

"Characterization of the exonuclease Eri1 in the binding and processing of RNA targets and analysis of its function in mouse development"

Dissertation der Fakultät für Biologie
der Ludwig-Maximilian-Universität München
zur Erlangung des Doktorgrades



vorgelegt von
Nicola Rath

München 2010

Erklärung

Hiermit erkläre ich, Nicola Rath, dass die vorliegende Arbeit mit dem Titel: "Characterization of the exonuclease Eri1 in the binding and processing of RNA targets and analysis of its function in mouse development" von mir selbstständig und ohne unerlaubte Hilfsmittel angefertigt wurde und ich mich dabei nur der ausdrücklich bezeichneten Quellen und Hilfsmittel bedient habe. Diese Arbeit wurde weder in der jetzigen noch in einer abgewandelten Form einer anderen Prüfungskommission vorgelegt.

München, der 28.04.2010

Nicola Rath

Erstgutachter: Prof. Dr. Dirk Eick

Zweitgutachter: Prof. Dr. Michael Schleicher

Tag der Einreichung: 03.05.2010

Tag der mündlichen Prüfung: 04.10.2010

Contents

Abbreviations	iv
Abstract	vi
Zusammenfassung	vii
1 Introduction	1
1.1 The eukaryotic transcriptome	1
1.2 Coding and structural RNAs	2
1.2.1 Messenger RNAs	2
1.2.2 Canonical histone mRNAs	3
1.2.3 Ribosomal RNAs	5
1.3 Regulatory RNAs	7
1.3.1 Mechanisms of RNA interference	7
1.3.2 MicroRNAs in development and cell differentiation	9
1.4 Embryonic development in vertebrates	10
1.4.1 Skeletal patterning and the organization of Hox clusters	11
1.4.2 Regulation of Hox gene expression	12
1.5 Functional protein-RNA interactions	14
1.6 The 3' exonuclease Eri1	15
1.6.1 The structure of Eri1	15
1.6.2 Eri1 and canonical histone mRNAs	16
1.6.3 Eri1 and RNA interference	17
1.7 Aim of the work	19
2 Material and methods	20
2.1 Material	20
2.1.1 Chemicals and biochemicals	20
2.1.2 Enzymes	20
2.1.3 Kits	21
2.1.4 Solutions	21
2.1.5 Vectors	22
2.1.6 Oligonucleotides	25
2.1.7 Antibodies	27
2.1.8 Cell culture	27
2.1.9 Mice	27
2.1.10 Instruments	28
2.2 Methods	29
2.2.1 Molecular biological standard methods	29
2.2.2 Breeding and genotyping of mice	32
2.2.3 Preparation of embryos	32
2.2.4 Generation of mouse embryonic fibroblasts	32
2.2.5 Cell culture	33
2.2.6 Transfection of cells	33
2.2.7 Infection of cells with adeno- and retroviruses	33
2.2.8 Flow cytometry analysis	34
2.2.9 Hydroxyurea treatment of cells	34

2.2.10	Measurement of cell growth	35
2.2.11	Confocal microscopy	35
2.2.12	Western blot analysis	35
2.2.13	Immunohistochemistry stain on embryos	36
2.2.14	Whole mount in situ hybridization of embryos	36
2.2.15	Methods employed in German Mouse Clinic.....	37
2.2.16	Skeletal analysis.....	38
2.2.17	Molecular phenotyping of embryos	38
2.2.18	RNA-immunoprecipitation (RIP)	40
2.2.19	Quantitative PCR.....	42
2.2.20	Dual-luciferase reporter assay	43
3	Results	45
3.1	Characterization of mouse Eri1: the knockout phenotypes, the expression patterns and the binding and processing of target RNAs	45
3.1.1	Description of the Eri1-knockout mouse.....	45
3.1.2	Eri1 is ubiquitously expressed in mice	49
3.1.3	The SAP domain and linker sequence of Eri1 determine its localization to the nucleolus	50
3.1.4	Eri1 binds 5.8S rRNA as well as its rRNA precursor and catalyses 5.8S rRNA processing.....	51
3.1.5	Reduced cell growth of primary Eri1-deficient MEF cells	57
3.1.6	Eri1 binds to histone mRNA and initiates cell cycle-dependent degradation	58
3.2	Dysmorphology phenotype of Eri1-knockout mice	65
3.2.1	Eri1-knockout mice show a homeotic transformation	65
3.2.2	High expression of Eri1 in the prevertebrae of embryos	69
3.2.3	Molecular phenotyping of Eri1-knockout embryos	71
3.2.4	Literature and database research to reveal Eri1 target candidates..	73
3.2.5	Shift of Hox gene expression in Eri1-knockout embryos.....	75
3.2.6	Eri1 reduces mature miR-196a levels in MEF cells.....	78
3.2.7	The exonuclease activity of Eri1 inhibits miR-196-mediated silencing of Hoxc8 through its 3' UTR.....	79
4	Discussion.....	83
4.1	Severe phenotypes in Eri1-knockout mice	83
4.1.1	Growth defects, postnatal death and male sterility.....	83
4.1.2	Results from the screen in the German Mouse Clinic	84
4.2	Limitations of molecular phenotyping of embryos	85
4.3	Expression and intracellular localization of Eri1	86
4.4	The RNA target molecules of Eri1	88
4.4.1	Ribosomal RNA processing	88
4.4.2	Histone mRNA degradation.....	89
4.4.3	How does Eri1 recognize its target RNAs?	91
4.5	Eri1 regulates skeletal patterning	92
4.5.1	Shared phenotypes of Eri1- and Hoxc8-knockout mice	93
4.5.2	Hox expression pattern in embryos.....	94
4.5.3	Eri1 regulates mature miR-196a levels	96
4.5.4	The impact of Eri1 on miR-196-mediated Hoxc8 silencing	97
4.5.5	Model depicting the role of Eri1 in skeletal patterning.....	98
4.6	Conclusion.....	99

References 100

Supplementary 108

Publications 110

Curriculum vitae..... 111

Acknowledgements 112

Abbreviations

%	percent
+/+	wildtype
-/-	knockout
°C	degree Celsius
A	adenine
Ago	Argonaute
Ala	alanine
APS	ammonium persulphate
Arg	arginine
bp	base pairs
BSA	bovine serum albumin
C	cytosine
cDNA	complementary DNA
CDS	coding sequence
Chr	chromosome
DAPI	4',6-diamidino-2'-phenylindol-dihydrochloride
DNA	deoxyribonucleic acid
dNTP	deoxynucleotide triphosphate
dpc	days post coitum
ds	double-stranded
DTT	dithiothreitol
<i>E. coli</i>	<i>Escherichia coli</i>
eGFP	enhanced green fluorescent protein
Eri1	enhanced RNAi1
ETS	external transcribed spacer
FACS	fluorescence-activated cell sorting
FCM	flow cytometry
FCS	fetal calf serum
FDR	false discovery rate
g	gramm
G	guanine
gDNA	genomic DNA
h	hour
HET	heterozygous
HRP	horse radish peroxidase
HU	hydroxyurea
Ig	immunoglobulin
IRES	internal ribosome entry site
ITS	internal transcribed spacer
kb	kilo base pairs
kDa	kilo Dalton
KO	knockout
LB media	Luria-Bertani media
Lys	lysine
M	molar

MEF	mouse embryonic fibroblasts
min	minute
miR	microRNA
miRNA	microRNA
mM	millimolar
MOI	multiplicity of infection
mRNA	messenger RNA
ms	millisecond
ncRNA	non-coding RNA
nt	nucleotide
PAGE	polyacrylamide gel electrophoresis
PBS	phosphate buffered saline
PCR	polymerase chain reaction
pH	potentia hydrogenii
PMSF	phenylmethylsulfonyl fluoride
pre-	precursor
pri-	primary
PVDF	polyvinylidene fluoride
rDNA	ribosomal DNA
RIP	RNA immunoprecipitation
RISC	RNA-induced silencing complex
RNA	ribonucleic acid
RNAi	RNA interference
RNA-Pol	RNA polymerase
RNase	ribonuclease
rpm	rounds per minute
rRNA	ribosomal RNA
RT	room temperature
RT-PCR	reverse transcription-PCR
s	second
S	Svedberg units
SDS	sodium dodecyl sulfate
shRNA	small hairpin RNA
siRNA	small interfering RNA
SLBP	stem-loop binding protein
snoRNA	small nucleolar RNA
snRNA	small nuclear RNA
snRNP	small nuclear ribonucleoprotein
T	thymidine
tRNA	transfer RNA
U	uracil
UTR	untranslated region
v/v	volume per volume
WT	wildtype
w/v	weight per volume

Abstract

The *Eri1* (enhanced RNAi) gene is conserved from fission yeast to humans and codes for a protein consisting of an amino-terminal SAP domain and a carboxy-terminal 3' exonuclease domain. In this study mouse *Eri1* protein was analyzed for its impact on three RNA target molecules: ribosomal RNA, histone mRNA and miRNA. The *Eri1* protein was found to be enriched in nucleoli, the sites of ribosome biogenesis. Consistent with this finding, RNA-immunoprecipitations revealed binding of *Eri1* to 5.8S rRNA as well as its precursor and it could be demonstrated that *Eri1* performs in 5.8S rRNA 3' end processing. Furthermore, histone mRNA could be co-immunoprecipitated with *Eri1* in living cells and functional data demonstrate that the exonuclease activity of *Eri1* is crucial for the initiation of cell cycle-dependent histone mRNA degradation. Detailed analyses using *Eri1* point mutants identified critical amino acids for binding of the RNA target molecules in the nucleic acid-binding SAP domain as well as in the linker sequence between the SAP and exonuclease domain. Together, these results suggest an impact of *Eri1* on fundamental cellular processes such as protein biogenesis, DNA replication and cell division.

Systematic analysis of *Eri1*-knockout mice uncovered a number of phenotypes. The most prominent ones were growth retardation, postnatal death and male sterility. Further, a skeletal dysmorphology phenotype was found, revealing an additional pair of ribs in *Eri1*-knockout mice. To investigate the underlying molecular mechanism analyses were performed on various levels. First, a detailed description of the skeleton showed a duplication of the thoracic vertebra T7 and an extension of the homeotic transformation to the first sacral vertebra. Second, literature and database research revealed a high degree of similarity between *Hoxc8*-knockout mice and *Eri1*-knockout mice. Third, molecular analysis of the *Hoxc8* mRNA expression pattern indicated a shift of the anterior expression border of *Hoxc8* comparing *Eri1*-knockout and wildtype embryos. Finally, *Eri1* could be shown to reduce miR-196a levels in MEF cells, and luciferase reporter assays demonstrated an inhibition of miR-196a-mediated *Hoxc8* 3' UTR silencing by *Eri1*. These data led to the current model in which *Eri1* regulates *Hoxc8* silencing by miR-196a in embryos and thus controls skeletal patterning during mouse development.

Zusammenfassung

Das *Eri1* (enhanced RNAi) Gen ist von der Spaltheife bis zum Menschen konserviert und kodiert für ein Protein mit einer amino-terminalen SAP-Domäne und einer carboxy-terminalen 3' Exonuklease-Domäne. In dieser Studie wurde der Einfluss von dem Eri1-Protein der Maus auf drei RNA-Zielmoleküle analysiert: ribosomale RNA, Histon-mRNA und miRNA. Eine Anreicherung des Eri1-Proteins wurde in Nukleoli, den Orten der Ribosombiogenese, gefunden. In Übereinstimmung mit diesem Ergebnis zeigten RNA-Immunpräzipitationen eine Bindung von Eri1 an 5.8S rRNA sowie an die ribosomale Vorläufer-RNA und es konnte nachgewiesen werden, dass Eri1 5.8S rRNA am 3' Ende prozessiert. Des Weiteren konnte Histon-mRNA mit Eri1 in lebenden Zellen ko-immunpräzipitiert werden und funktionelle Daten beweisen, dass die Exonuklease-Aktivität von Eri1 für die Initiierung der Degradation Zellzyklus-abhängiger Histon-mRNAs notwendig ist. Detaillierte Analysen mit Eri1-Punktmutanten identifizierten kritische Aminosäuren für die Bindung von RNA-Zielmolekülen in der Nukleinsäure-bindenden SAP-Domäne sowie in der Region zwischen SAP- und Exonuklease-Domäne. Zusammengefasst machen diese Ergebnisse deutlich, dass ein Einfluss von Eri1 auf elementare zelluläre Prozesse wie Proteinbiogenese, DNA-Replikation und Zellteilung besteht.

Bei der systematischen Analyse von Eri1-„Knockout“-Mäusen wurde eine Reihe von Phänotypen entdeckt. Die markantesten waren Wachstumsverzögerung, postnataler Tod und Sterilität bei männlichen Mäusen. Weiterhin wurde eine Skelettfehlbildung mit einem zusätzlichem Rippenpaar in Eri1-„Knockout“-Mäusen gefunden. Zur Erforschung des zugrundeliegenden molekularen Mechanismus wurden Analysen auf verschiedenen Ebenen durchgeführt. Erstens zeigte eine detaillierte Beschreibung des Skeletts eine Duplikation des 7. Brustwirbels und eine Ausdehnung der homeotischen Transformation bis zum ersten sakralen Wirbel. Zweitens machten Literatur- und Datenbanknachforschungen eine hohe Ähnlichkeit zwischen *Hoxc8*-„Knockout“-Mäusen und *Eri1*-„Knockout“-Mäusen deutlich. Drittens kennzeichnete die molekulare Analyse der *Hoxc8* mRNA-Expression eine Verschiebung der anterioren Expressionsgrenze von *Hoxc8* in *Eri1*-„Knockout“-Mäusen im Vergleich zu Wildtyp-Mäusen. Letztlich konnte gezeigt werden, dass Eri1

miR-196a-Level in MEF-Zellen reduziert und Luziferase-Reporter Experimente bewiesen eine Inhibierung der miR-196a-vermittelten Hoxc8 3' UTR-Stillegung durch Eri1. Diese Daten führten zu dem aktuellen Modell, in dem Eri1 die Hoxc8-Stillegung durch miR-196a im Embryo reguliert und folglich die Skelettmusterung während der Mausentwicklung kontrolliert.

1 Introduction

1.1 The eukaryotic transcriptome

All living cells store their hereditary information in the same genetic code in the form of deoxyribonucleic acid (DNA), a long, double-stranded winding molecule that contains the instructions needed to build and maintain cells. For these instructions to be carried out, DNA must be transcribed into corresponding molecules of ribonucleic acid (RNA), referred to as transcripts. The transcriptome comprises the entire set of transcripts in a cell. For a long time the description of the transcriptome was limited to the transcription products of known annotated genes: These products were mainly messenger RNAs (mRNAs) as well as stable non-coding RNAs (ncRNAs), such as ribosomal RNAs (rRNAs), transfer RNAs (tRNAs), small nuclear RNAs (snRNAs) and small nucleolar RNAs (snoRNAs). However, the catalogue of transcribed sequences became more complex, first with the discovery of naturally occurring interfering RNAs, such as small interfering RNAs (siRNAs) and microRNAs (miRNAs). Lately, new technologies revealed that the transcription landscape in higher eukaryotes was found to imply high portions of transcripts originating from intergenic regions. This widespread genomic transcription is often called 'pervasive transcription', because contrary to genes, the transcripts are not restricted to well-defined functional features (Jacquier, 2009).

Additionally to the complexity in sequence, recent findings have revealed that enormous diversity can be generated on the RNA level. Regulatory networks control RNA transcription as well as post-transcriptional events (Figure 1). For example, ribosomal RNAs are further modified by pseudouridylation (Ψ) and ribose methylation (CH₃) at specific residues. In alternative splicing, exonic sequences are removed as part of an intron to generate alternative mRNAs that direct the synthesis of distinct protein isoforms. Interfering RNAs might inhibit protein synthesis or even lead to mRNA degradation (Mendes Soares and Valcarcel, 2006). Consequently, numerous proteins tightly regulate gene expression to ensure spatio-temporal expression, meaning that the correct complement of RNA and proteins is present in the right cell at the correct time.

Accordingly, in contrast to the clear description of genomes, transcriptomes are entities as diverse as the cell types, developmental stages and environmental conditions that the organism harbors or faces.

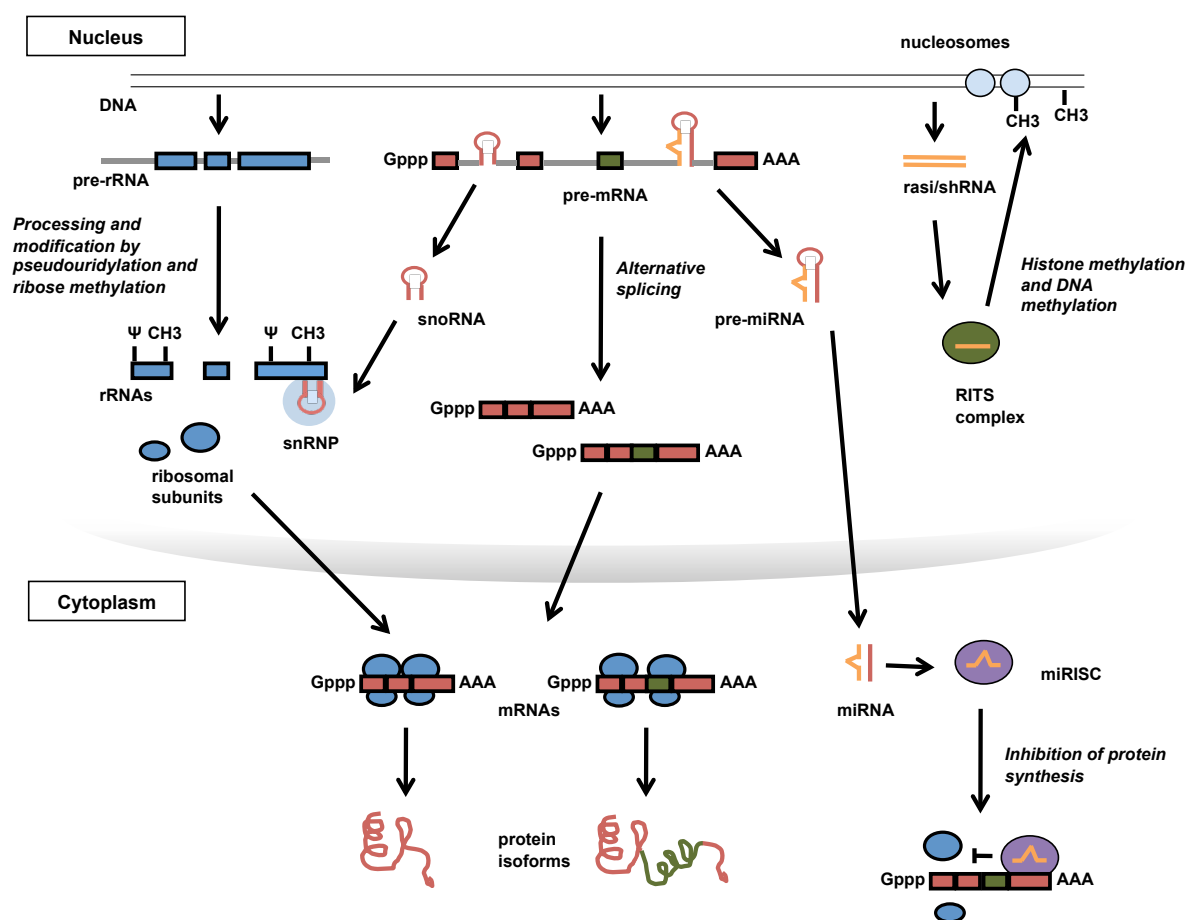


Figure 1: An overview of the eukaryotic transcriptome. miRNA, microRNA; mRNA, messenger RNA; rasiRNA, repeat associated small interfering RNA; RISC, RNAi-induced silencing complex; miRITS, miRNA-induced transcriptional silencing; rRNA, ribosomal RNA; shRNA, small hairpin RNA; snRNP, small nuclear ribonucleoprotein; snoRNA, small nucleolar RNA. (Adapted from Mendes Soares and Valcarcel, 2006)

1.2 Coding and structural RNAs

1.2.1 Messenger RNAs

Protein coding genes represent only a small fraction of eukaryotic genomes. New insights indicate that the generation of organismal complexity from the relative small number of genes is mainly achieved through the regulation of RNA complexity. The primary products of transcription of eukaryotic protein-coding genes are subject to extensive processing. A single primary transcript can lead to the generation of

multiple mRNAs, proteins and functions due to post-transcriptional events; for example, through alternative splicing, alternative polyadenylation and RNA editing. Protein-coding genes are transcribed exclusively by RNA polymerase II (RNA-Pol II) to synthesize mRNA precursors (pre-mRNAs). The processing of the pre-mRNAs to their mature form often occurs co-transcriptionally. The standard modifications involve capping, splicing and cleavage/polyadenylation (Figure 1). In brief, the 7-methyl G5'ppp5'N cap is an identifying mark on all RNA-Pol II transcripts. Three enzymes contribute to the capping of mRNAs: RNA triphosphatase, guanylyltransferase and 7-methyltransferase. The cap is added when the RNA is about 25 bp long, soon after its 5' end emerges from the RNA exit channel of the polymerase (Shuman, 1997). Introns can be removed by the spliceosome, a large, dynamic complex comprising five uridine-rich small nuclear ribonucleoproteins (snRNPs) and a number of additional proteins. Splicing can occur either co-transcriptionally or post-transcriptionally (Wetterberg et al., 1996). At the end of the gene, the pre-mRNA is cleaved at the poly(A) motive and a poly(A) tail is added to the exposed 3' end. Finally, the mature mRNA will be transported to the cytoplasm to be translated into proteins.

1.2.2 Canonical histone mRNAs

Histones are the primary protein component of chromatin. The canonical histone mRNAs encode the four core histones – H2A, H2B, H3 and H4 – which make up the nucleosome, and the linker H1 histones, which are found between nucleosomes. Two of each core histones form a heterooctamer, which is used to wrap the DNA around twice. In 1974 it has already been discovered that histones are involved in chromosomal DNA packaging (Kornberg, 1974; Kornberg and Thomas, 1974; Olins and Olins, 1974), but only recently a crucial role for histones in regulating gene expression was recognized. In this process extensive modification of the histone proteins plays an important role. Furthermore, the accurate positioning of nucleosomes within chromatin is essential for proper transcriptional regulation, the demarcation of heterochromatic boundaries and the epigenetic inheritance of gene expression patterns. Thus the cell must carefully coordinate the replication of DNA, the synthesis of estimated 10^8 molecules of each histone type per mammalian cell and the rapid deposition of new and old histones to reform chromatin during each relatively short S-phase (Marzluff et al., 2008).

In mouse there are 65 distinct canonical histone mRNAs, which code for the five types of histone proteins. These canonical histone mRNAs are the only metazoan mRNAs, which are not polyadenylated but contain a unique 3' end structure. They are encoded by replication-dependent histone genes and must rapidly reach high levels of expression during S-phase. In contrast, the replication-independent histone variants are polyadenylated and their synthesis persists also outside S-phase. Transcription of the canonical histone genes and processing of the resulting pre-mRNA occur in association with the Cajal body in the nucleus. The genes are transcribed by RNA-Pol II and their rate of transcription increases as cells approach S-phase (DeLisle et al., 1983). Additionally, the formation of histone mRNAs by 3' end processing is most effective during S-phase, coupling histone synthesis with DNA replication (Harris et al., 1991).

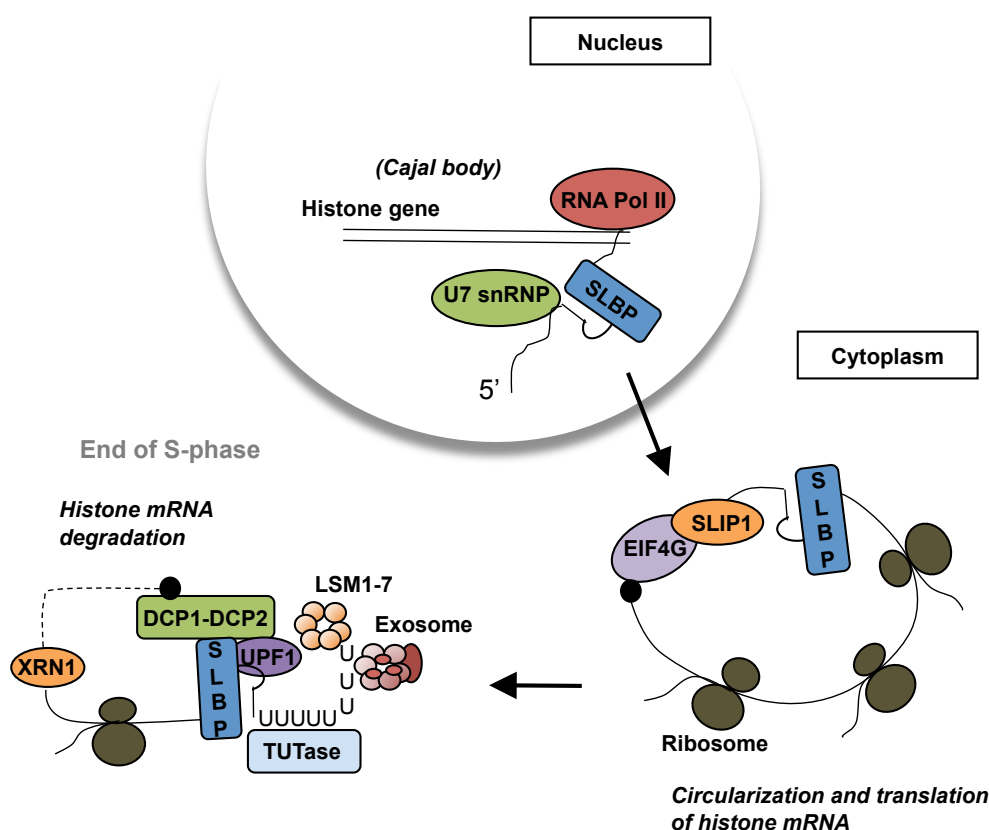


Figure 2: Global view of histone mRNA metabolism in mammalian cells. DCP, mRNA decapping enzyme; EIF4G, eukaryotic translation initiation factor 4- γ ; LSM, Sm-like protein; Pol, polymerase; SLBP, stem-loop binding protein; SLIP1, SLBP-interacting protein 1; snRNP, small nuclear ribonucleoprotein; TUTase, terminal uridylyltransferase; XRN1, 5'–3' exoribonuclease 1. (Adapted from Marzluff et al. 2008)

The genes encoding metazoan canonical histones lack introns, and thus one endonucleolytic cleavage reaction is the only processing event necessary to form mature histone mRNA (Figure 2). Cleavage requires binding of the stem-loop binding protein (SLBP) and is carried out by a multi-component machinery containing U7 snRNP (Mowry and Steitz, 1987). SLBP remains bound to the histone mRNA as it relocates to the cytoplasm, where histone mRNA is circularized through a complex of proteins including at least SLBP, SLBP-interacting protein 1 (SLIP1) and eukaryotic translation initiation factor 4- γ (EIF4G). Subsequently, translation of histone mRNA takes place. At the end of S-phase, a short U-tail is added to histone mRNA in the cytoplasm. The LSM1–7 ring binds the oligo(U) to cooperate in the recruitment of the decapping complex and a conserved complex of 3' to 5' exonucleases, termed the exosome to degrade the mRNA. In addition, the cyclin A/cyclin-dependent kinase 1 complex (CycA/CDK1) phosphorylates SLBP to trigger its degradation by the proteasome preventing further accumulation of histone mRNAs and eventually histone proteins (Marzluff et al., 2008).

1.2.3 Ribosomal RNAs

One of the most important tasks of any cell is to synthesize ribosomes. There are about 10^6 ribosomes in a growing cell, so the cell has to synthesize 10^6 copies of each type of ribosomal RNA (rRNA) in each cell generation; these represent about 80% of the total RNA. In eukaryotes, the process of rRNA transcription, processing and assembly occurs sequentially in the nucleolus, the nucleoplasm and the cytoplasm. The nucleolus is a distinct subnuclear compartment with over 700 proteins identified in the proteome of human nucleoli (Andersen et al., 2005; Andersen et al., 2002; Scherl et al., 2002). The primary function of the nucleolus is ribosome subunit biogenesis, but besides pre-mRNA processing factors also other proteins have been identified that are involved in cell-cycle control as well as DNA replication and repair (Boisvert et al., 2007).

The ribosomal DNA (rDNA) genes are encoded in so-called nucleolar organizer regions, which are located on acrocentric chromosomes. Nucleoli form at the end of mitosis around the rDNA genes and result in a subnuclear compartment that locally concentrates the transcription and processing machineries that are responsible for generating ribosome subunits. The rDNA genes are arranged in long tandem arrays separated by non-transcribed spacer regions. The transcription of rDNA genes

requires a specialized RNA polymerase, RNA-Pol I, which produces uncapped and unpolyadenylated rRNA transcripts. The primary pre-rRNA most likely starts to fold spontaneously and to interact with small RNAs and proteins during transcription. Indeed proper transcriptional elongation by RNA-Pol I is required for efficient pre-rRNA processing and pre-ribosome assembly (Schneider et al., 2007).

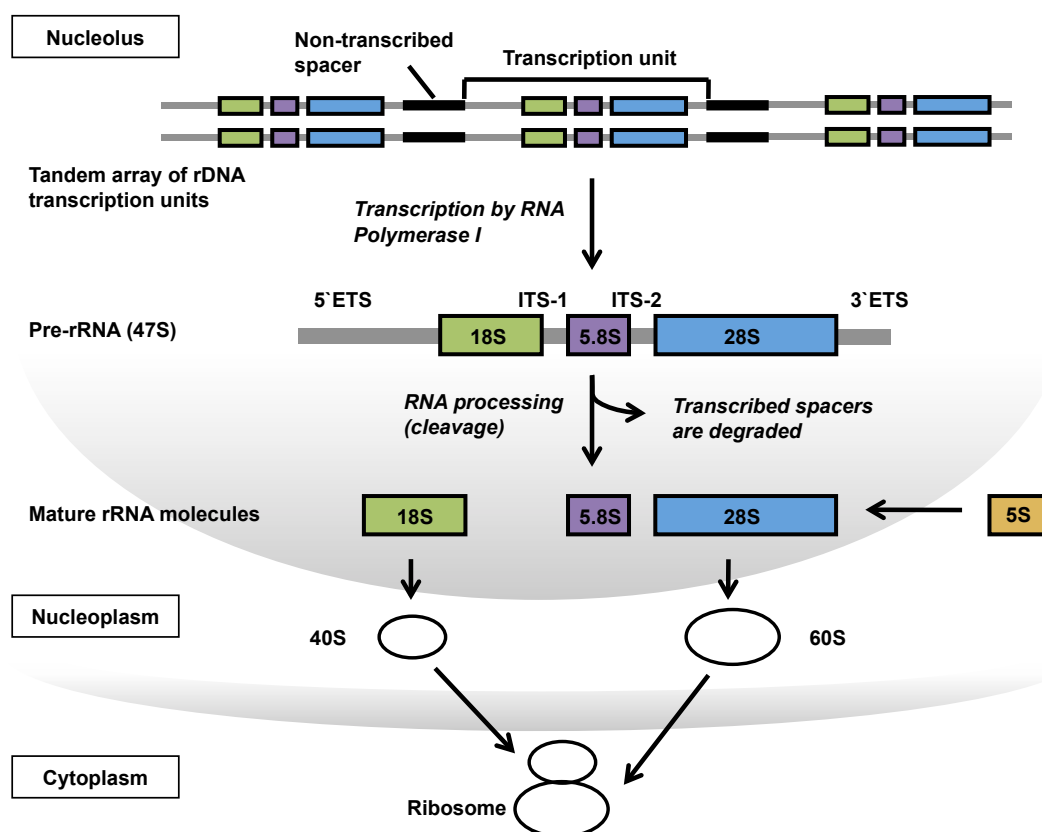


Figure 3: Synthesis and processing of rRNA for ribosome biogenesis in mammals. ETS, external transcribed spacer; ITS, internal transcribed spacer; rDNA, ribosomal DNA; rRNA, ribosomal RNA.

The primary transcript (47S pre-rRNA) of ~14 kb in size is processed into 18S, 5.8S, and 28S mature rRNAs (Figure 3). About half of the primary rRNA transcript is comprised of regions termed external transcribed spacers (5'ETS and 3'ETS) and internal transcribed spacers (ITS-1 and ITS-2). The latter are removed and rapidly degraded during rRNA maturation (Eichler and Craig, 1994). Processing of pre-rRNA requires more than 150 non-ribosomal factors that transiently associate with the developing pre-ribosomes (Henras et al., 2008; Tschochner and Hurt, 2003). For example, the exosome is involved in multiple steps in pre-rRNA maturation (Houseley et al., 2006; Mitchell et al., 1997; Raijmakers et al., 2004). The most

common covalent modifications found in rRNA are methylation and 2'-O-ribose pseudouridylation (Figure 1). Both of these modifications are catalyzed in the nucleolus by small nucleolar ribonucleoproteins (snoRNPs) that act on the pre-rRNA substrate (Kiss, 2002). Contrary to the long precursor RNA, which is transcribed by RNA-Pol I and has to be processed further, the 5S rRNA is transcribed from a separate cluster of genes by RNA-Pol III. The 5.8S and 28S rRNAs assemble with the 5S rRNA transcript to form the large 60S subunit, whereas the 18S rRNA alone assembles into the small 40S ribosome subunit. The pre-40S and pre-60S ribosome subunits are both exported into the cytoplasm, where final assembly and maturation steps occur. As a last step, the mature ribosomal subunits bind to mRNA to form functional ribosomes (Boisvert et al., 2007).

1.3 Regulatory RNAs

RNA interference (RNAi) was discovered by Andrew Fire and Craig Mello in 1998. This finding was awarded with the Nobel Prize for Medicine in 2006. The discovery that sequence-specific gene silencing occurs in response to the presence of double-stranded RNAs in the worm (Fire et al., 1998) and the subsequent demonstration that RNAi operates also in mammalian cells (Elbashir et al., 2001) has had an enormous impact on biology, uncovering an unsuspected level of regulation of gene expression. During the last decade, remarkable progress has been made towards understanding the underlying mechanisms of RNAi. These small RNAs are able to regulate the fine-tuning and networking of complex suites of gene activity, thereby specifying cellular physiology, differentiation and development. Additionally, RNAi has become a powerful experimental tool for biological research as well as drug discovery and is currently being developed for human gene therapy.

1.3.1 Mechanisms of RNA interference

During RNAi, dsRNAs are processed into small RNAs of approximately 21 nucleotides, termed small interfering RNAs (siRNAs), which guide the destruction of complementary target mRNAs (Mello and Conte, 2004). Natural mechanisms related to RNAi are involved in developmental gene regulation mediated by microRNAs (miRNAs) and in transcriptional silencing and heterochromatin formation (Ambros, 2004; Lippman and Martienssen, 2004).

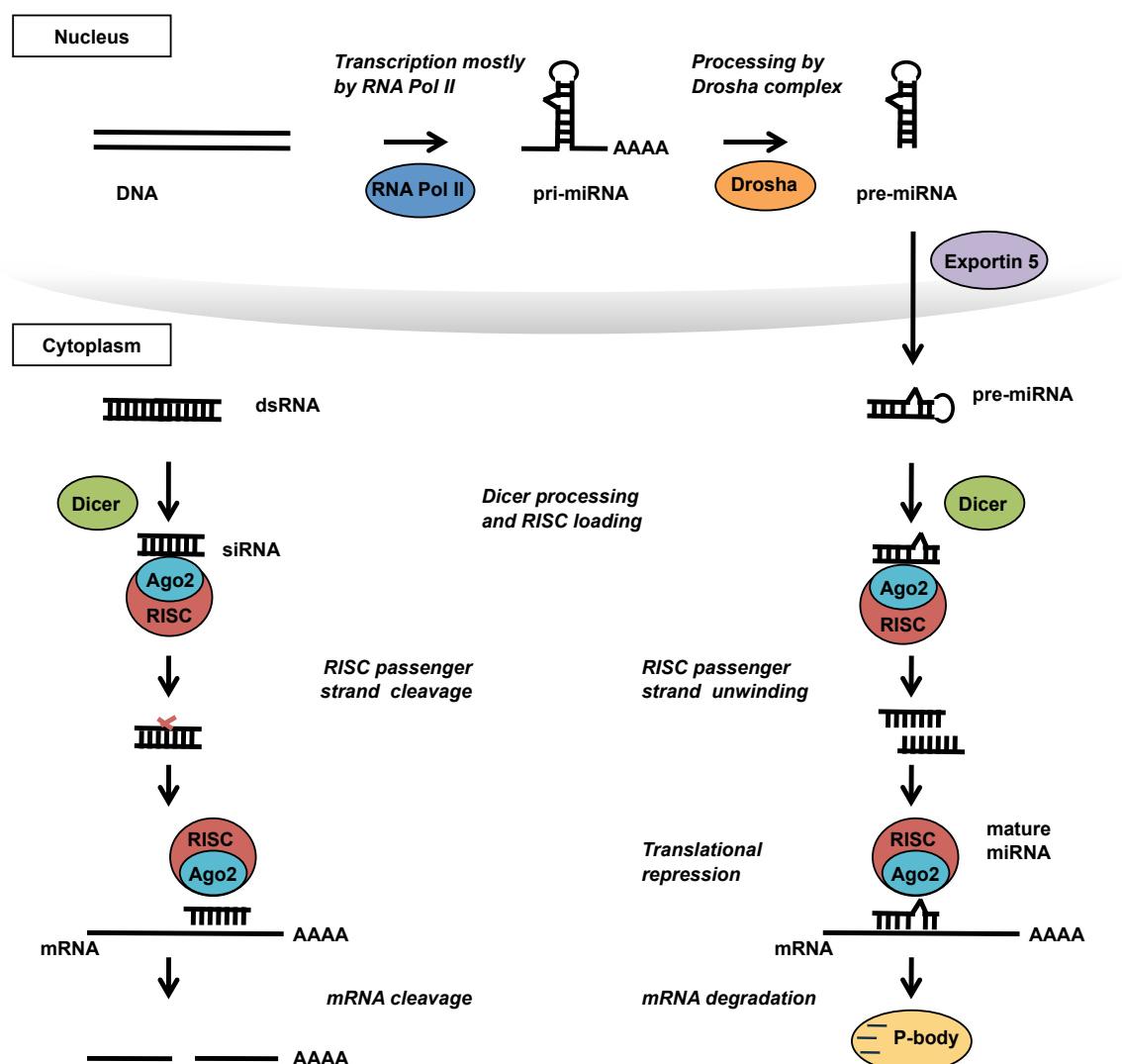


Figure 4: Mechanism of RNA interference in mammalian cells. Ago2, Argonaute-2; ds, double-stranded RNA; mRNA, messenger RNA; Pre-miRNA, precursor miRNA; Pri-miRNA, primary miRNA; RISC, RNAi-induced silencing complex; siRNA, small interfering RNA. (Adapted from Fougerolles et al., 2007)

Two main categories of small RNAs have been defined on the basis of their precursors: The cleavage of exogenous long dsRNA precursors in response to viral infection or after artificial introduction generates siRNAs, whereas the processing of genome-encoded stem-loop structures generates miRNAs (Figure 4). The synthesis of mature miRNAs begins with endogenously encoded primary miRNA transcripts (pri-miRNAs) that are mostly transcribed by RNA Pol II (Kim, 2005) and are processed by the nuclear-localized RNase III Drosha enzyme complex, which defines one end of the duplex and releases a precursor miRNA (pre-miRNA) of ~65–70 nucleotides. The pre-miRNA hairpin is exported to the cytoplasm by exportin 5, where Dicer completes the processing for loading onto the Argonaute 2/RNAi-

induced silencing complex (Ago2/RISC). When the RNA duplex loaded onto RISC has imperfect sequence complementarity, the passenger strand is unwound leaving a mature miRNA bound to active RISC. The mature miRNA recognizes target sites, typically in the 3' UTR of the mRNA, leading to direct translational inhibition. Binding of a miRNA to its target mRNA may also lead to mRNA target degradation in processing (P)-bodies. In the siRNA pathway the RNA duplex loaded onto the RISC has perfect sequence complementarity. AGO2 cleaves the passenger strand, so that active RISC containing the guide strand is produced. The guide strand recognizes target sites to direct mRNA cleavage, again carried out by the catalytic domain of AGO2 (de Fougères et al., 2007; Siomi and Siomi, 2009).

1.3.2 MicroRNAs in development and cell differentiation

The first miRNA, *lin-4*, was discovered in *C. elegans* and was shown to be essential for the normal temporal control of diverse postembryonic developmental events. *Lin-4* transcripts were found to contain sequences complementary to a repeated sequence element in the 3' UTR of *lin-14* mRNA. This suggested the post-transcriptional regulation of the heterochronic gene *lin-14* expression via an antisense RNA-RNA interaction (Lee et al., 1993; Wightman et al., 1993). In 2000, another *C. elegans* miRNA, *let-7*, was identified and shown to regulate developmental timing in the nematode (Reinhart et al., 2000). It was proposed that the sequential stage-specific expression of the *lin-4* and *let-7* regulatory RNAs triggers transitions in the complement of heterochronic regulatory proteins to coordinate developmental timing in *C. elegans*. However, unlike *lin-4*, which is conserved only in closely related species, *let-7* RNAs were detected and found to exhibit temporally controlled expression in samples from a wide range of animal species, including vertebrates (Pasquinelli et al., 2000). Since then, numerous regulatory small RNAs have been cloned from several species, and many of these exhibit spatially and/or temporally regulated patterns of gene expression (Aravin et al., 2006; Aravin et al., 2003; Lagos-Quintana et al., 2002; Landgraf et al., 2007; Lau et al., 2001; Lee and Ambros, 2001). The abundance of these tiny RNAs, their expression patterns, and their evolutionary conservation implied that, as a class, miRNAs have broad regulatory functions in animals. For example, while the two founding members of this class of regulatory RNAs both were found to control developmental timing, other miRNAs were shown to function in the neuronal

patterning in nematodes (Johnston and Hobert, 2003) or the modulation of hematopoietic lineage differentiation in mammals (Chen et al., 2004). *Drosophila* miRNAs, bantam and miR-14, have been implicated in the control of cellular proliferation and in the reduction of programmed cell death (Brennecke et al., 2003; Johnston and Hobert, 2003; Xu et al., 2003) and the muscle-specific miR-1 was found to control cardiac differentiation (Kwon et al., 2005a). Microarray based analysis of mouse miRNAs demonstrated tissue specific expression of many miRNAs (Liu et al., 2004). These observations led to the notion that a principal function of miRNAs is to control cell differentiation and development.

1.4 Embryonic development in vertebrates

Animal development begins with fertilization of the ovum, which initiates rapid cell division and a cascade of gene expression changes. The final pattern of a differentiated cell type is the outcome of a specific program for cell specialization. Although every cell contains the same genetic information, selective gene expression will produce many diverse cells in a final pattern of great complexity and precision.

During development, many cell movements occur to shape the vertebrate body. In gastrulation the cells from the exterior of the early embryo tuck into the interior to form a gut cavity and create the three germ layers: endoderm, mesoderm, and ectoderm. In vertebrates, the movements of gastrulation are organized by signals from the organizer, called node in a mouse embryo. This specifies the dorso-ventral (from back to belly) axis and gives shape to the anterior-posterior (from head to tail) axis, which has already been defined by the animal-vegetal asymmetry of the egg. The segmentation of the mesoderm into somites depends on a periodic pattern of gene expression, which is laid by a biochemical oscillator in the mesoderm and dictates the way the mass of cells will break up into separate blocks. The vertebral bodies and ribs evolve from somatic mesoderm, only the sternum is formed by the lateral plate mesoderm. In all vertebrates the axial skeleton is composed of similar components that extend from anterior to posterior along the body axis: the occipital skull bones and cervical, thoracic, lumbar, sacral, and caudal vertebrae. During evolution significant changes in the number and size of these elements occurred, but the basic character and the order in which they appear in vertebrate skeletons have remained remarkably similar.

1.4.1 Skeletal patterning and the organization of Hox clusters

An important mechanism during embryonic development is the correct patterning of the axial skeleton. The definition of the anterior to posterior (A-P) animal body axis is probably the ancestral role of Hox genes (Duboule and Dolle, 1989; Graham et al., 1989; Gruss and Kessel, 1991; Krumlauf, 1994). Hox proteins are transcription factors that contain a homeodomain and were first described in *Drosophila* for their ability to cause segmental homeotic transformations of the body plan (Lewis, 1978). In mammals there are four Hox gene clusters (Hoxa -d) containing 39 Hox genes that can be classified in 13 paralogous subgroups. The size of the Hox clusters is between 100 and 200 kb. In the Hox gene nomenclature, the numbers of the paralogous genes descend in the direction of transcription with Hox1 paralogues mapping to the 3' end of each cluster. The temporal and spatial colinearity is a striking phenomenon of Hox gene expression: Hox genes located at the 3' end of the cluster are expressed earlier, whereas genes more 5' are expressed at later stages of development. In addition, genes at the 3' end of the clusters are expressed more anterior, while genes at the 5' end are expressed in more posterior parts of the embryo. Thus the gene order in the cluster is collinear to the relative position of their distinct expression domains along the A-P axis of the embryo (Pearson et al., 2005) (Figure 5).

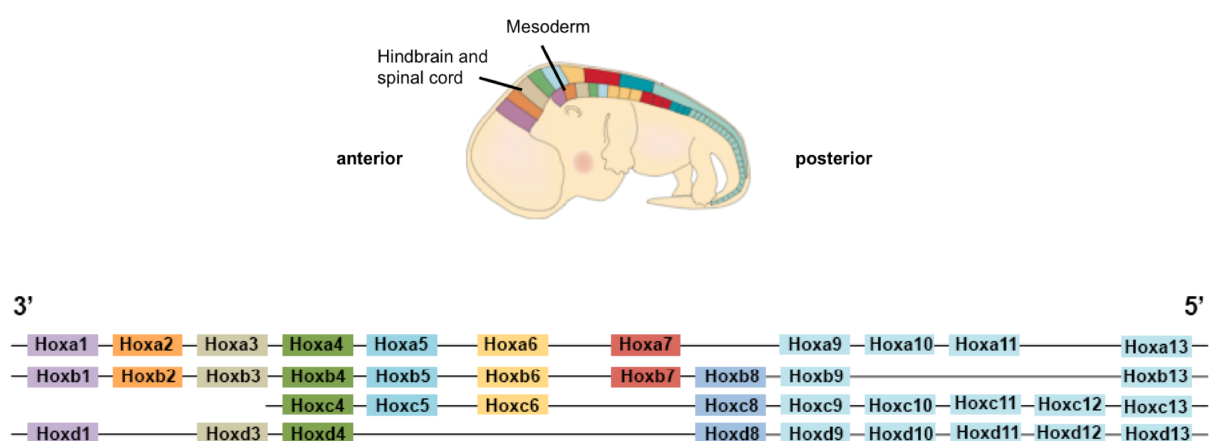


Figure 5: Hox expression and genomic organization. Mouse embryo with approximate Hox expression domains at embryonic day E12.5. The colors that denote the expression patterns of the Hox transcripts are color-coded to the genes in the Hox cluster diagrams. (Adapted from Pearson et al., 2005)

A specific combination of Hox gene transcription factor activity assigns the morphology of each vertebra (Kessel and Gruss, 1991). Because of Hox gene

expression in overlapping domains, a posterior prevalence model has been suggested, in which the patterning information at a given region relies on the more posterior expressed Hox gene (Duboule and Morata, 1994). Consequently, it is likely that particularly the establishment of the anterior boundary of Hox genes is an important step to accomplish an exact patterning of the embryo. Interestingly, it has been shown for *C. elegans* that after the initial boundaries are set, Hox gene expression patterns can still shift within the larger limits of their initial expression domains (Castelli-Gair and Akam, 1995; Salser and Kenyon, 1996). Several studies with mice also demonstrated that early Hox expression boundaries are subjected to both anterior and posterior changes before fixed boundaries are established at 12.5 days post coitum (dpc) (McIntyre et al., 2007; Wellik, 2007).

Hox mutant animals often exhibit morphological defects that involve changes in the A-P axial identity of the vertebrae. While for single Hox gene mutants both anterior and posterior homeotic transformations have been reported, loss of function of Hox paralogous groups always leads to anterior homeotic transformations of collinear regions throughout the skeleton (McIntyre et al., 2007). Additionally, data suggest that paralogous Hox genes show large functional redundancy, because double and triple mutant mice display a more severe and more penetrant phenotype (Chen and Capecchi, 1997; Condie and Capecchi, 1994; Davis et al., 1995; Fromental-Ramain et al., 1996a; Fromental-Ramain et al., 1996b; Horan et al., 1995; Manley and Capecchi, 1997; Manley and Capecchi, 1998).

Tandem duplications within the ancestral Hox cluster and subsequent genome duplication events have resulted in a relatively fixed arrangement of four Hox clusters in mammals, composed of two to four paralogous members (Wellik, 2007). The use of several Hox paralogous might be due to smaller differences in the coding sequence and in the 3' UTR. A slightly different regulatory modality has been observed for the single paralogous transcription factors, maybe because of diverse transcriptional as well as post-transcriptional regulation.

1.4.2 Regulation of Hox gene expression

The underlying mechanism of spatial and temporal colinearity is still elusive. An elaborate set of global and local transcriptional regulatory mechanisms seems to be involved (Deschamps, 2007; Heard and Bickmore, 2007). For example, it has been shown that Polycomb and Trithorax group complexes control the maintenance of *Hox*

gene expression in appropriate domains. The Polycomb complexes function as global enforcers of epigenetically repressed states, balanced by an antagonistic state that is mediated by Trithorax (Duboule and Morata, 1994; Schwartz and Pirrotta, 2007). When cells become committed to differentiation, the epigenetic state has to be reprogrammed. Recently, it has been shown that a directional transition of the chromatin status takes place on Hox clusters. A dynamic progression of transcription-competent modifications is employed that leads to an increase of activation marks and a decrease of repressive marks (Soshnikova and Duboule, 2009a; Soshnikova and Duboule, 2009b).

For regulation of Hox expression on the post-transcriptional level, miRNAs have been proposed. It has been suggested that miRNAs are fine-tuners of developmental gene expression programs (Stark et al., 2005). At least 30 of the 39 mammalian Hox 3' UTRs have one or more binding sites for vertebrate miRNAs. Hoxa7, Hoxb8, Hoxc8 and Hoxd8 have already been demonstrated experimentally as conserved targets of miR-196 (Mansfield et al., 2004; Yekta et al., 2004). Hoxc8, Hoxd8 and Hoxa7 have complementary sequences with canonical seed matches for miR-196 that mediate translational repression. Although Hoxb8 lacks perfect seed pairing, it has extensive complementarity to miR-196 making it a substrate for cleavage. Furthermore, it could be shown that miR-196 acts upstream of Hoxb8 *in vivo* in the context of hindlimb development. The presented data indicated that the miRNA functions in a fail-safe mechanism acting as an inhibitor of Hoxb8 preventing its induction by ectopic retinoic acid (Hornstein et al., 2005). This supports the idea that many miRNAs in vertebrates may function as a secondary level of gene regulation.

The Hox miRNAs, miR-10 and miR-196a, are encoded at two or three paralogous locations in the Hox clusters (Figure 6).

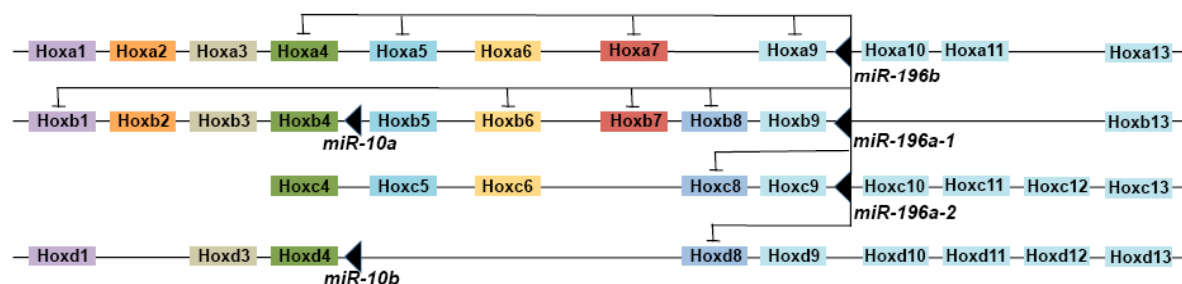


Figure 6: Predicted repression of Hox genes by miR-196. Depiction of the mouse Hox clusters including the Hox miRNAs miR-10 and miR-196. (Adapted from Yekta et al., 2008)

The miRNAs are regulated spatially and temporally like the adjacent Hox genes as has been shown for miR-10a and Hoxb4 or miR-196a and Hoxb8 for mouse embryonic day E10.0 (Mansfield et al., 2004). Interestingly, the members of the miR-196 family have been predicted to target only Hox genes that are located more 3' in the cluster, while leaving unaffected the activity of Hox genes located more 5' in the cluster (Yekta et al., 2008). Thus the genomic organization, the collinear expression and the conserved miRNA-recognition motifs in 3' genomically encoded Hox mRNAs make it likely that these miRNAs shape the boundaries of those Hox proteins. Recently it has been shown that during chick development antagomir-mediated neutralization of miR-196 led to an expansion of the anterior limit of Hoxb8 and thereby induced a cervical to thoracic homeotic transformation (McGlenn et al., 2009).

1.5 Functional protein-RNA interactions

RNA regulatory proteins induce changes in tissue and developmental mRNA profiles. It is challenging to investigate, how these regulatory proteins work in complexes to control the fate of transcribed RNA. New biochemical strategies to map RNA binding protein (RNABP)-RNA interactions *in vivo* are yielding transcriptome-wide insights into mechanisms of RNA processing. In general, researchers wish to distinguish between the primary (direct) and secondary (indirect) effects of RNA regulatory factors. However, it is often hard to distinguish between the direct and indirect consequences of cellular manipulation, because any perturbation in a cell is likely to disrupt the RNA profile. Several approaches have emerged for the biochemical identification of functional RNABP-RNA interactions *in vivo*. These include immunoprecipitation (IP) of the RNA-binding protein followed by purification of the co-precipitating RNA and analysis by RT-PCR or microarrays. The strategy is limited by the need to use relatively low stringency conditions to maintain protein-RNA interaction, so that discrimination between direct and indirect interaction or identification of the RNA-protein-binding site is impossible. Further, co-immunoprecipitation of other RNABPs and RNABP-RNA reassociation *in vitro* cannot be controlled (Licatalosi and Darnell, 2010). An alternative method for identifying regulatory RNABP-RNA interactions is the RNA-immunoprecipitation (RIP) assay, which involves formaldehyde-mediated crosslinking as a first step (Gilbert et al., 2004; Niranjanakumari et al., 2002) (section 2.2.18). This method yields a population

of RNA sequences that are directly bound by the RNABP of interest and consequently allows determining RNABP-RNA interactions occurring in live cells. In the future, the generation of transcriptome-wide maps of functional RNABP–RNA interactions will reveal the rules underlying RNA regulation and networks of biologically linked transcripts.

1.6 The 3' exonuclease Eri1

The *Eri1* (enhanced RNAi-1) gene is conserved from fission yeast to humans. In *C. elegans* two equally abundant splice variants of the *Eri1* gene have been found, *Eri1a* (~1.4 kb) and *Eri1b* (~1.8 kb). In mice and humans only the shorter splice variant (~1.0 kb) has been detected. The mouse *Eri1* gene is encoded on chromosome 8 and is expressed as a 345 amino acid protein.

Analyses of purified recombinant Eri1 proteins expressed from *C. elegans*, *S. pombe*, and human cDNAs have shown that Eri1 degrades single stranded RNA 3' overhangs, but that it is not efficient in degrading RNA duplexes. Single stranded DNAs have also been found to be very poor substrates for Eri1 (Dominski et al., 2003; Iida et al., 2006; Kennedy et al., 2004; Yang et al., 2006). The exonuclease Snipper is a homolog of Eri1 in *Drosophila*, which efficiently degrades structured RNA and DNA substrates as long as there exists a minimum 3' overhang of 2 nt to initiate degradation (Kupsco et al., 2006).

1.6.1 The structure of Eri1

The *Eri1* gene encodes a protein with an amino-terminal SAP (SAF-A/B, Acinus and PIAS) domain and a carboxy-terminal 3' exonuclease domain. The SAP domain, has been defined as sequence of 35 residues containing an invariant glycine and a conserved distribution of hydrophobic, polar and bulky amino acids. It is present in a number of eukaryotic proteins in conjunction with other domains that link these proteins with the RNA or DNA metabolism.

The structure of the nuclease domain of the human Eri1 homolog, called 3'hExo or formerly named THEX1 (Three prime histone exonuclease-1), complexed with rAMP (riboadenine-5'-monophosphate) was determined in the presence of Mg²⁺ ions (Cheng and Patel, 2004) (Figure 7). Ribonucleotide 5'-monophosphates (rNMPs) are the products of the 3'-5' exonuclease hydrolysis reaction and are thus believed to

mimic interactions associated with nuclease activity. The data revealed, that the nuclease domain adopts an α/β globular fold. In the active site of the nuclease domain two magnesium cations are coordinated to D134, E136, D234 and D298, and together with H293 provide a platform for hydrolytic cleavage of bound RNA in the 3'-5' direction. The bound rAMP is positioned within a deep active-site pocket. The nuclease domain is similar to 3' exonucleases of the DEDD-family characterized by the presence of these four invariant acidic amino acids after which the family name has been originated (Zuo and Deutscher, 2001). The DEDD-family includes both DNA- and RNA-specific enzymes.

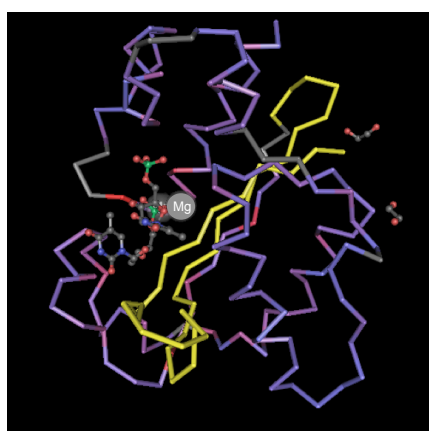


Figure 7: Simplified structure of the mouse Eri1 protein. Red: nuclease domain coordinating two Mg^{2+} ions. Yellow: Exon 3, which has been targeted to create a conditional knockout mouse model. (Adapted from the RCSB Protein Data Bank)

1.6.2 Eri1 and canonical histone mRNAs

1.6.2.1 Eri1 binds to the stem loop of histone mRNAs

The replication-dependent histone mRNAs end with a highly conserved 26-nucleotide sequence that contains a 6-nucleotide stem and a 4-nucleotide loop, followed in vertebrates by an ACCCA sequence (Dominski and Marzluff, 1999). The human Eri1, named 3'hExo, has been shown to bind oligos mimicking this 3' stem loop of canonical histone mRNAs *in vitro* (Dominski et al., 2003). It has further been demonstrated that Eri1 can bind to stem loop-RNA alone or in conjunction with the stem-loop binding protein (SLBP), but SLBP and Eri1 do not directly interact with each other in the absence of stem loop-RNA. Tight binding and sequence-specific recognition of the RNA by SLBP requires the 5' flank of the stem, the two invariant uridines at position 12 and 14 in the loop and the 5 nucleotides 5' to the stem loop region (Battle and Doudna, 2001; Martin et al., 2000; Williams and Marzluff, 1995). In contrast, Eri1 was demonstrated to recognize the 3' flank of the stem, the loop and

the 3' single stranded ACCCA sequence (Dominski et al., 2003). Thus SLBP and Eri1 bind to opposite faces of the histone stem loop (Figure 8).

Furthermore, it was suggested that Eri1 selects histone mRNA targets by sequence-specific binding through its SAP domain. In 2006, the crystal structure of Eri1 in complex with stem loop RNA was solved and suggested that the SAP domain is indispensable for binding to histone RNA (Y. Cheng and D. Patel, submitted to the Protein Data Bank). Functional assays supported these data showing that a SAP domain deletion mutant as well as specific mutations in the SAP domain and the linker sequence abolished binding of Eri1 to stem loop-RNA (Yang et al., 2006).

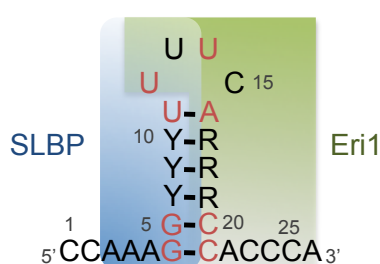


Figure 8: Binding of SLBP and Eri1 to the stem loop structure of the histone mRNAs. Consensus sequence of the 3' end of metazoan histone mRNAs. The absolutely conserved nucleotides are colored red. R and Y denote purine and pyrimidine, respectively. (Adapted from Dominski et al., 2003 and the Eri1 structure at the RCSB Protein Data Bank)

1.6.2.2 Does Eri1 regulate histone mRNAs in a cell cycle dependent manner?

Recombinant Eri1 was shown to degrade stem loop RNA in a 3' to 5' direction, thus it was suggested that Eri1 initiates degradation of histone mRNAs (Dominski et al., 2003). Lately the same group presented data that disproved a role for Eri1 in histone mRNA degradation. They introduced a 80-90% knockdown of Eri1 in Hela cells, but hydroxyurea-induced degradation of replication-dependent histone mRNAs failed to reveal any contribution of Eri1 in the degradation process (Mullen and Marzluff, 2008). A physiological role for Eri1 binding to histone mRNAs in cells therefore remains unclear.

1.6.3 Eri1 and RNA interference

Eri1 has been shown to have an impact on different RNAi and RNAi-related pathways. It is involved in the regulation of exogenous (exo-) siRNAs (Kennedy et al., 2004) as well as endogenous (endo-) siRNAs (Duchaine et al., 2006), and it has been demonstrated to affect heterochromatin formation (Bühler et al., 2006; Iida et al., 2006).

1.6.3.1 Eri1 is a regulator of siRNAs

The *C. elegans Eri1* gene was found in a screen for inhibitors of RNA interference in neurons (Kennedy et al., 2004). It had been shown before that dsRNAs vary in different cell types in their ability to trigger RNA interference; e.g. the nervous system of *C. elegans* is refractory to RNAi. The group of Gary Ruvkun discovered that worms with *Eri1* mutations accumulated more siRNAs after exposure to dsRNA or siRNAs than did wildtype animals. Thus it was proposed that Eri1 is a negative regulator of RNAi, which normally functions to limit duration, cell-type specificity or endogenous functions of RNAi. It was further suggested, that Eri1 inhibits RNAi by degrading the 3' overhangs of siRNAs and thereby makes them fail to enter the RNAi-induced silencing complex (RISC) or alternatively that the 3' recessed siRNAs may be unstable *in vivo*. In agreement with a decreased efficiency of RNAi in neurons, the Eri1b form fused to GFP was seen in a subset of neurons. In these neurons, Eri1 predominantly localized to the cytoplasm. Eri1 was further found to be expressed in the developing somatic gonad and the spermatheca of adult worms (Kennedy et al., 2004).

In addition to down-regulating the response to exogenous siRNAs, Eri1 was shown to be required for the production of several endogenous siRNAs in *C. elegans*. The pathways for exo-siRNA and endo-siRNA use in part separate enzymes while sharing others including Dicer (DCR-1) (Lee et al., 2006). Mass spectrometry data of Dicer immunoprecipitations revealed that Eri1b exists in a complex with DCR-1 and functionally both proteins were required for the generation of endogenous siRNAs in *C. elegans* (Duchaine et al., 2006). In the new model Eri1 binds to short stem loops in a group of endogenous RNAs, which causes the removal of unpaired 3' nucleotides. Thus a structure is generated that can prime an RNA-dependent RNA polymerase for the synthesis of double stranded RNA species. These RNAs will subsequently be cleaved by DCR-1 and introduced into the RNAi-pathway. If Eri1 is deleted, the proposed pathway for endogenous siRNA production cannot take place any more. Consequently, the Eri1 phenotype might be caused by the release of limiting components from the endogenous to the exogenous RNAi pathway in these mutants. Therefore, exogenous siRNAs show an increased effect in worms with Eri1 mutation.

1.6.3.2 Regulation of heterochromatin assembly by Eri1

Eri1 has also been shown to be an important regulatory factor in RNAi-mediated heterochromatin assembly. In fission yeast, heterochromatin assembly is initiated by siRNAs derived from heterochromatic regions and it requires the RNA-induced transcriptional silencing (RITS) complex (Cam and Grewal, 2004; Cam et al., 2005; Verdel et al., 2004; Volpe et al., 2002). Deletion of *Eri1* caused an increase in siRNAs associated with the RITS complex and therefore enhanced heterochromatin silencing (Iida et al., 2006). Furthermore, it has been shown that *de novo* silencing mediated by siRNAs is under a strong negative control by Eri1. Eri1 interfered with heterochromatin assembly *in trans*. Hence, deletion of *Eri1* allowed siRNAs to silence the expression of a second allele, which was located on another chromosome in an experimental RNAi-induced gene silencing in *S. pombe* (Bühler et al., 2006).

1.7 Aim of the work

The primary aim of the present work was to functionally characterize the impact of mouse Eri1 on RNA target molecules and to analyze the consequence of *Eri1*-deletion in mice. Only two RNA target molecules have been proposed for Eri1 so far. It has been shown that human Eri1 binds to histone mRNA *in vitro* (Dominski et al., 2003; Yang et al., 2006), but the physiological role remained unclear. Further, Eri1 was reported to be a regulator of siRNA-mediated RNAi in *C. elegans* and in fission yeast (Bühler et al., 2006; Duchaine et al., 2006; Iida et al., 2006; Kennedy et al., 2004). A possible function for Eri1 on miRNAs in the mammalian system has not been described yet.

RIP is the method of choice to reveal functional protein-RNA interactions *in vivo*. Hence this method should be established and applied to find RNA target molecules of Eri1. Further, binding specificity should be analyzed employing Eri1-mutants. Since RNAs identified in the RIP assay directly bind to Eri1, they are possible targets for its exonuclease activity. This should be analyzed in functional assays. A systematic screen in cooperation with the German Mouse Clinic should be accomplished to reveal phenotypes of *Eri1*-knockout mice. One prominent phenotype should subsequently be studied for its underlying molecular mechanism.

2 Material and methods

2.1 Material

2.1.1 Chemicals and biochemicals

Chemical	Company
Ampicillin	Roche
Biozym DNA Agarose	Biozym Scientific GmbH
BSA (Albumin Fraktion V)	Roth
Chloroform min. 99%	Sigma-Aldrich
Deoxynucleotide (dNTP) set	Fermentas
Dimethyl sulfoxide (DMSO)	Sigma-Aldrich
Dynabeads MyOne Tosylactivated	Invitrogen
Dynabeads Protein G	Invitrogen
Ethidium bromide 1% (w/v)	Serva
Glycogen blue	Ambion
Hydroxyurea	Sigma
Kanamycin sulfate	Roth
Milk powder	Roth
Paraformaldehyde	Sigma-Aldrich
1 kb Plus DNA Ladder	Invitrogen
Tri@Reagent	Invitrogen
0.05% Trypsin/ 0.02% EDTA in PBS	Pan biotech GmbH
Trypton	Merck
Tween 20	Applichem
Urea	Applichem
Yeast extract	Serva
β -Mercaptoethanol 99%	Sigma-Aldrich

2.1.2 Enzymes

Enzyme	Company
Gateway LR Clonase II Enzyme Mix	Invitrogen
Herculase® II Fusion DNA Polymerase	Stratagene
Proteinase K	Invitrogen
Restriction enzymes	New England Biolabs
T4 DNA Ligase (10,000 U/ml)	New England Biolabs
Taq Polymerase (5,000 U /ml)	Invitrogen
Taq Polymerase (5,000 U /ml)	New England Biolabs
Topoisomerase I (<i>E. coli</i>) (5.000 U/ml)	New England Biolabs

2.1.3 Kits

Kit	Company
TOPO TA Cloning Kit	Invitrogen
pENTR/D-TOPO Cloning Kit	Invitrogen
pCR8/GW/TOPO TA Cloning Kit	Invitrogen
Nucleobond®Xtra Maxi Kit	Macherey-Nagel GmbH & Co. KG
pENTR/D-TOPO Cloning Kit	Invitrogen
peqGOLD Plasmid Miniprep Kit I	PeqLab Biotechnologie GmbH
QIA®PCR purification Kit	Qiagen
QIA®quick gel extraction Kit	Qiagen
QuickChange	Stratagene
TaqManMicroRNA Assay	Applied Biosystems
Universal Probe Library	Roche
ViraBind Adenovirus Miniprep Kit	Cell Biolabs Inc.

2.1.4 Solutions

Standard Solutions	Composition
20x SSC	3M NaCl 0.3 M Sodium citrate, pH=7.0
10x PBS	137 mM NaCl 27 mM KCl 100 mM NaH ₂ PO ₄ 17 mM KH ₂ PO ₄ dissolve in ddH ₂ O
5x Loading buffer	100 mM EDTA 30% (v/v) Glycerine 0.25% (w/v) Bromophenolblue dissolve in ddH ₂ O
10x TE	100 mM Tris/HCl pH 8.0 10 mM EDTA, pH=8.0
5x TBE	0.445 M Tris-Borat, pH=8.0 10 mM EDTA, pH=8.0
20% SDS	20% SDS (w/v) dissolve in ddH ₂ O

Western blot solutions	Composition
RIPA buffer	20 mM Tris-HCl, pH 7.5 250 mM NaCl 10 mM MgCl ₂ 1% NP-40 0.1% SDS 0.5% Na-desoxycholate 1 mM DTT complete protease inhibitor cocktail tablet (Roche)/50 ml

4x SDS sample buffer	200 mM Tris/HCl pH=6.8 8% w/v SDS 4% Glycerol 0.1% w/v Bromphenol blue 10% v/v β -Mercaptoethanol
5x SDS-PAGE running buffer	25 mM Tris-Base 200 mM Glycine 10% (w/v) SDS ddH ₂ O
1x Western blot buffer	25 mM Tris-Base 192 mM Glycin 20% v/v Methanol pH=8.4
1x TBS-T	20 mM Tris-Base 137 mM NaCl 3.8 ml 1M HCl 0.1% (v/v) Tween 20 dissolve in 1l ddH ₂ O
APS	10% APS w/v in ddH ₂ O

2.1.5 Vectors

For the generation of most expression constructs the Gateway system (Invitrogen) was used. Therefore the expression plasmids first had to be converted into gateway destination vectors via ligation of the gateway cassette behind the respective promoter. The open reading frame of the gene of interest was PCR amplified and cloned into one of the so-called entry-plasmids (pENTR11, pENTR-D Topo, pCR8-GW), which contain a gateway cloning cassette. For some applications a myc- or eGFP-tag was added to the cloning cassette. Point mutations were introduced into the gene of interest via site-directed mutagenesis with the Quickchange kit (Stratagene) (section 2.2.1.3). Finally, recombination reactions from the entry-plasmids into expression plasmids were performed with the LR clonase kit (Invitrogen) (section 2.2.1.8).

2.1.5.1 Entry-plasmids

Table 1: Entry-plasmids for LR reactions into expression plasmids.

Entry plasmid	Insert	Tag
pENTR11	Eri1 wildtype	myc, eGFP
pENTR11	Eri1 A176D	myc, eGFP
pENTR11	Eri1 R101A	myc, eGFP
pENTR11	Eri1 K107A K108A	myc, eGFP
pENTR11	Eri1 D130G E132G	myc, eGFP
pENTR11	Eri1 N96A K107A	myc, eGFP

pENTR11	Eri1 delta N	myc, eGFP
pENTR11	Eri1 SAP only	myc, eGFP
pENTR11	attL sites without ccdb gene	no tag
pCR8 GW-TOPO	eGFP	no tag
pENTR-D Topo	pri-miR-196a	no tag
pENTR-D Topo	pri-miR-150	no tag
pENTR-D Topo	Hoxc8 3' UTR	no tag
pENTR-D Topo	Hoxc8 3' UTR/miR-196a sites mutated	no tag

Mouse Eri1 cDNA (NM_026067) was PCR amplified from IMAGE clone 5354985. The primers for site-directed mutagenesis are listed in section 2.1.6 and the point and deletion mutants are shown in figure 2-1.

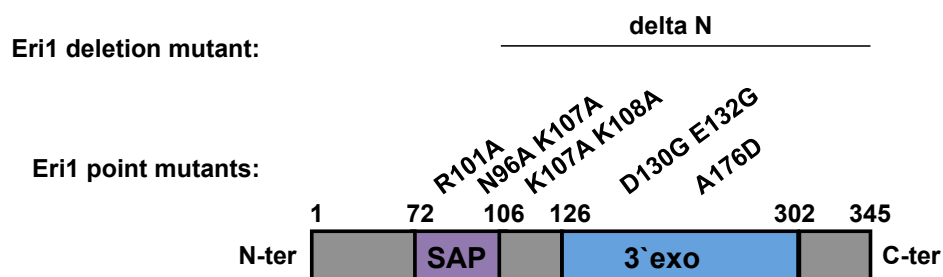


Figure 9: Schematic depiction of the structure of Eri1 and the employed point and deletion mutants.

The pri-miRNAs, pri-miR-196a and pri-miR-150, have been amplified from mouse genomic DNA (C57BL/6 mouse strain) with the primers listed in section 2.1.6, to get a 702 bp fragment in the case of miR-196a and a 725 bp fragment in the case of miR-150.

Hoxc8 3' UTR was also amplified from mouse genomic DNA (C57BL/6 mouse strain). For the Hoxc8 3' UTR/miR-196a sites mutated construct, all four conserved miR-196a binding site sequences have been mutated (actaCCt>actaAAt) within the seed sequence. Primers for the amplification and the four site-directed mutagenesis reactions are listed in section 2.1.6.

2.1.5.2 Expression plasmids

pMSCV-puro and pLNCX2 are retroviral expression plasmids from Clontech, that were converted into gateway destination vectors via ligation of the gateway cassette.

Recombination reactions of Eri1 wildtype, point and deletion mutants as well as control sequences were performed into the pMSCV-puro, pLNCX2 and pDest12.2 (Invitrogen) using the LR clonase kit.

The adenoviral pCAGAdDu plasmid was constructed by insertion of a gateway cassette, an internal ribosome entry site (IRES), the open reading frame of green fluorescent protein (GFP) and the bovine growth hormone polyadenylation sequences in the context of a CMV early enhancer and chicken beta-actin (CAG) promoter. The sequences for Eri1 wildtype, Eri1 D130G E132G, pri-miR-196a and pri-miR-150 were inserted by LR reaction.

2.1.5.3 Plasmids for dual luciferase assay

The pAdpsiCHECK2 adenoviral plasmid for the dual luciferase activity assays was cloned based on the psiCHECK2 dual luciferase construct (Promega), in the context of an adenoviral backbone of pAd-PI (Invitrogen). A gateway cassette was placed between the renilla luciferase open reading frame and the polyadenylation signal. The sequences for Hoxc8 3' UTR or Hoxc8 3' UTR/miR-196a sites mutated (actaCct>actaAAt) were inserted by LR reaction. For the control reporter the gateway cassette was deleted.

2.1.5.4 Plasmids for knockdown experiments

For knockdown experiments a mouse Eri1 specific sequence (si6: ggatggatgtgaacttcca) was cloned into the pSUPER-puro retroviral vector from R. Agami (The Netherlands Cancer Institute, Amsterdam, The Netherlands) (Brummelkamp et al., 2002). For the control vector a scrambled DNA sequence was cloned.

2.1.5.5 Additional constructs

The large T-plasmid for the immortalization of MEF cells was kindly provided by W. Hammerschmidt (HelmholtzZentrum München, Germany).

For the production of retroviruses, amphotropic packaging plasmids were co-transfected with the respective expression plasmids.

2.1.6 Oligonucleotides

Table 2: Oligonucleotides, synthesized by the company METABION.

Labeling	Sequence (5'-3')	Application
MEXO A	gggtggtatatcctcagttacttttg	Mouse genotyping of the Eri1 fl/fl allele
MEXO B	gccataaccttgaacctgca	
MEXO C	gcaacccgaggtaaaaggag	
del Cre for	gaaagtcgagtaggcgtgtacg	Mouse genotyping of the deleter Cre allele
del Cre rev	cgcataaccagtgaacacgcat	
eGFP NcoI for	gagaccatggtgagcaagggcgagg	eGFP tag/ eGFP control
eGFP Sall rev2	gagagtcgacccttgtacagctcgtccatg	
eGFP STOP rev	ttactgtacagctcgtccatg	
rfa XhoI for	tgctcggagatcacaagttgtacaaaaaagc	Introduce gateway cassette into pAdpL
rfa PmeI rev	tgcgttaaacatcaccactttgtacaagaagc	
BglII-ClaI-BglII oligo	gatccatcgatg	ClaI site linker to clone pSiCHECK2 into pAdpL
Test-LR pAdpSiCHECK2 for	cggtgctgaagaacgagcagt	Sequence insert in pAdpSiCHECK2
M13 for	tgtaaaacgacggccagt	Sequence insert of a Gateway plasmid
M13 rev	caggaaacagctatgacc	
mExo aa 101 for	gtcaaggatgttctaagaaggcactgaaaaact attacaagaagc	Quick change Eri1 R101A
mExo aa 101 rev	gcttctgtataacttttctcagtccttcttagaacatc cttgac	
mExo aa 107/8 for	aaactattacgcgcgagcaagttgatgctgaaa gagagctccgc	Quick change Eri1 K107A K108A
mExo aa 107/8 rev	gcgagctctctttcagcatcaacttctgcgcccgcg taatagttt	
mExo aa 176 for	ggccagaagtcaatgatcagcttcagagttatgc	Quick change Eri1 A176D
mExo aa 176 rev	gcagaactctgaaagctgatcattgactctggcc	
Hoxc8UTR for	cacaaaagagagagaaaatcagccc	PCR on mouse gDNA to clone the Hoxc8 UTR
Hoxc8UTR rev	aattctttttttattatgactcagc	
Hoxc8-mut196asite1 for	gacactcacaactctaactaaatgacagatagttgc agctctg	Quick change on Hoxc8 UTR to mutate miR-196a binding site 1
Hoxc8-mut196asite1 rev	cagagctgcaactatctgacatttagtaggttg agtgc	
Hoxc8-mut196asite2 for	ataaatcttaacataactaaataaagggaaacctgc aataatctggggg	Quick change on Hoxc8 UTR to mutate miR-196a binding site 2
Hoxc8-mut196asite2 rev	cccccaagattatgcaggttccctttatttagtatgtt aaagatttat	
Hoxc8-mut196asite3 for	cctccagcgtattttatcactaaatagaaagaaa tctgctttgag	Quick change on Hoxc8 UTR to mutate miR-196a binding site 3
Hoxc8-mut196asite3 rev	ctcaaagcaggatttcttctatatttagtgataaaat acgctggagg	
Hoxc8-mut196asite4 for	cccaacaactgagactgaatagcccgcggtct	Quick change on Hoxc8 UTR to mutate miR-196a binding site 4
Hoxc8-mut196asite4 rev	agaccggcgggctattcagctcagttgttggg	
Pri-miR-196a for	cacctgctgagaggccaagtaggt	PCR on mouse gDNA to

Pri-miR-196a rev	cctacaacccaaaggcttga	clone pri-miR-196a
Pri-miR-150 for	caccaggggaagtgctaggct	PCR on mouse gDNA to clone pri-miR-150
Pri-miR-150 rev	gttgagtgatgggaacacc	
RT-PCR 5ETS for	gagaggtgctggagagctgt	(Semi-) quantitative PCR for mouse rRNA
RT-PCR 5ETS rev	ggcggagagcctcgcg	
RT-PCR 18S for	cgctgagaagacggtcgaac	(Semi-) quantitative PCR for mouse rRNA
RT-PCR 18S rev	cacctgctccacacgcg	
RT-PCR 5.8S for	gtggatcactcggctcgt	(Semi-) quantitative PCR for mouse rRNA
RT-PCR 5.8S rev	agtgcgttcgaagtgtcgt	
RT-PCR ITS-2 for	ggagagcgagggcgagaac	(Semi-) quantitative PCR for mouse rRNA
RT-PCR ITS-2 rev	gggtgaaggagaagcggagac	
RT-PCR 28S for	cggctgggcgctgtc	(Semi-) quantitative PCR for mouse rRNA
RT-PCR 28S rev	gttactcgccgttactgagg	
RT-PCR 3ETS for	gtgtgggagcctcgtgcc	(Semi-) quantitative PCR for mouse rRNA
RT-PCR 3ETS rev	gatcccaccgtcggtcacc	
RT-PCR out 3ETS for	ggcgggctcactctggac	(Semi-) quantitative PCR for mouse rRNA
RT-PCR out 3ETS rev	gacatctggtcgacctctgcg	
RT-PCR 5S for	gtctacggccataaccacctg	(Semi-) quantitative PCR for mouse rRNA
RT-PCR 5S rev	gcctacagcaccgggtattcc	
h5ETS for5	gttcgtgtgtgggtgactt	(Semi-) quantitative PCR for human rRNA
h5ETS rev5	gcggtacgaggaaacacct	
h18S for 1	aaacggctaccacatccaag	(Semi-) quantitative PCR for human rRNA
h18S rev 1a	cctccaatggatcctcgta	
hITS-1 for	cgggtgggggctttac	(Semi-) quantitative PCR for human rRNA
hITS-1 rev	gtcgaaggttcacaccac	
h5.8S for2	gactcttagcggatgactc	(Semi-) quantitative PCR for human rRNA
h5.8S rev2	gacgctcagacaggcgtag	
h28S for	tcagcggaggaaaagaaact	(Semi-) quantitative PCR for human rRNA
h28S rev	gcctcgatcagaaggacttg	
h3ETS for2	ccttctcggtcttgagact	(Semi-) quantitative PCR for human rRNA
h3ETS rev2	gcagacgccggctaagt	
qmExos	cggctcagcagactcaaaca	Light cyclor qPCR
qmExoas	ggccgtccatcataatccat	
Hist2h4 for	ccagctggtgtttcagattaca	Light cyclor qPCR with probe #6 (UPL)
Hist2h4 rev	accctgcctagacccttc	
UPL-Hoxc8 for	catgccagcatacactctc	Light cyclor qPCR with probe #15 (UPL)
UPL-Hoxc8 rev	atagggattaaataggaactccttctc	
UPL-Hoxb8 for	cagctcttccctggatgc	Light cyclor qPCR with probe #1 (UPL)
UPL-Hoxb8 rev	atagggattaaataggaactccttctc	
UPL-2 pri-miR196a for	gcggacctctgttaggaaaa	Light cyclor qPCR with probe #6 (UPL)
UPL-2 pri-miR196a rev	gctaaaatggccacgcaat	
PBGD F	cagtgatgaaagatgggcaac	Light cyclor qPCR with probe #22 (UPL)
PBGD R	aacagggacctggatggtg	
HPRT1 F	tgatagatccattcctatgactgtaga	Light cyclor qPCR with probe #95 (UPL)
HPRT1 R	aagacattcttccagttaaagttag	

2.1.7 Antibodies

Antibody	Company
Monoclonal anti-Eri1 (5G8-111, 5G8-112)	HMGU monoclonal antibody facility
Polyclonal anti-Eri1 (A28)	Millbrook
Monoclonal anti-Hoxc8 (C952-12E)	Covance
Polyclonal anti-GFP (A11122)	Invitrogen
Monoclonal anti-c-Myc (9E10)	Abcam
Monoclonal anti-alpha tubulin (5-B-1-2)	Santa Cruz Biotechnology
Monoclonal anti-rat IgG1 (Tib-170)	HMGU monoclonal antibody facility

2.1.8 Cell culture

2.1.8.1 Cell medium

Medium and Additive	Company
Dulbecco's Modified Eagle Medium (DMEM)	Gibco, Invitrogen
Fetal Calf Serum (FCS)	BioWhittaker, Lonza
HEPES (1 M)	Gibco, Invitrogen
PenStrep (10 000 U/ml)	Gibco, Invitrogen

2.1.8.2 Cell lines

The human embryonic kidney cell lines (HEK293A and HEK293gag/pol) were purchased from ATCC as well as the human lung adenocarcinoma epithelial cell line (A549).

Primary or immortalized mouse embryonic fibroblast cells (MEF cells) were produced from NMRI x C57BL/6 wildtype and Eri1-knockout embryos or C57BL/6 wildtype and Dicer^{fl/fl} embryos, respectively (section 2.2.5).

2.1.9 Mice

BALB/c, NMRI and C57BL/6 mice were obtained from Taconic or Jackson Laboratories. C57BL/6 Eri1^{fl/fl} (the exon 3 of the Eri1 gene is flanked by LoxP sites, 'floxed') mice were bred with CMV-Cre transgenic mice (6.C-Tg(CMV-cre)1Cgn) to obtain C57BL/6 Eri1^{fl/fl} x del Cre mice for the generation of *Eri1*-knockout mice.

2.1.10 Instruments

Device	Official name and Company
Accuracy weighing machine	KERN ABJ-220-4M (Kern und Söhne GmbH) KERN EW 220-3NM (Kern und Söhne GmbH)
Agarose gel chambers	Peqlab Biotechnologie GmbH
Bacterial incubator	Brutschrank BINDER BF 53 (Binder Labortechnik) Innova 4400 incubator shaker (New Brunswick Scientific GmbH)
Blotting chamber	BioRad
Centrifuges and Rotors	Beckman Coulter Avanti-J-26XP (Beckman Coulter) JS-7.5 Swinging-Bucket Rotor (Beckman Coulter) JA-10 Rotor, Fixed Angle (Beckman Coulter) Allegra®X-12R Centrifuge (Beckman Coulter) Rotor FX 6100 (Beckman Coulter) Rotor SX 4750 (Beckman Coulter)
CO ₂ incubator	Forma Direct Heat CO2 Incubator HEPA Class 100 (Thermo Electron Corporation)
Coasting mixer	Tube Roller-Mixers, SRT1 (Stuart) (ScienceLab)
Confocal microscope	Type: 301-185.104-000 Order-No: 500277 (Leica)
Energy supplier	Stromgeber EC105 (Thermo Electron Corporation) BioRad energy supplier (BioRad)
FACS machine	BD FACS Calibur Flow Cytometer (BD Biosciences)
Fluorescence microscope	Axiovert 200M (Zeiss)
Gel documentation	(Peqlab Biotechnologie GmbH)
Ice machine	Scotsman AF 200 (Scotsman Icesystem)
Luminometer	Orion Microplate Luminometer, Berthold Detection systems
Magnet stirrer	RCT basic safety control (IKA)
Microscope	Axiovert 40C (Zeiss)
Microwave	Bosch
pH meter	pH-Meter inoLab® pH 720 (Wissenschaftlich Technische Werkstätten)
Protein gel chamber	BioRad
Spectro photometer	Eppendorf BioPhotometers (Eppendorf) Thermo Scientific NanoDrop™ 1000 Spectrophotometer (Thermo Fisher Scientific Inc.)
Sterile-working bench	BDK, Luft und Reinraumtechnik
Table centrifuge	Centrifuge 5415D (Eppendorf) Centrifuge 5417R (Eppendorf)
Thermo cycler	Biometra TGradient Thermal Cycler 96 (Biometra) DNA Engine 48/48 Dual Alpha Unit With Two Heated Lids (BioRad) Light Cycler 480II (Roche)
Thermo mixer	Thermomixer compact (Eppendorf) Thermomixer comfort (Eppendorf)
UV-lamp	Transilluminator model. TS-40 (Ultra-Violet Products Ltd.)
Vortexer	Vortex Genius 3 (IKA)
Waterbath	WB7 (Mettler)

2.2 Methods

2.2.1 Molecular biological standard methods

2.2.1.1 Bacterial culture

Chemical competent *E. coli* DH5alpha bacteria (Invitrogen) were used to amplify plasmid DNA. The transfer of plasmids into bacteria requires that the cell membrane is permeable for the plasmids, which is achieved by a short time heat incubation at 42°C. 50 µl of *E.coli* bacteria were thawed on ice, mixed with the plasmid DNA and incubated for 30 min on ice. For the plasmid uptake, the bacteria were placed into a 42°C waterbath for 45 s and briefly equilibrated on ice. 250 µl of LB medium was added and cells were incubated for 1 h at 37°C while shaking (600 rpm). The suspension was plated onto LB-agar plates containing the respective antibiotic. LB plates were incubated over night at 37°C. Single colonies were selected for downstream applications. For storage, single colonies were scraped off the LB agar plates and a fresh overnight bacterial culture was stored at -80°C, mixed at an 1:1 ratio with glycerol. LB media and LB agar were prepared with 'ready to mix'-powder (SERVA), supplemented with ampicillin (100 µg/ml), spectinomycin (50 µg/ml) or kanamycin (30 µg/ml) for selection of bacterial resistance.

2.2.1.2 PCR reaction

Cyclic reaction series of denaturation, reannealing of forward and reverse primer and polymerization with a thermostable DNA polymerase allow the *in vitro* amplification of DNA (Saiki et al., 1988). A standard PCR reaction, e. g. for the genotyping of mice, contained: 150 ng DNA template, 0.5 µl of 100 pmol/µl forward primer, 0.5 µl of 100 pmol/µl reverse primer, 1 µl dNTP-mix (5 mM each), 2.5 µl 10x PCR Rxn Buffer, 1 µl 50 mM MgCl₂ and 0.5 µl (5 Units) Taq DNA polymerase (Invitrogen). The mixture was filled up with ddH₂O to a volume of 25 µl. Cycling reactions were: 95°C for 3 min; 31 cycles of 95°C for 15s, 58°C for 30s, 72°C for 60 s, 72° for 10 min, hold at 4°C. A minimum of 15 µl of the PCR reaction was analyzed on an agarose gel.

2.2.1.3 Site-directed mutagenesis

In vitro site-directed mutagenesis is a technique for studying protein structure-function relationships. The Quik Change site-directed mutagenesis kit (Stratagene) is

used to make point mutations, switch amino acids, and delete or insert single or multiple amino acids. The basic procedure utilizes a dsDNA vector with the insert of interest and two synthetic oligonucleotide primers containing the desired mutation. The Quik Change primers, listed in section 2.1.6, were chosen according to the manufacturer's protocol. The reaction mix was prepared and the oligonucleotide primers extended during temperature cycling by PfuTurbo DNA polymerase. After amplification, the PCR product was *DpnI* digested for one hour to degrade the methylated and hemimethylated parental template. Then 5 µl of the PCR product were transformed into competent DH5alpha bacteria. One of the resulting colonies was selected for sequencing.

2.2.1.4 Vector restriction enzyme digests

Digests were carried out in 20 µl volume with a DNA content of 1 µg for 1 h with 5 U of each enzyme. For digestions over night, a minimum volume of at least 50 µl is recommended. For digests of the pCAGAdDU adenoviral vector, 20 µg vector were digested over night at 37°C using 30 U of the restriction endonuclease *PacI*.

2.2.1.5 PCR purification and gel extraction

PCR product purification was performed using the QIAquick PCR Purification Kit according to the manufacturer's protocol (Qiagen). In cloning approaches, the restriction digested vector was separated in a 1% agarose gel containing ethidium bromide. Under 254 UV nm light, vector and insert bands were carefully cutted out and extracted from the agarose gel using the QIAquick Gel Extraction Kit according to the manufacturer's protocol (Qiagen).

2.2.1.6 Annealing of oligonucleotides

To obtain a double stranded DNA oligonucleotide linker for the conversion of a *Bgl* II restriction site into a *Cla* I restriction site in the psiCHECK2 vector, sense and antisense oligonucleotides were annealed. The oligonucleotides were dissolved in nuclease free water to a concentration of 100 pmol/µl. For annealing of the oligonucleotides, 25 µl of each oligonucleotide were added to 150 µl annealing buffer (50 mM Tris pH 8.0, 70 mM NaCl), and incubated 15 min at 95°C, then slowly cooled down to 4°C reducing the temperature every 30 s by 0.5°C in a PCR machine.

2.2.1.7 Ligation of DNA fragments

For the ligation of the digested vector with an insert, the fragments were incubated with T4 DNA ligase (New England Biolabs) at RT for 1 h according to the manufacturer's protocol. For the ligation of plasmids with more than 20 kb, the reaction was done at 16°C overnight.

2.2.1.8 Lambda recombination reaction

Gateway is a universal cloning technique based on the site-specific recombination properties of bacteriophage lambda. The Gateway LR Clonase enzyme mix contains a proprietary blend of Int (Integrase), IHF (Integration Host Factor) and Xis (Excisionase) enzymes that catalyze the *in vitro* recombination between an entry-plasmid (containing a gene of interest flanked by attL sites) and a destination vector (containing attR sites) to generate a new expression plasmid. Only destination vectors that have recombined are selected. This is ensured by differences in antibiotic resistance between the destination and the entry vector and the expression of a death gene (*ccdB*) in clones that have not recombined. LR reactions were carried out according to the manufacturer's protocol, using 150 ng entry-plasmid and 150 ng destination vector.

2.2.1.9 Trizol RNA extraction

RNA was extracted from cells, immunoprecipitation samples, or embryos by mixing with 1 ml of Trizol (Invitrogen) according to the manufacturer's protocol. Shortly, the contents were mixed with 200 µl chloroform and incubated at RT for 2 min. The organic and aqueous phases were separated by centrifugation at 12,000g for 15 min at 4°C. The aqueous phase was collected and subjected to isopropanol precipitation in the presence of 1 µl glycoblue-carrier (Ambion) for 10 min at RT. RNA precipitates were collected by centrifugation at 12,000g for 10 min at 4°C, washed with 75% ethanol, air-dried and resuspended in 20 µl RNase-free water.

2.2.1.10 Reverse transcriptase reaction

Genomic DNA elimination and reverse transcription of RNA was done according to the QuantiTect Reverse Transcription Kit (Qiagen). 1 µg Trizol-purified RNA was incubated in gDNA 'wipeout buffer' at 42°C for 2 min. For the reverse transcription a mix prepared from Quantiscript Reverse Transcriptase, Quantiscript RT Buffer, and

3 µg Random Primers (Invitrogen) was used. The entire reaction took place at 42°C for 15-20 min and was then inactivated by incubation at 95°C for 3 min.

2.2.1.11 Acrylamide-Urea RNA gels

RNA was extracted using Trizol reagent (Invitrogen) and resuspended in RNase free water (section 2.2.1.9). 5 µg RNA were vacuum dried and resuspended in 2x loading buffer (RNA Loading Buffer PA, BioDynamics Laboratory Inc.). Samples were separated on 7% acrylamide, 8 M urea gels (24.04 g Urea, 11.8 ml 30% acrylamide, 5 ml 10x TBE, 25 µl TEMED, 250 µl 10% APS, a.d. 50 ml with water) in 1x TBE buffer and visualized by ethidium bromide staining.

2.2.2 Breeding and genotyping of mice

BALB/c, NMRI and C57BL/6 mice were housed in a specific pathogen-free barrier facility. For genotyping the tip of the mouse tail was lysed in 200 µl genotyping buffer (100 mM Tris-HCl, pH 8.5, 5 mM EDTA, 0.2% SDS, 200 mM NaCl, 0.2 mg/ml proteinase K) by incubation overnight at 800 rpm at 55°C. The Proteinase K was heat-inactivated at 95°C for 15 min the next day. 300 µl of water were added and 0.4 µl were used as template for the genotyping-PCR (section 2.2.1.2). To genotype embryos, the yolk sac was lysed in 100 µl genotyping buffer and 0.4 µl of undiluted sample were taken for PCR amplification.

2.2.3 Preparation of embryos

For the preparation of embryos, breeding pairs were caged together in the late afternoon and the females were examined for the presence of vaginal plug on the following morning, which was defined as 0.5 day post coitum (dpc). Pregnant females were sacrificed at the required gestational stages and embryos were dissected free of maternal and extraembryonic tissue in PBS. Embryo genotypes were determined by PCR (section 2.2.2).

2.2.4 Generation of mouse embryonic fibroblasts

For cell culture experiments, mouse embryonic fibroblasts (MEF) were generated from *Eri1*-knockout, *Eri1*-heterozygous, wildtype and *Eri1*^{fl/fl} (the exon 3 of the *Eri1* gene is flanked by LoxP sites, 'floxed') embryos at 12.5 dpc or 13.5 dpc. The trunk of the embryos excluding the head was sliced into very small pieces, incubated with

trypsin for 2 min and then cultivated in normal MEF cell medium (section 2.2.5). Cells were directly taken into experiments where primary MEF cells were required, i.e. the cell screen experiment. For other experiments, the cells were immortalized via ecotropic retroviral infection with an SV40 large T antigen plasmid followed by hygromycin selection at 100 µg/ml for two weeks. These MEF cells could then be expanded in cell culture and be infected with retroviruses and adenoviruses.

2.2.5 Cell culture

HEK293 cells and MEF cells were grown in Dulbecco's modified Eagle's medium (DMEM). The medium was supplemented with 10% fetal calf serum (FCS), 10 mM HEPES and 100 mg/ml penicillin/streptomycin. Cells were cultured at 37°C in a 5% CO₂ humidified incubator. Stocks from cell lines were stored in liquid nitrogen in a mixture of 90% FCS and 10% DMSO in NUNC-freezing tubes. The cells were first placed into a -80°C freezer to slowly cool down. The next day, the cells were transferred into a liquid nitrogen container for long-time storage.

2.2.6 Transfection of cells

HEK293A or HEK293gag/pol cells were split to about 60-80% confluency at least 6 hours prior to transfection. For one cell culture dish (92 x 17 mm) a mixture of 10 µg virus construct and 50 µl cold 2 M CaCl₂ was filled up with sterile water to 500 µl total volume and then added drop-wise to 500 µl 2 x HBS (For 500 ml: 8.0 g NaCl, 6.5 g HEPES, 10 ml Na₂HPO₄ (Na₂HPO₄ stock solution: 5.25 g Na₂HPO₄ in 500 ml water), pH 7.0) on a vortexer. For retrovirus production amphotropic packaging vectors (1 µg amphi-env construct and 1 µg gag/pol construct) were added to the transfection mixture. After 15 min incubation time at RT the co-precipitates of DNA and calcium phosphate were added to the HEK293 cells. The next day the medium was replaced with fresh medium. Transfected cells were analyzed or kept in culture if used for adenovirus- or retrovirus-production.

2.2.7 Infection of cells with adeno- and retroviruses

Type 5 replication-deficient adenoviruses were produced from *PacI*-digested adenoviral vectors. The vectors were transfected into HEK293A cells using the calcium phosphate method (section 2.2.6). In a second round of infection the viruses were amplified in HEK293A cells and viral stocks were purified using mini columns

according to the manufacturer's instructions (Cell Biolabs). Titers were determined in A549 cells by FACS approximately 40 h after infection. MEF cells were infected with adenoviruses at a multiplicity of infection (MOI) of 10-1000. Importantly, an MOI of 50 of the pCAGAdDU-virus was needed to reconstitute MEF cells to about endogenous levels of Eri1 expression.

Retroviral supernatants were produced by calcium phosphate transfection of amphotropic packaging vectors and retroviral expression vectors in HEK293gag/pol cells. Supernatants were collected 48-72 h post transfection, passed through 0.45 μ m filters, mixed with polybrene at a final concentration of 5 μ g/ml and added to the MEF cells. The medium was replaced the next day and infected MEF cells were analyzed two or three days after.

2.2.8 Flow cytometry analysis

Flow cytometry (FCM) analysis is a method that can be used for measuring the number of virus-infected cells in a cell sample and the level of infection. Therefore a fluorescent marker, i.e. GFP, is co-expressed with the gene of interest either as a tag or after an IRES sequence. For FCM infected MEF or A549 cells were scraped off the plates and analyzed in a 1:4 dilution of trypsin in PBS. FCM was performed on a FACS Calibur device (Becton Dickinson) and raw data were analyzed with Flow Jo (Treestar) software.

2.2.9 Hydroxyurea treatment of cells

Hydroxyurea (HU) is used for cell cycle related studies, because it is a potent inhibitor of DNA synthesis and depletes the cellular deoxyribonucleotide pool through inhibition of ribonucleotide reductase. Through this pharmacological treatment the situation in the cell at the end of S-phase is simulated. MEF cells were incubated for 45 min in DMEM supplied with 5 mM Hydroxyurea (1 M Hydroxyurea stock solution: 0.76 g Hydroxyurea, 10 ml PBS). After the HU-treatment, the cells were directly harvested in 1 ml Trizol for RNA extraction, followed by the analysis on an acrylamide-urea gel (section 2.2.1.11) and qRT-PCR (section 2.2.19.1).

2.2.10 Measurement of cell growth

MEF cells from wildtype and Eri1-knockout embryos at 13.5 dpc were taken into culture (section 2.2.3, 2.2.4) to measure the doubling time. The primary MEF cells were seeded in 96 well plates, 5000 cells in 200 μ l DMEM. The Cellscreen (Innovatis) was used according to the manufacturer's instructions to take pictures of exactly the same cells and their progeny over a culture period of 24 h or 48 h, respectively. Percentages of the surface area covered with cells were determined by automated analysis of each picture using the PA adhesion software (Innovatis). At least eight replicates of each culture were used to calculate the cell-doubling time.

2.2.11 Confocal microscopy

Cells were transfected and split the next day to seed 3×10^5 cells on a glass cover slip. The day after, the cells were fixed with 4% PFA for 20 min at RT with agitation, washed three times for 5 min each in wash buffer WB (PBS + 0.5% Nonidet P-40, 0,01% NaN_3) and blocked by incubation in WB/FCS (WB,10% FCS) for 30 min at RT. Staining was performed by incubation with the primary Pes1 antibody in WB/FCS (1:10 dilution) for 1h at RT. After three washing steps, the cells were stained with the secondary Cy5 antibody in WB/FCS (1:200 dilution) for 45 min at RT. Finally, after two more washing steps, the cells were stained for 1 min in DAPI solution (15 μ g DAPI (Sigma D8417)/100 ml 2xSSC buffer) and then put in PBS/0.01% NaN_3 before mounting.

2.2.12 Western blot analysis

For SDS-PAGE, gel solutions with 8-12% acrylamide in the resolving part and 5% in the stacking part were prepared. 30% ammonium persulphate (APS) and 0.001% N,N,N',N'-tetramethylethylenediamine (TEMED) were added to the gel solution to induce polymerization. MEF cells or embryo parts were washed in PBS and lysed in 20-300 μ l RIPA-buffer. Lysates were incubated for 30 min on ice and then centrifuged at 14,000g, 4°C for 15 min. Protein samples were boiled in 4x SDS sample buffer for 5 min at 95°C and subsequently loaded into the slots of the gel. In addition, a protein size maker (Precision Plus Protein All Blue Standards, Biorad) was loaded into one slot of the gel. Electrophoresis was applied for 50 minutes at 130 V. The electrophoretic transfer of polypeptides from polyacrylamide (PAA) gel to

a polyvinylidene fluoride (PVDF) membrane was performed by using a wet gel transfer apparatus (Biorad). The PVDF membrane was briefly activated in 100% methanol and soaked for 5 min in Western blot buffer (25 mM Tris-Base, 192 mM glycine, 20% v/v methanol) for 10 min. The PAA gels were carefully removed from the electrophoresis chamber and the Western blot 'sandwich' was assembled. The transfer was carried out for 2 h at 100 V and 250 mA in ice-cold buffer. For protein detection with antibodies, the membranes containing the separated polypeptides were blocked in TBS/5% milk for 1 h at RT. After blocking, the membrane was washed with TBS/0.05% Tween (3 x 5 min) and the diluted primary antibody was added 1 h at RT or over night at 4°C. After washing (3 x 5 min) the membrane was incubated with the secondary antibody conjugated with horse radish peroxidase (HRP) for 1 h at RT. While washing (3 x 10 min) the membrane, the ECL chemiluminescent substrate was prepared (ECL Western Blot Detection Kit). Following incubation of the membrane with the ECL solution for 5 min at RT, the solution was drained off. The membrane was placed in a plastic foil to prevent drying and then placed in a dark developing cassette and exposed to an ECL film. The exposure time of the film was between 2 s and 2 h.

2.2.13 Immunohistochemistry stain on embryos

For immunohistochemistry (IHC) stains embryos were taken from pregnant females at 11.5 dpc or 12.5 dpc (section 2.2.3). The embryos were washed in PBS, then fixed in 4% neutral buffered formalin or 4% buffered paraformaldehyd for 24 h, embedded in paraffin and 1 µm serial slides were cut for immunohistochemistry. Eri1-immunohistochemistry was performed using the discovery immunohistochemistry autostainer (Discovery®XT Instrument, Ventana medical systems, Illkirch CEDEX, France) and affinity-purified rabbit anti mouse Eri1-antibodies (A28), which were diluted 1:100. Image capturing was done using the dotslide virtual microscopy system (2.0; Olympus GmbH, Hamburg, Germany).

2.2.14 Whole mount in situ hybridization of embryos

Embryos were obtained from timed pregnancies (section 2.2.3), dissected in phosphate buffered saline (PBS) and fixed in 4% paraformaldehyde (PFA) in PBS at 4°C overnight. *In situ* hybridizations were performed as previously described (Kloosterman et al., 2006; Sweetman et al., 2008). All embryos were stained using

BM Purple (Roche) according to the manufacturer's instructions. The double DIG labeled probe for miR-196a was purchased directly from Exiqon. The *in situ* hybridizations were performed using an Intavis *In Situ* Pro robot. The pictures of embryos from whole mount *in situ* hybridizations were taken using a Leica MZ16F microscope and a Leica DFC320 camera.

2.2.15 Methods employed in German Mouse Clinic

Table 3: Methods employed in the screen at the German Mouse Clinic.

Screen	Goal	Method
Dysmorphology, Bone and Cartilage	morphological analysis of body, skeleton, bone, and cartilage	morphological observation, bone densitometry, X-ray
Behavior	locomotion and anxiety-related behavior sensory motor gaiting	open field Acoustic startle & PPI
Neurology	assessment of muscle, spinocerebellar, sensory, and autonomic function	modified SHIRPA protocol grip strength Rotarod
Eye	assessment of morphological alterations of the eye	funduscopy laser interference biometry slit lamp biomicroscopy
Nociception	detection of altered pain response	hot plate assay
Energy Metabolism	measurement of altered body weight regulation, body temperature and energy balance	bomb calorimetry
Clinical Chemistry and Hematology	determination of clinical-chemical and hematological parameters in blood glucose tolerance	blood autoanalyzer, ABC-animal blood counter simplified IpGTT
Steroid Metabolism	analysis of steroid hormones in blood plasma: testosterone and DHEA	ELISA
Immunology	analysis of peripheral blood samples for immunological parameters	flow cytometry, Multiplex Bead Array
Allergy	analysis of total plasma IgE	ELISA
Cardiovascular function	assessment of functional cardio-vascular parameters, analysis of plasma ANP	non-invasive tail-cuff blood pressure measurement, sur- face limb ECG / Echo, heart weight, ELISA
Lung Function	assessment of alterations in breathing patterns	whole body plethysmography (Buxco [®])
Molecular Phenotyping	RNA expression profiling	DNA-chip technology
Pathology	microscopic and macroscopic examination	histology, immunochemistry

2.2.16 Skeletal analysis

2.2.16.1 X-ray and computed tomography (CT) scanner

For x-ray analysis the Faxitron X-ray Model MX-20 (Specimen Radiography System, Illinois, USA) and the NTB Digital X-ray Scanner EZ 40 (NTB GmbH, Diepholz, Germany) were used. The anesthetized mouse was fixed on an X-ray-permeable plate, placed in the machine and scanned with a voltage of 25 kV and an integration time of 40 ms. Using iX-Pect software the image was taken. Analysis was done qualitatively by visual inspection of the images as well as quantitatively by using the ruler tool of iX-Pect software. For micro-computed tomography (μ CT) a VAMP Tomoscope 10010 m, version 1.2 (VAMP GmbH, Erlangen, Germany) was used. CT images were captured according to the manufacturer's instructions and reconstructed using the ImpactView 3.0 software supplied by the manufacturer. More CT analyses were performed with a LaTheta LCT-100A (Bruker) and the corresponding LaTheta 2.1 Software. Mice were imaged with a 0.2 mm slice thickness. 3D reconstruction was performed with the 3D Doctor software.

2.2.16.2 Skeletal stain

Skeletal preparations were generated as previously described (Fuchs et al., Screening for bone and cartilage phenotypes in mice (2006), In: Standards of mouse model phenotyping, 1st edition, Wiley-VCH Verlag GmbH. pp. 35–86). For analysis, vertebrae were dissected and photographed with Leica DFC320 and the corresponding software for image acquisition.

2.2.17 Molecular phenotyping of embryos

Isolation of total RNA

The 4 wildtype and 4 Eri1-knockout embryo littermates were taken from pregnant females at 12.5 dpc (section 2.2.3). The embryos, exclusive heads, were thawed in buffer containing chaotropic salt (RLT buffer, Qiagen) and homogenized using a Polytron homogenizer. Total RNA from individual samples was obtained according to the manufacturer's protocols using RNeasy Midi kits (Qiagen). The concentration was calculated from OD_{260/280} measurements and 2- μ g-RNA aliquots were run on a formaldehyde agarose gel to check for RNA integrity. The RNA was stored at -80°C in RNase free water (Qiagen).

Chip hybridization

Two chip hybridizations were performed with RNA from each individual mutant embryo. Each chip hybridization was performed against a pool of reference RNAs. For each individual mutant embryo the chip experiments include a colorflip experiment (in total eight hybridizations).

Reverse transcription and fluorescent labeling

For labeling 15 µg of total RNA were used for reverse transcription and indirectly labeled with Cy3 or Cy5 fluorescent dye according to the TIGR protocol (Hegde et al., 2000). Labeled cDNA was dissolved in 50 µl hybridization buffer (6x SSC, 0.5% SDS, 5x Denhardt's solution and 50% formamide) and mixed with 50 µl of reference cDNA solution (pool from six control animals) labeled with the second dye. This hybridization mixture was subjected to a prehybridized microarray in a HS4800 Hybstation (Tecan) and incubated at 42°C for 16 h. After hybridization slides were washed with 3x SSC, 1x SSC, 0.5x SSC and 0.1x SSC at room temperature. Slides were dried with nitrogen. Dried slides were scanned with a GenePix 4000A microarray scanner and the images were analyzed using the GenePix Pro6.0 image processing software (Axon Instruments, USA).

Significance of regulation

The TIGR software package for Microarray analysis (TM4; Chu *et al.*, 2002, Saeed *et al.*, 2003) was used for normalization (MIDAS: Microarray Data Analysis System; Quackenbush 2002) and identification of genes with significant differential regulation (SAM, Significance Analysis of Microarrays; Tusher *et al.*, 2001). Expression data were normalized performing a total intensity normalization to transform the mean log₂ ratio to zero. To eliminate low-quality array elements several filtering methods were applied. They include: background checking for both channel with a signal/noise threshold of 2.0, one bad tolerance policy parameter and flip dye consistency checking (Yang *et al.*, 2002). SAM was used to identify genes with statistically significant changes in expression. Genes were ranked according to their relative difference value $d(i)$, a score assigned to each gene on the basis of change in gene expression levels relative to the standard deviation. Genes with $d(i)$ values greater than the threshold were selected as significantly differentially expressed. The percentage of such genes identified by chance is the false discovery rate (FDR). To

estimate the FDR, nonsense genes were identified by calculating permutations of the measurements. The selection of the top differentially expressed genes with reproducible up- or down-regulation includes less than 10% false positives (FDR).

Functional classification of regulated genes

For *in silico* analysis of differentially expressed genes EASE, a module of the DAVID database assigning genes to Gene Ontology (GO) functional categories was employed. EASE analysis including a Bonferroni multiplicity correlation evaluated the set of differentially expressed genes for over- representation of two categories of GO terms: Biological processes and molecular functions (Dennis *et al*, 2003).

2.2.18 RNA-immunoprecipitation (RIP)

In vivo formaldehyde fixation of cells

Actively dividing mouse embryonic fibroblasts (1.7×10^7 cells) were first washed with PBS, treated with trypsin, and then washed twice with PBS. The cells were fixed in 20 ml 1% formaldehyde/PBS buffer, prepared from a 36.5-38% aqueous solution (Sigma), for 10 min at room temperature with rotation. Crosslinking reactions were quenched with glycine (pH 7.0) at a final concentration of 0.25 M, followed by incubation at room temperature for 5 min with rotation. The cells were harvested by centrifugation at 280g for 4 min followed by a PBS wash.

Solubilization of crosslinked complexes by sonication

Fixed cells were resuspended in 2 ml RIPA buffer (50 mM Tris, pH 7.5, 1% Nonidet P-40 (NP-40), 0.5% sodium deoxycholate, 0.05% SDS, 1 mM EDTA, 150 mM NaCl) containing complete protease inhibitors mix (Roche) and 1 mM dithiothreitol (DTT). The cells were then lysed by three rounds of sonication, 30 s each, at an amplitude setting of 15% (Branson Digital Sonifier) in an ice-water bath. Insoluble material was removed by centrifugation at 16,000 *g* for 10 min at 4°C.

Preclearing lysates

Cell lysates were precleared by mixing with 20 μ l MyOne Tosylactivated Dynabeads (Invitrogen) that have been covalently coupled to a monoclonal anti-rat IgG1 (TIB170) according to the manufacturer's protocol. The mixture was rotated for 1 h at

4°C. The precleared lysate was removed and used for immunoprecipitation. An aliquot was saved for RNA extraction (100 µl input).

Immunoprecipitation of crosslinked RNA-protein complexes

TIB170 antibody coated Dynabeads (20 µl) were coated with 3 ml supernatant of 5G8-111 hybridoma containing anti-Eri1 antibody for 1 h at 4°C, followed by three wash steps with RIPA buffer. The precleared lysate was mixed with the antibody-coated beads, 20 U of RNasin (Promega) was added and incubated with rotation at RT for 2 h. The beads were washed five times with 1 ml of high-stringency RIPA buffer (50 mM Tris, pH 7.5, 1% NP-40, 1% sodium deoxycholate, 0.1% SDS, 1 mM EDTA, 1 M NaCl, 2 M urea, and 0.2 mM phenylmethylsulfonyl fluoride (PMSF)) for 10 min rotation at RT.

Reversal of crosslinks and RNA purification

The beads containing the immunoprecipitated samples were collected and resuspended in 100 µl of 50 mM Tris, pH 7.0, 5 mM EDTA, 10 mM DTT and 1% SDS. Samples (resuspended beads) were incubated at 70°C for 45 min to reverse the crosslinks. The RNA was extracted from 100 µl by mixing with 1 ml Trizol (Invitrogen) following the standard protocol (section 2.2.1.9).

Analysis of immunoprecipitated RNA by semiquantitative RT-PCR

RNA (1/5 of the total sample) was subjected to genomic DNA elimination and reverse transcription of RNA according to the QuantiTect Reverse Transcription Kit (Qiagen) (section 2.2.1.10). PCR was performed in 50 µl volume containing 1× Taq buffer (20 mM Tris, pH 8.4, 50 mM KCl,) 1.5 mM MgCl₂, 0.2 mM dNTP, 1 pmol of each specific primer, 5 U of Taq DNA polymerase, and 1 µl of RT product. After an initial incubation at 95°C for 3 min, the reaction mixtures were subjected to 28–32 cycles of amplification using the following sequence: 95°C for 15 s, 55°C for 30 s, and 72°C for 30 s. 15 µl of each reaction mixture were run on a 2% agarose gel and visualized by ethidium bromide staining. The primers for semiquantitative PCR amplification are listed in section 2.1.6.

RIP assays on HEK293 cells expressing GFP or GFP-tagged Eri1 constructs were performed with the following modifications: extracts containing 2 mg of protein were

immunoprecipitated in 1 ml volume with 10 µg polyclonal anti-GFP (A11122) antibody. The anti-GFP antibody was coupled to 25 µl Protein G Dynabeads (Invitrogen) according to the manufacturer's protocol.

2.2.19 Quantitative PCR

2.2.19.1 qRT-PCR using the universal probe library

For an accurate qualitative and quantitative detection of RNAs the universal probe library system (UPL, Roche) was used. It is based on short hydrolysis probes that are labeled at the 5' end with fluorescein and at the 3' end with a dark quencher dye. The sequences of the 165 UPL probes have been selected to detect 8- and 9-mer motifs that are very prevalent in the transcriptomes ensuring optimal coverage of all transcripts in a given transcriptome. PCR primers for the quantitative real-time PCR experiments were designed with the Primer design tool from Roche Applied Science: 'universal probe library' (<https://www.roche-applied-science.com/sis/rtqpcr/upl/index.jsp?id=UP030000>) listed in section 2.1.6. All primer/UPL-probe sets were tested for an efficiency of close to 2. For qRT-PCR measurements, the cDNA template was synthesized by a reverse transcription reaction including a gDNA wipeout step using the QuantiTect Reverse Transcription Kit (Qiagen) as previously described (section 2.2.1.10). The qPCR reaction mixture consisted of 10 µl MM (Light Cycler 480 Probes Master 2x conc., Roche), 1 µl forward Primer (4 pmol/µl), 1 µl reverse Primer (4 pmol/µl), 0.2 µl UPL probe (Roche), 2.8 µl H₂O (Roche) and 5 µl cDNA template (about 1:30 diluted in H₂O). The qPCRs were run in 96-well-plates on a Light Cycler 480 (Table 4). Calculations of relative RNA levels were performed in correlation to a housekeeping gene (pbgd). Individual samples were always measured in duplicates to ensure reliability.

Table 4: PCR program on the Light Cycler 480 for real-time PCR using the UPL library (Roche).

Program step	Cycles	Target (°C)	Hold	Ramp rate (°C/s)
Pre-incubation	1	95°C	10 min	4.4
Amplification	45	95°C	10 sec	4.4
		60°C	30 sec	2.2
		72°C	1 sec	4.4
Cooling	1	40°C	30 sec	2.2

2.2.19.2 qRT-PCR of miRNAs

For the measurement of miRNAs the TaqMan MicroRNA assays kit (Applied Biosystems) was used. The two-step protocol requires a reverse transcription step with a miRNA-specific primer, followed by a qPCR step with TaqMan probes. The assays target only mature microRNAs, not their precursors. To convert a specific miRNA to cDNA, first strand synthesis was carried out using the TaqMan microRNA reverse transcription kit (Applied Biosystems) and stem-loop primers, specific for miR-196a, miR-196b, miR-181a and U6 snRNA as reference (Applied Biosystems) according to the manufacturer's protocol. The qPCR reaction mixture consisted of 10 μ l MM (Light Cycler 480 Probes Master 2x conc., Roche), 1.3 μ l specific forward and reverse Primer + TaqMan probe (Applied Biosystems), 7.67 μ l H₂O (Roche) and 1.33 μ l cDNA template. The qPCRs were performed on the LightCycler 480 (Table 5). U6 snRNA was taken as a reference for relative quantification.

Table 5: PCR program on the Light Cycler 480 for real-time PCR using miRNA Taqman primers (Applied Biosystems).

Program step	Cycles	Target (°C)	Hold	Ramp rate (°C/s)
Pre-incubation	1	95°C	10 min	4.4
Amplification	45	95°C	15 sec	4.4
		60°C	1 min	2.2
Cooling	1	40°C	30 min	2

2.2.20 Dual-luciferase reporter assay

Genetic reporter systems are widely used to study the regulation of eukaryotic gene expression. The term 'dual' refers to the simultaneous expression and measurement of two individual reporter enzymes within a single system. The experimental reporter is correlated with specific experimental conditions, while the activity of the second 'control' reporter provides an internal control that serves as a baseline for infection efficiency. The psiCHECK2 (Promega) encodes for both reporter genes on the very same plasmid. Because of low transfection efficiency of MEF cells, first the commercial psiCHECK2 plasmid had to be converted to an adenoviral expression plasmid (pAdpsiCHECK2) (section 2.1.5.3). Then the sequences for Hoxc8 3' UTR and Hoxc8 3' UTR/miR-196a sites mutated (actaCCt>actaAAt) were fused to the Renilla luciferase gene. For the dual-luciferase assays MEF cells were plated onto

12-well plates at $1-2 \times 10^5$ cells per well and cells were co-infected with the indicated adenoviruses in triplicates. Two days after infection, Renilla and Firefly luciferase activities were assayed using a Dual-Luciferase Reporter System (Promega) and a luminometer (Orion Microplate Luminometer, Berthold Detection Systems). Infected cells were washed once with PBS and lysed in 150 μ l of 1x passive lysis buffer (Promega) for 20-30 min at RT on a shaker. Then cells were subjected to one freeze and thaw cycle followed by centrifugation at 20,000 g for 5 min. 20 μ l of each lysate was pipetted into the reader plate of the luminometer.

3 Results

3.1 Characterization of mouse *Eri1*: the knockout phenotypes, the expression patterns and the binding and processing of target RNAs

In order to understand the molecular function of *Eri1* in mice (section 3.2), the phenotypes of the *Eri1*-knockout mouse were first systematically analyzed (section 3.1.1). Then organs and tissues were examined for *Eri1* expression in adult mice (section 3.1.2) and the intracellular localization of the *Eri1* protein was determined (section 3.1.3). Protein-intrinsic binding specificity and the processing activity of *Eri1* towards two of its target RNAs, namely the ribosomal RNA and the histone mRNA, was analyzed (section 3.1.4 and 3.1.6). Additionally, the growth rate of primary *Eri1*-deficient MEF cells was measured (section 3.1.5).

3.1.1 Description of the *Eri1*-knockout mouse

Eri1-knockout mice were analyzed on two different genetic backgrounds, on a C57BL/6 inbred background and on an NMRI x C57BL/6 mixed background that was generated by crossing in an NMRI outbred strain. An inbred strain is defined by at least 20 consecutive generations of sister x brother or parent x offspring matings and the strain has to be traceable to a single ancestral pair in the 20th or subsequent generation. Except for the sex difference, mice of an inbred strain are genetically as alike as possible by being homozygous at virtually all of their loci.

In contrast, the mice of an outbred strain are genetically undefined; no two wildtype individuals from an outbred strain are the same. Outbred mice are intentionally not bred with siblings or close relatives. Hence unlike fully inbred strains, outbred mice have normal levels of heterozygosity for polymorphisms, recapitulating the genetic situation in humans. An advantage of using outbred strains is, amongst others, the better resistance to diseases, this applies also for intentionally caused conditions by genetic modifications.

3.1.1.1 Growth defects in *Eri1*-knockout mice

Eri1-knockout mice were smaller in body size than wildtype littermates. This was especially pronounced when littermates on the C57BL/6 inbred strain background were compared (Figure 10a), but the difference was also penetrant after crossing in an NMRI outbred strain to generate mice on a NMRI x C57BL/6 mixed background. The growth defect was similarly reflected by the body weight, comparing *Eri1*-knockout, *Eri1*-heterozygous and wildtype mice from one litter. Comparing the differences in weight among males or females, the wildtype and *Eri1*-heterozygous littermates were heavier than the *Eri1*-knockout mice of the same sex (Figure 10b).

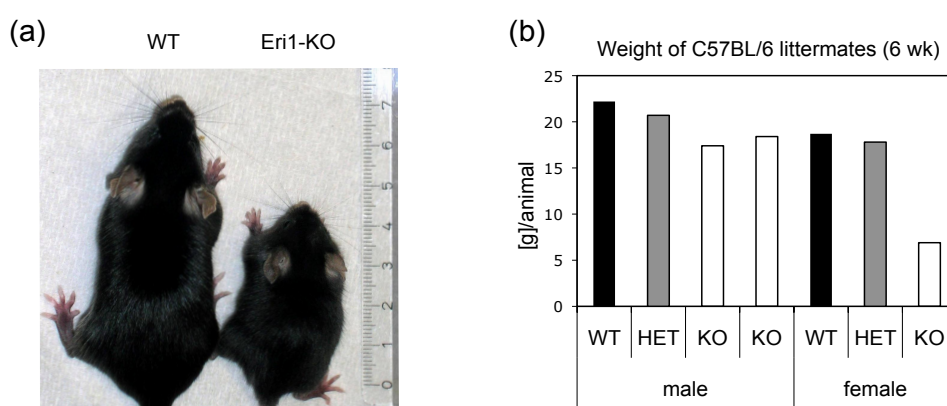


Figure 10: Reduced body size and weight of *Eri1*-knockout mice. (a) Picture of a C57BL/6 wildtype mouse (7.4 cm) and its *Eri1*-knockout littermate (4.6 cm) 6.5 weeks after birth. (b) Weight of male and female littermates from one litter on a C57BL/6 inbred strain background. wildtype (black), *Eri1*-heterozygous (gray) and *Eri1*-knockout (white) 6 weeks after birth.

3.1.1.2 Postnatal death and male sterility of *Eri1*-knockout mice

On the C57BL/6 inbred background about 90% of *Eri1*-knockout mice died during the first days after birth, so that the p-value for an *Eri1*-knockout to survive till weaning age was calculated to be only $p = 1.1 \times 10^{-10}$ (Table 6).

Table 6: Effect of strain background on the reduced viability of *Eri1*-knockout mice.

Strain	Genotype representation, Actual (Expected) ^{*1}			p ^{*2}
	<i>Eri1</i> ^{+/+}	<i>Eri1</i> ^{+/-}	<i>Eri1</i> ^{-/-}	
C57BL/6	55 (42)	109 (84)	4 (42)	1.1×10^{-10}
(NMRI x C57BL/6) F ₂	197 (180)	410 (360)	116 (180)	1.6×10^{-7}

^{*1} The number of animals with the indicated *Eri1* genotype. Expected numbers assuming Mendelian inheritance of *Eri1* alleles are shown in parentheses.

^{*2} Chi-squared test for deviation from the expected Mendelian distribution.

In contrast *Eri1*-heterozygous mice had similar chances for survival as wildtype mice (Figure 11). Standard analyses did not reveal the cause for the neonatal mortality, but the postnatal death of the *Eri1*-knockout mice could partly be rescued by crossing in mice from the NMRI outbred strain (Table 6).

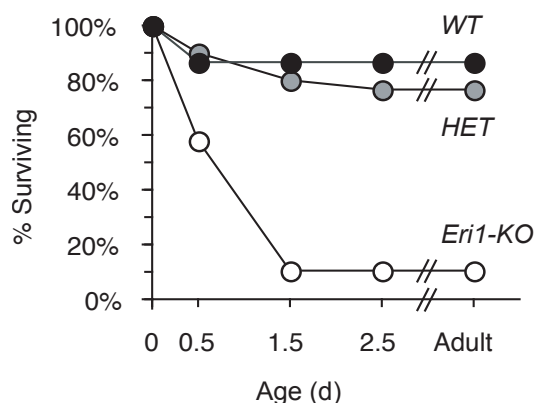


Figure 11: Postnatal death of *Eri1*-knockout mice. Survival curve of C57BL/6 *Eri1*-knockout mice (open circles), *Eri1*-heterozygous (grey circles), and wildtype (black circles) littermates. (In collaboration with K. Mark Ansel.)

On a mixed NMRI x C57BL/6 background *Eri1*-knockout mice were viable, but the male mice showed the phenotype of sterility that was likely to be caused by the underdeveloped testes that were observed for this genotype (Figure 12). Consequently, only *Eri1*-heterozygous male mice on C57BL/6 inbred background or NMRI x C57BL/6 mixed background could be used for further breeding.

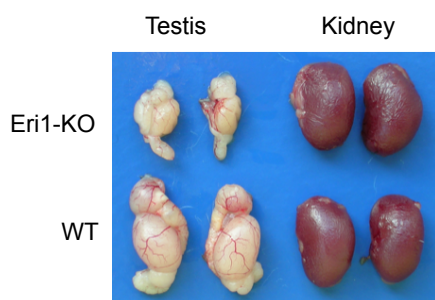


Figure 12: Smaller testis in *Eri1*-deficient mice. Picture of testis and kidney from NMRI x C57BL/6 *Eri1*-knockout and wildtype littermates.

3.1.1.3 Summary of the phenotypes of *Eri1*-knockout mice found in the screens of the German Mouse Clinic

For a detailed description of the *Eri1*-knockout mouse phenotype a large scale breeding strategy was planned and realized to generate 25 *Eri1*-knockout and 25 wildtype littermates, males and females each, for a first systematic screen in the German Mouse Clinic. The analyzed mice were an F2 generation on a mixed background: *Eri1*-heterozygous mice on a C57BL/6 background were mated with wildtype mice on an NMRI background. The progeny (F1 *Eri1*-heterozygous males

and F1 *Eri1*-heterozygous females) was intercrossed to generate the cohort for the analyses in the German Mouse Clinic. Subsequently, a secondary systematic screen with 12 *Eri1*-knockout, 12 *Eri1*-heterozygous and 12 wildtype littermates, males and females each, was performed to provide further information about the uncovered phenotypes. Out of the 14 different categories that have been analyzed, an *Eri1*-specific phenotype was observed in nine of them (Table 7).

Table 7: Summary of the results from primary and secondary screens on *Eri1*-knockout, *Eri1*-heterozygous and wildtype mice in the German Mouse Clinic.

Screen	<i>Eri1</i> -knockout mouse specific phenotype
Allergy	No.
Behavior	Slight decrease in locomotion activity, increased anxiety in the open field and light/dark box test.
Cardiovascular malfunction	No.
Clinical chemistry and hematology	Homozygous <i>Eri1</i> -knockout mice develop a macrocytic blood cell count with slightly reduced hemoglobin values, increased ferritin and transferrin levels as well as an increased alkaline phosphatase activity, while heterozygous mice share the wild-type phenotype concerning these parameters.
Dysmorphology	An additional thoracic vertebra and/or an extra pair of ribs in most of the mutants.
Energy metabolism	Only small significant differences were revealed. For the metabolic parameter 'efficiency in energy turnover' an increase was seen in <i>Eri1</i> -knockout mice.
Eye malfunction	No.
Immunology	The analysis of <i>Eri1</i> -mutant mice in the primary immunology screen showed statistically significant lower frequencies of NK1.1+ cells in mutant mice compared to controls. Furthermore, in female mice a higher proportion of CD44 expressing cells within the CD4+ T cell cluster has been found. The analysis of the blood plasma revealed statistically higher levels of IgG1 and IgG2b in mutants compared to controls.
Lung dysfunction	No.
Molecular phenotyping	Embryos (E12.5) on pure C57BL/6 background were chosen for this secondary screen. The data analysis of the microarray experiments including various statistical methods detected several genes differentially regulated between mutant and reference tissues in the embryo. Several of the regulated genes have known expression during embryogenesis.
Neurology	Reduction of grip force that could be a consequence of the reduced body weight.

Nociception	No.
Pathology	Compared to the control mice, the <i>Eri1</i> -mutant mice showed a reduction of the body weight and body length, which was however not statistically significant. The presence of testicular hypoplasia could be confirmed in 5 of 6 mutants and an arrest of spermatogenesis was found in all male mice. In the femurs, we observed a tendency to a reduction in the amount of metaphyseal trabeculae, mainly in male mutant mice.
Steroid metabolism	For dehydroepiandrosterone (DHEA) significantly reduced levels were found in mutant females. In case of testosterone, mutants did not display sex-specific differences and mutant male mice presented very low concentrations of testosterone, even below the limit of quantification. Unfortunately these findings could not be confirmed in a second cohort of mice.

3.1.2 *Eri1* is ubiquitously expressed in mice

The expression pattern of *Eri1* in mice was analyzed to get a hint for *Eri1*'s function in mammals. Western blot analysis of a panel of tissues indicated that *Eri1* is ubiquitously expressed, and it was represented highly in total tissue protein extracts from the spleen, thymus and testis (Figure 13).

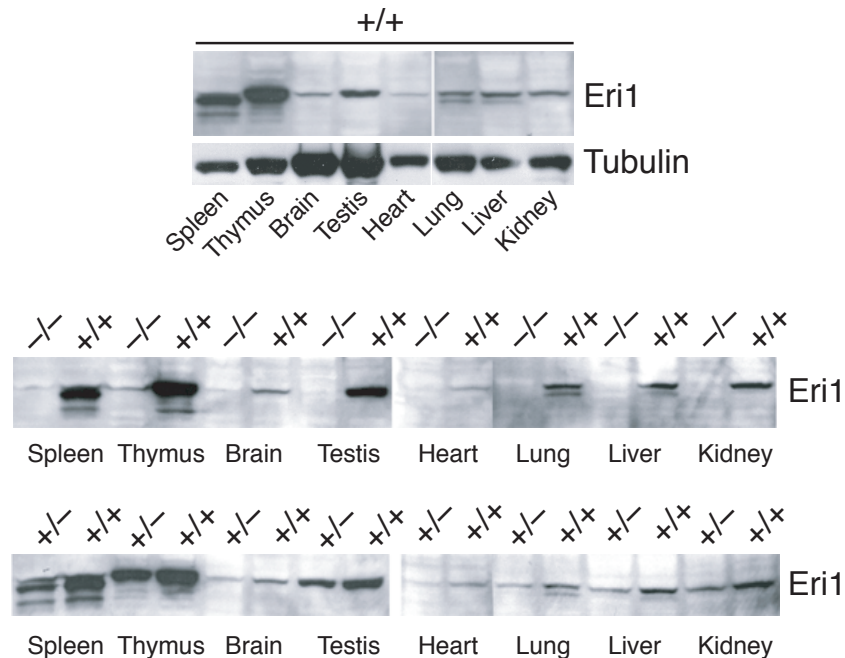


Figure 13: Ubiquitous expression of *Eri1* protein in various organs of adult mice. Tissue protein extracts from one *Eri1*-knockout, *Eri1*-heterozygous and wildtype mouse of the NMRI x C57BL/6 F2 generation were examined with the monoclonal 5G8 rat-anti *Eri1* antibody by Western blotting.

Together, the increased expression of Eri1 in the testis, the male sterility phenotype and the smaller testis size upon absence of Eri1 (3.1.1.2) supported Eri1's function in testis development. The ubiquitous expression pattern gave a hint for the involvement of Eri1 in a general processing pathway or even in several pathways that occur in all cell types. There was only half the amount of Eri1 protein expressed in all tissues from the *Eri1*-heterozygous mouse and no Eri1 protein could be detected in the Eri1-knockout mouse (Figure 13). Hence, this Western blot result also assured that the conditional *Eri1*-knockout mouse model worked outright and showed that Eri1 is expressed in a dose dependent manner when one allele is expressed compared to two alleles.

3.1.3 The SAP domain and linker sequence of Eri1 determine its localization to the nucleolus

Microscopic analysis was performed to determine the subcellular localization of Eri1 in HEK293A cells. For this experiment an N-terminal eGFP-tag was fused to wildtype and mutant sequences of *Eri1*. Localization of the fusion protein was found in both, the cytoplasm and nucleus, and within the nuclear compartment Eri1 was enriched in the nucleolus (Figure 14a). The presence of Eri1 in the nucleolus was confirmed by colocalization with the nucleolar marker Pes-1.

To determine whether the RNA/DNA-binding SAP domain or the adjacent linker sequences influence localization, two mutant Eri1 proteins were tested, which had been shown, in the context of human Eri1, to impair histone mRNA stem-loop binding *in vitro* (Yang et al., 2006) (Figure 14a,b). Murine Eri1 harboring orthologous mutations in conserved residues in either the SAP domain (R101A) or the adjacent linker sequence (K107A/K108A) localized more diffusely throughout the nucleus, and were not as enriched in the nucleoli as compared to the wildtype protein (Figure 14a,b). These observations showed that nuclear import remains intact after inactivation of residues critical for RNA binding, but that accumulation in the nucleoli is driven by the ability of the Eri1 protein to bind to RNA and/or DNA. A naturally occurring polymorphism found in C57BL/6 mice was also analyzed, which results in an amino acid substitution (A176D) in the catalytic domain of Eri1. The increased negative charge of the protein by this additional residue did not affect the subcellular localization (Figure 14a,b).

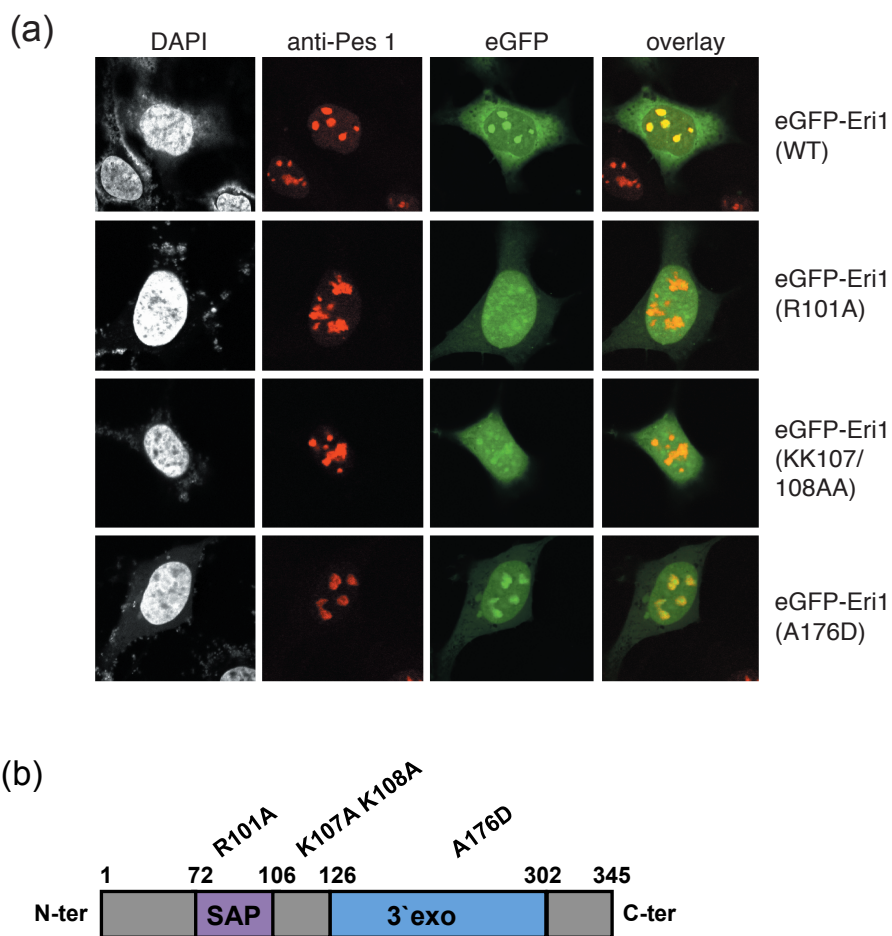


Figure 14: Eri1 accumulation in the nucleolus is driven by the function of the RNA/DNA-binding SAP domain and the linker sequence. (a) HEK293A cells were transiently transfected with eGFP-tagged *Eri1* using pDEST12.2. Eri1 wildtype and Eri1 proteins with point mutations within the SAP domain (R101A) or linker sequence (K107A K108A) or in the exonuclease domain (A176D) were analyzed for colocalization with endogenous Pes-1. (In collaboration with Elke Glasmacher.) (b) Schematic depiction of the structure of Eri1 and the employed point and deletion mutants.

3.1.4 Eri1 binds 5.8S rRNA as well as its rRNA precursor and catalyses 5.8S rRNA processing

The finding that Eri1 localized to the nucleolus dependent on its SAP domain and linker sequence and that specific residues are important for interaction with nucleic acids suggested an interaction of Eri1 with rRNA, which is transcribed in the nucleolus.

3.1.4.1 Eri1 is associated with 5.8S rRNA in vivo

RIP assays were established to show direct binding of the Eri1 protein to RNAs and to analyze the impact of SAP domain deletion or the exchange of critical amino acids on RNA binding. In IP assays the protein of interest is pulled out of the cell lysate by

an antibody – either directly specific for the protein itself or indirectly for a protein-tag – and the co-immunoprecipitated RNAs are purified and subsequently analyzed, i.e. by RT-PCR. Other than in the classical IP assay, the RIP protocol starts with a formaldehyde-mediated protein-RNA crosslinking step, which allows washing at more stringent conditions during the following precipitation steps. This reduces the co-immunoprecipitation of unspecific background RNA and prevents *in vitro* reassociation of protein-RNA complexes. Additionally, the lysate containing the crosslinked protein-RNA complexes is subjected to sonification to shear the RNA and to avoid the co-immunoprecipitation of unspecifically bound RNAs. These modifications to the classical protocol allowed the co-immunoprecipitation of only those RNAs, which are directly associated to Eri1 in living cells.

RIP assays using a monoclonal anti-Eri1 antibody revealed that 5.8S rRNA specifically co-immunoprecipitated with Eri1 in wildtype MEF cells, whereas no 5.8S rRNA could be amplified by semi-quantitative RT-PCR in the RIP-sample from *Eri1*-knockout MEF cells (Figure 15a). This result could be reconfirmed by an RIP experiment on HEK293 cells that had been transfected with a GFP-*Eri1* or a GFP-control expression construct. Performing the assay with a polyclonal anti-GFP antibody, 5.8S rRNA could again only be co-immunoprecipitated in the sample expressing GFP-*Eri1* (Figure 15b).

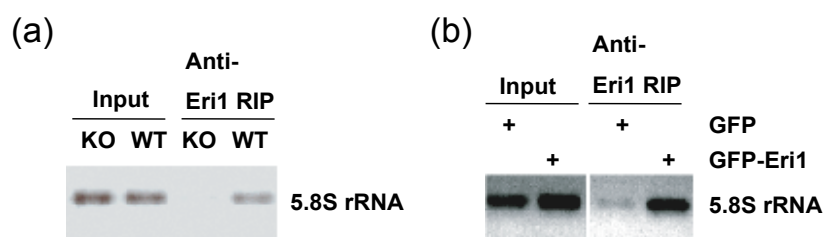


Figure 15: RNA-immunoprecipitation of Eri1 reveals association with 5.8S rRNA. (a) The RIP assay was performed on *Eri1*-knockout and wildtype MEF cells using an anti-Eri1 monoclonal antibody. Subsequently, the co-immunoprecipitated RNA was Trizol-purified, reverse transcribed and amplified by semi-quantitative PCR with primers specific for 5.8S rRNA. For visualization the PCR-product was run on a 2% agarose gel and stained with ethidium bromide. (b) RIP experiment with anti-GFP polyclonal antibody on HEK293 cells transfected with LNCX2-GFP or LNCX2-GFP-*Eri1*, respectively.

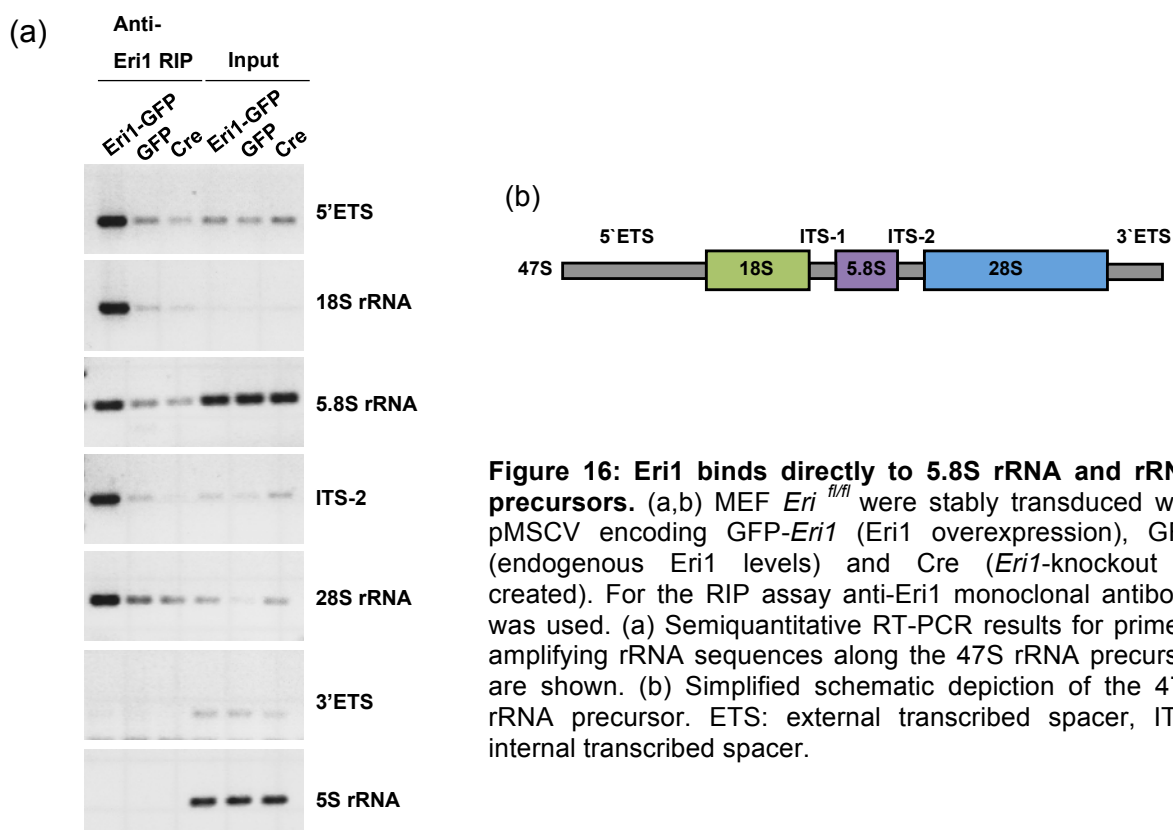
The input samples were harvested prior to the immunoprecipitation steps, thus before the samples were incubated with the respective antibodies. The RT-PCR

results for this inputs showed only marginal differences in the amount of 5.8S rRNA in cells with or without Eri1 protein expression (Figure 15a,b). These results assured that equal quantities of 5.8S rRNA were present in all immunoprecipitations. It could further be concluded that the absence of Eri1 does not have an obvious impact on upstream ribosomal RNA maturation steps. If Eri1 would affect earlier ribosomal RNA processing, less mature 5.8S rRNA would be expected in the *Eri1*-knockout input sample.

3.1.4.2 Eri1 interacts with 5.8S rRNA and rRNA precursors

Although Eri1 might not be important for early ribosomal maturation steps, it could be shown that Eri1 interacts with ribosomal RNA precursors. This association is consistent with its nucleolar localization (section 3.1.3).

For the RIP assay immortalized *Eri1^{fl/fl}* MEF cells were produced from an embryo that has the *Eri1* exon 3 flanked by loxP sites, 'floxed' (fl/fl). Excision of the exon 3 by a recombination event prevents the production of Eri1 proteins. *Eri1^{fl/fl}* MEF cells were stably transduced with retroviruses (1) to create Eri1 overexpression situation (GFP-Eri1) or (2) to keep endogenous Eri1 levels (GFP) or (3) to generate an *Eri1*-knockout situation (Cre recombinase).



GFP-Eri1 as well as the endogenous Eri1 co-immunoprecipitated sequences from the 5' ETS, 18S rRNA, 5.8S rRNA, ITS-2 and 28S rRNA. This indicated Eri1 association with the rRNA molecules present in the 45S rRNA precursor (Figure 16a,b). Significant interaction of Eri1 with the 3' ETS could not be detected. Within the Eri1 associated ribosomal RNAs, 5S rRNA could only be detected as a faint band, probably indicating the degree of unspecific background interaction. This provides support for the specificity of Eri1 binding to 5.8S rRNA and its precursor.

3.1.4.3 The SAP domain and linker sequence of Eri1 support binding to 5.8S rRNA

The analysis was extended to include the Eri1 mutations that had been published in the context of human Eri1 to impair histone mRNA binding (Yang et al., 2006). Two of the mutants, the SAP domain (R101A) mutant and the linker region (K107A K108A) mutant, had already been studied in the localization experiments in this thesis (section 3.1.3). The additional mutants were a truncated Eri1 protein with an amino terminal deletion spanning the SAP-domain (delta N-Eri1, aa107-345) and a catalytically inactive Eri1 bearing mutations that exchange two acidic amino acids in the exonuclease domain (D130G E132G), which are critical for coordinating a magnesium ion (Cheng and Patel, 2004). The two acidic amino acids, aspartic acid (D130) and glutamic acid (E132), were substituted with glycine (G), because of its conformational flexibility as the smallest amino acid.

Binding of point mutants of the Eri1 protein to the 5.8S rRNA was tested under conditions of endogenous expression of Eri1 or overexpression. GFP-tagged proteins were typically expressed at substantially higher levels than myc-tagged proteins, the latter reached approximately endogenous Eri1 expression levels. This difference in expression levels, even when expressed from otherwise identical vectors, indicates a stabilization of Eri1 protein through aminoterminal fusion with GFP.

First, RIP assays were performed on MEF cells that had been reconstituted with myc-tagged Eri1 proteins using the monoclonal anti-Eri1 antibody. The results showed that the catalytically inactive (D130G E132G) mutant still bound efficiently to the 5.8S rRNA, whereas the linker region (K107A K108A) mutant was reproducibly impaired in binding as compared to wildtype Eri1 (Figure 17a,b,d). The delta N mutant and the SAP domain (R101A) mutant of human Eri1 were also published not

to bind the histone stem-loop RNA in solution (Yang et al., 2006). However, these mutants could not be included in this experiment, because the monoclonal anti-Eri1 antibody recognizes an epitope in the N-terminus that was absent in both mutants. The polymorphism A176D, which is found in the C57BL/6 mouse strain did not affect 5.8S rRNA binding (Figure 17a,b,d).

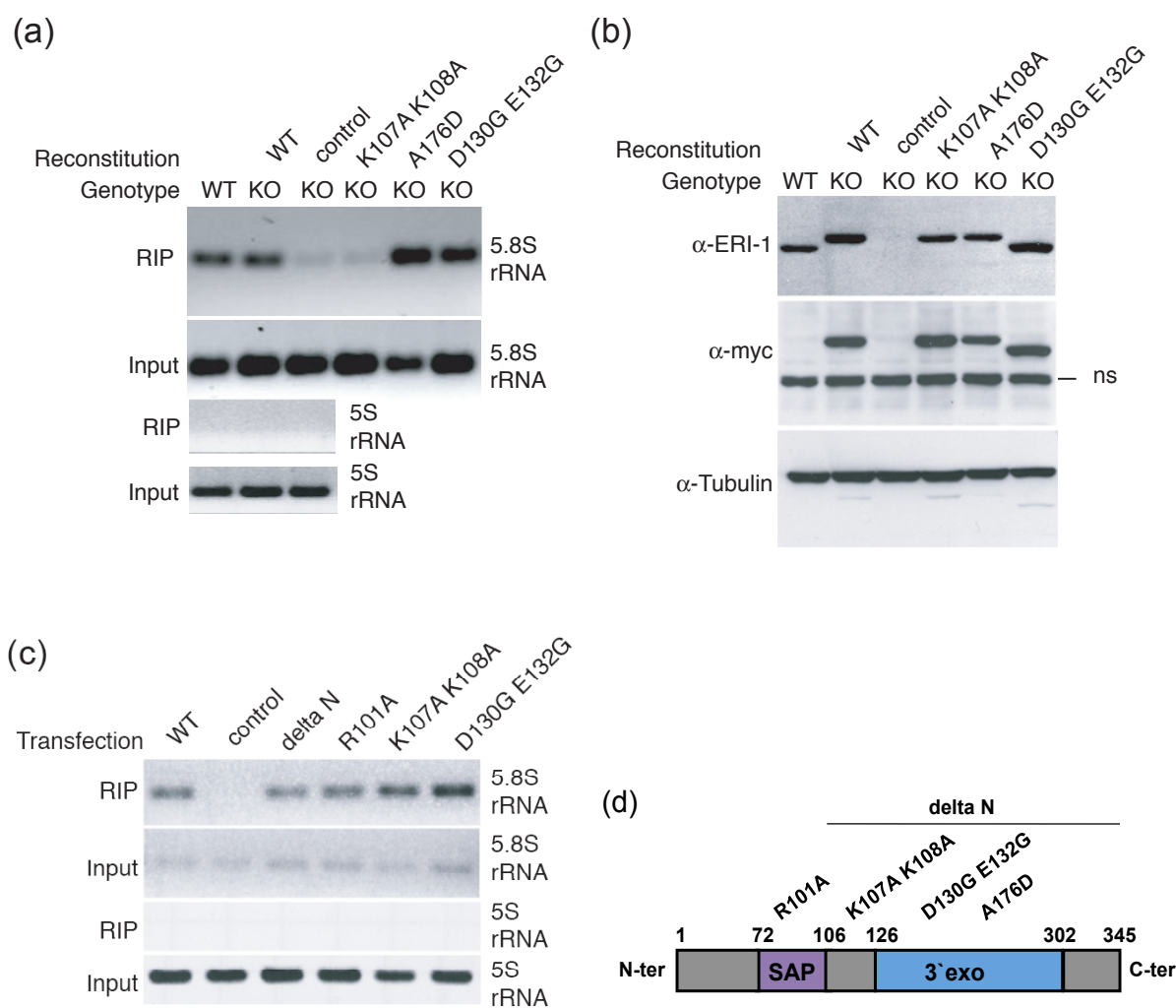


Figure 17: The SAP domain and linker sequence of Eri1 support binding to 5.8S rRNA at endogenous expression levels. (a) A RIP assay for Eri1 was performed with anti-Eri1 monoclonal antibody. Wildtype and *Eri1*-knockout MEF cells were left untransduced or transduced with control retrovirus (pMSCV) or retroviruses encoding myc-tagged (WT) and the indicated *Eri1* mutants. (b) Immunoblots using polyclonal anti-Eri1 and monoclonal anti-myc antibodies to detect Eri1 and myc-Eri1 expression in MEF cells of the indicated genotypes that were used in the RIP assay. (c) RIP assay using anti-GFP polyclonal antibody. HEK293 cells were transiently transfected with pDEST12.2 expression constructs for GFP-*Eri1* (WT), the indicated mutants or GFP-expressing vector (control). Equal expression levels were judged by fluorescent microscopy. (d) Schematic depiction of the structure of Eri1 and the employed point and deletion mutants.

Next, the association of 5.8S rRNA with Eri1 wildtype and mutant forms, including the delta N and R101A mutants, was tested in HEK293 cells. For these experiments,

GFP-tagged Eri1 proteins were overexpressed by transient transfection and RIP assays were performed with GFP-specific antibodies that immunoprecipitate all mutants with equal efficiency. Consistent with the results from RIP assays using endogenous Eri1 expression levels, the catalytically inactive (D130G E132G) mutant could still associate with 5.8S rRNA. Whereas at overexpression levels the sequences in the N-terminal SAP domain (Δ N and R101A mutants) and linker region (K107A K108A mutant) were no longer required for Eri1 interaction with 5.8S rRNA (Figure 17c,d). The reason for these differences may lie in the high expression levels attained in transfected HEK293 cells. The findings indicate that the N-terminal region of Eri1 supports rRNA binding but is not required for the interaction with 5.8S rRNA at least in an artificial system using high expression levels.

3.1.4.4 In Eri1-deficient cells the 5.8S rRNA is extended at the 3' end

With the knowledge of mouse Eri1 binding to 5.8S rRNA as well as its precursor and *Eri1* encoding for an exonuclease domain, Eri1's function in 5.8S rRNA processing was analyzed. Therefore, 5.8S rRNA running behavior was tested on large denaturing acrylamide-urea gels. For this approach wildtype-MEF cells were either infected with retroviruses encoding an shRNA against Eri1 to create an Eri1 knockdown, or with retroviruses encoding scrambled shRNAs as a control. During rRNA processing, alternative 5' endonucleolytic cleavage sites generate the major short (S) as well as the less abundant long (L) forms of 5.8S rRNA. Both isoforms appeared on acrylamide-urea gels in Eri1-knockdown and wildtype MEF cell RNA extracts. Importantly, both showed similar retardation in migration after Eri1-knockdown compared to wildtype (Figure 18a).

The apparent increase in molecular weight is likely to reflect a change at the 3' end of 5.8S RNA. This was validated by an approach from K. Mark Ansel, in which 5.8S rRNA was isolated from the liver of wildtype and *Eri1*-knockout mice and subsequently sequenced (Ansel et al., 2008). The 5.8S rRNA 3' end from wildtype cells uniformly terminated at the previously reported position. In contrast, the 5.8S rRNA 3' end from *Eri1*-knockout cells was variable, and 15 out of 16 clones contained a 1- or 2- nucleotide 3' end extension (Figure 18b). Thus Eri1 is crucial to ensure the fidelity of 5.8S rRNA maturation.

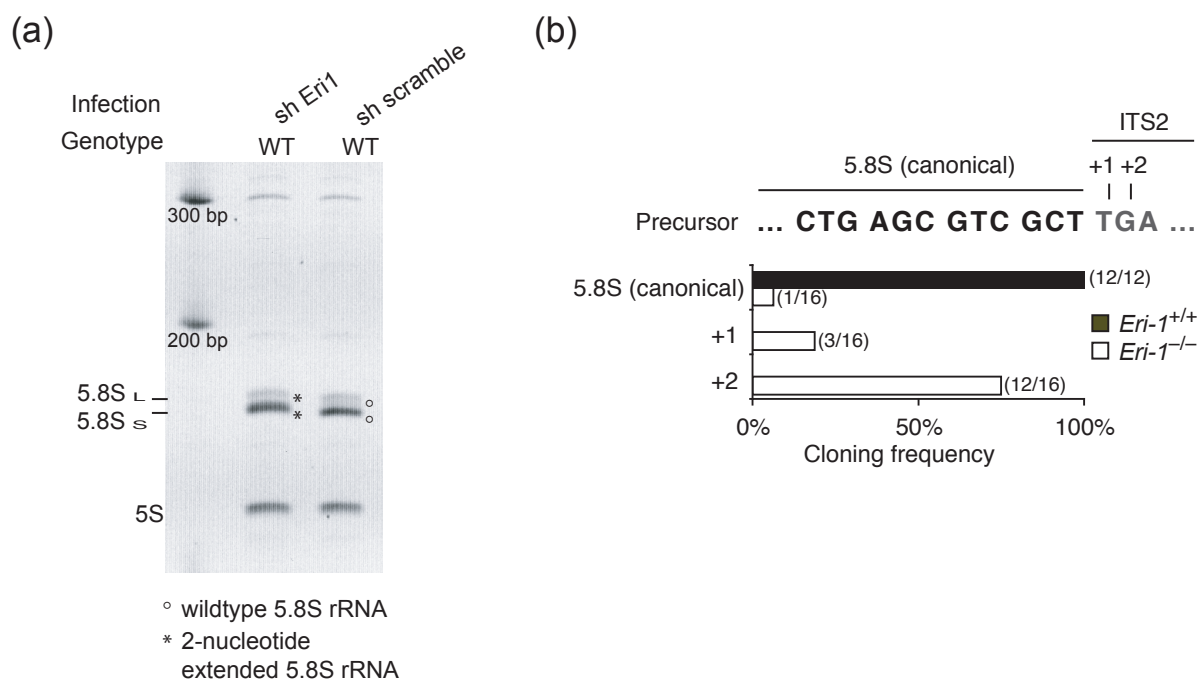


Figure 18: In *Eri1*-deficient cells the 5.8S rRNA 3' end is extended. (a) Ethidium bromide-stained RNA from wildtype MEF cells infected with an shRNA against *Eri1* or control shRNAs, respectively. 5.8S_S: short isoform of 5.8S rRNA, 5.8S_L: long isoform of 5.8S rRNA. The according Western blot is shown in Figure 3-14g. (b) Histogram shows the frequency of sequences obtained from *Eri1*-wildtype (black bars; n=12) and *Eri1*-knockout (white bars; n=16) that correspond to the predicted 5.8S sequence or extended sequences as shown above. All sequence extensions matched the expected ITS2 sequences (+1, T; +2, TG), except for one +2 clone that contained a TT extension. (K. Mark Ansel)

3.1.5 Reduced cell growth of primary *Eri1*-deficient MEF cells

The growth rate of primary embryonic cells was observed for a possible connection between the defect in 5.8S rRNA processing in *Eri1*-deficient MEF cells (Figure 18) and the phenotype of a reduced body size observed in *Eri1*-deficient mice (Figure 10). Primary MEF cells were generated from *Eri1*-knockout and control embryos (E13.5) and cell proliferation was measured using the Cellscreen (Innovatis). Pictures were taken of exactly the same cells and their progeny over a culture period of 24 h or 48 h, respectively. The percentages of the surface area covered with cells were determined by automated image analysis and used to calculate the doubling time of the primary MEF cell population. The data revealed that *Eri1*-knockout MEF cells grew significantly more slowly (P-value = 0.006) than cells obtained from their wildtype and heterozygous littermates (Figure 19). Ribosomes are among the most crucial factors for cell growth; hence the reduced cell growth might be caused by impaired ribosome synthesis in *Eri1*-deficient MEF cells.

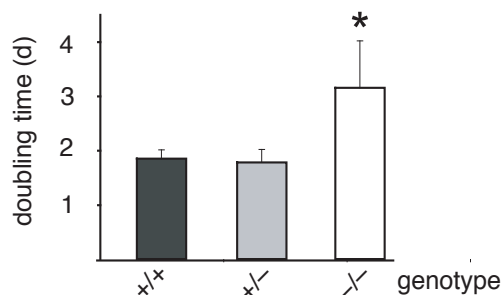


Figure 19: Reduced growth of primary *Eri1*-knockout MEF cells. Mean (\pm s.d.) doubling times for three independent experiments using two measurements obtained between passages 6 and 9 of MEF cells derived from a total of six *Eri1*-knockout embryos and controls. At least eight replicates of each primary MEF cell culture were measured.

3.1.6 *Eri1* binds to histone mRNA and initiates cell cycle-dependent degradation

3.1.6.1 *Eri1* is associated with *Hist2h4* mRNA *in vivo*

Dominski and colleagues have published the binding of the human *Eri1* to histone mRNA *in vitro* (Dominski et al., 2003). The interaction was confirmed in mouse cells. The RIP assay was used to show *in vivo* binding of histone mRNA, i.e. *Hist2h4* (histone cluster 2 histone H4), to the mouse *Eri1* protein. Immunoprecipitation of endogenous *Eri1* protein as well as the myc-tagged *Eri1* protein revealed the association with *Hist2h4* mRNA (Figure 20).



Figure 20: RNA-immunoprecipitation of *Eri1* reveals association with *Hist2h4* mRNA. A RIP assay for *Eri1* was performed with anti-*Eri1* monoclonal antibody. Wildtype and *Eri1*-knockout MEF cells left uninfected or reconstituted by transduction with pMSCV encoding myc-*Eri1* (WT) and the indicated mutants. The according Western blot is shown in Figure 17b.

It was proposed that 3'hExo interacts with histone mRNA in a sequence-specific manner through its SAP domain (Dominski et al., 2003; Yang et al., 2006). Consistent with the findings for 5.8S rRNA binding, the catalytically inactive mutant

(D130G E132G) and the C57BL/6 variant (A176D) could still bind to Hist2h4 mRNA, whereas the linker region mutant (K107A K108A) was impaired in binding at endogenous reconstitution levels (Figure 20, Figure 17b). These results provided support for a stem-loop specific histone mRNA substrate selection.

3.1.6.2 Eri1 regulates replication-dependent histone mRNAs, which is supported by specific amino acids in the SAP domain and linker sequence

The molecular basis for Eri1 substrate selection was analyzed further in the context of Eri1-dependent histone mRNA degradation at the end of S-phase by using the information from the crystal structure of human Eri1 bound to stem-loop RNA of the histone Hist2a (Y. Cheng and D. Patel, submitted to the Protein Data Bank). The crystal structure revealed two amino acids in the Eri1 SAP domain and linker sequence that located in close proximity and making physical contact with the conserved U13 nucleotide within the loop of the stem-loop structure of histone mRNAs (Figure 21). A new Eri1 SAP/linker sequence mutant was created by changing these critical two amino acids, asparagine (N69) and lysine (K107), into the non-polar amino acid alanine (A). Alanine was chosen to avoid protein misfolding of the Eri1 SAP domain by introduction of other charged amino acids.

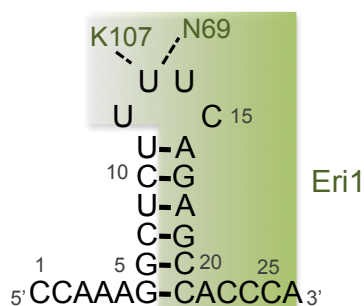


Figure 21: Contacts between histone stem loop RNA and Eri1. Intermolecular hydrogen bonding involving U13 of the histone RNA and K107 and N69 of the Eri1 protein is indicated by a dashed line.

The N69A K107A mutant was first analyzed for its exonuclease function towards 5.8S rRNA by testing the 5.8S rRNA running behavior on a large denaturing acrylamide-urea gel. Infection with retroviruses coding for wildtype Eri1 or mutant forms of Eri1 reconstituted *Eri1*-knockout MEF cells to about endogenous Eri1 levels (Figure 23g). As already seen for the RNA extracts from wildtype and Eri1-knockdown cells (Figure 18), a major short (S) and a less abundant long (L) form of 5.8S rRNA appeared on the gel and the *Eri1*-knockout cells revealed a 1-2 bp extension of both forms. Irrespective of its tag the Eri1 SAP/linker sequence (N69A

K107A) mutant was able to trim the 3' end of 5.8S rRNA, while the catalytically inactive (D130G E132G) mutant was impaired and the function of the delta N mutant seemed to be constricted (Figure 22). The result led to the conclusion that these both amino acids, N69 and K107, are not crucial for 5.8S rRNA processing.

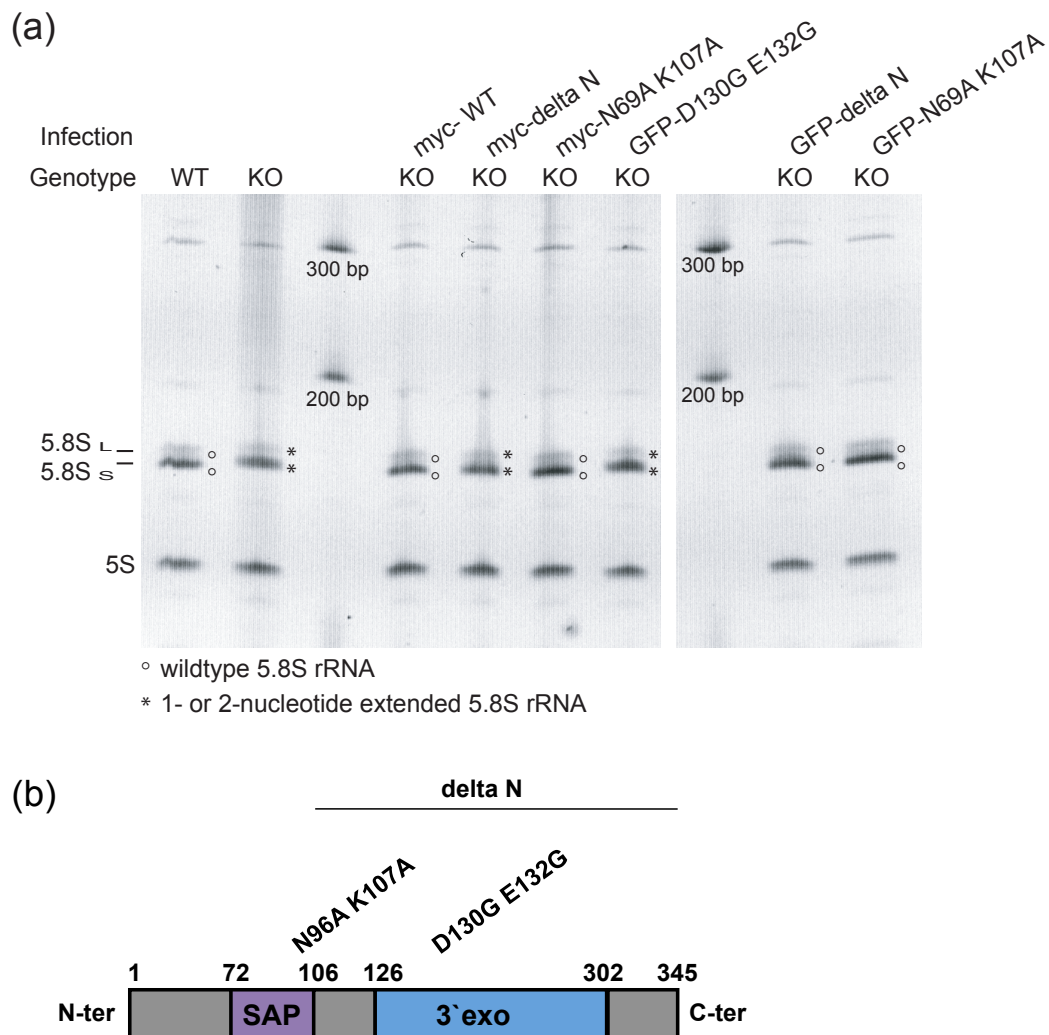


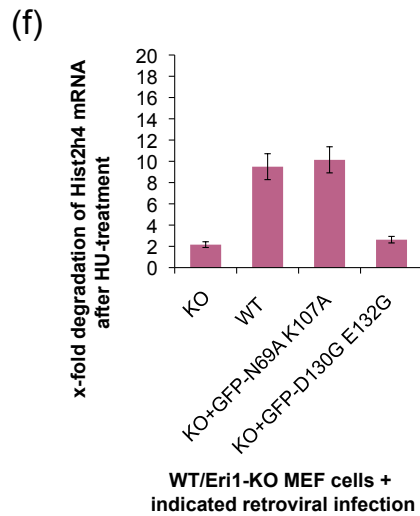
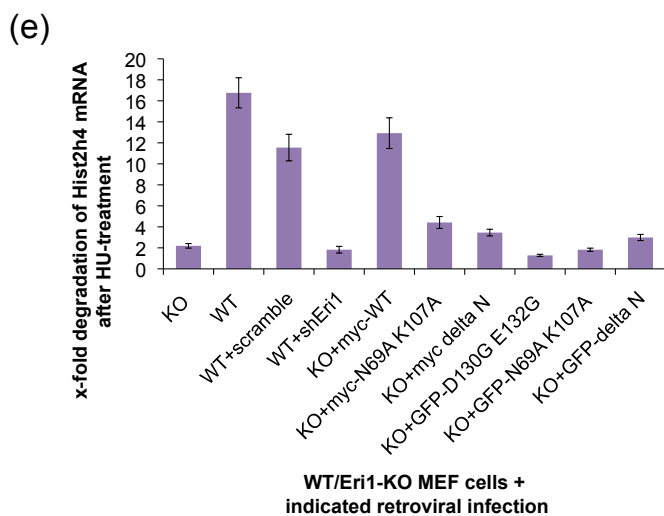
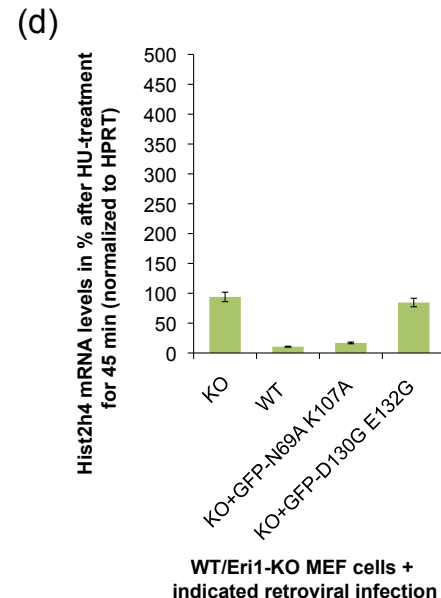
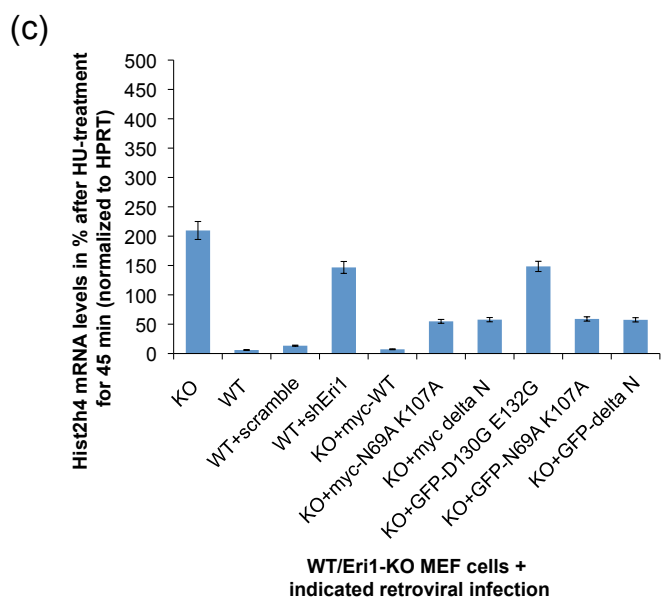
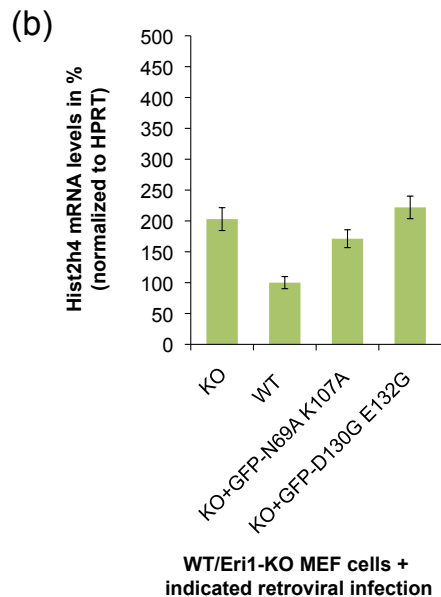
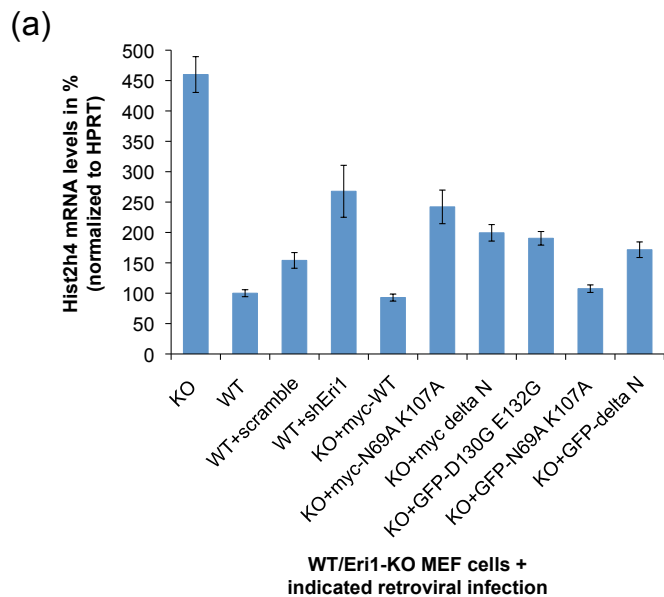
Figure 22: The Eri1 SAP/linker (N69A K107A) sequence mutant is not impaired in 5.8S rRNA 3' end trimming. (a) Ethidium bromide-stained RNA from wildtype and *Eri1*-knockout MEF cells left untransduced or infected with the indicated mutants, respectively. 5.8S_S: short isoform of 5.8S rRNA, 5.8S_L: long isoform of 5.8S rRNA. The according Western blot is shown in Figure 3-14g. (b) Schematic depiction of the structure of Eri1 and the employed point and deletion mutants.

Our lab has shown that Eri1 is needed for the degradation of stem-loop containing histone mRNAs at the end of S-phase (Höfig et al., in preparation). In the experiments, cells were treated with hydroxyurea (HU), which is used to mimick end of S-phase to trigger degradation of histone mRNAs. To compare *Eri1*-knockout MEF cells and control-wildtype MEF cells in their ability to regulate replication-dependent

histone mRNAs, Hist2h4 mRNA was measured by qRT-PCR in cells before HU-treatment, representing asynchronous growing cells, and in cells 45 min after addition of 5 mM hydroxyurea, representing the status in cells at the end of S-phase. The calculated ratio between these two time points represented the factor of degradation of Hist2h4 mRNA upon HU-treatment. This approach was extended comparing Hist2h4 mRNA degradation in wildtype MEF cells with or without Eri1 knockdown as well as in *Eri1*-knockout MEF cells with or without Eri1 reconstitution. For the reconstitution, retroviruses were produced to express wildtype-Eri1, the delta N deletion mutant, the catalytically inactive (D130G E132G) mutant and the SAP/linker sequence (N69A K107A) mutant. The assumption in this experiment was that a direct association of Eri1 with histone mRNAs is crucial for degradation at the end of S-phase. Hence, the Eri1 SAP/linker sequence (N69A K107A) mutant should be impaired in binding and processing of Hist2h4 mRNA, if sequence specific binding mediated by these two amino acids is irreplaceable.

In two independent experiments Hist2H4 mRNA levels have been measured by qRT-PCR in asynchronously growing MEF cells. The expression of Hist2H4 mRNAs was normalized to HPRT mRNAs and are displayed in percentage of histone mRNA that was measured in the wildtype MEF cells (Figure 23a,b). Consistent effects on the overall level of histone mRNAs in asynchronously growing cells were seen: low Hist2h4 levels in Eri1-sufficient and two to five fold increased levels of Hist2h4 in Eri1-deficient cells. The level of Hist2h4 mRNA in MEF cells after reconstitution with the myc- or GFP-tagged mutants, N69A K107A, delta N, and D130G E132G, tended to resemble rather the knockout than the wildtype situation. The variance of histone mRNA expression levels may also be affected by clonal variation, growth condition, relative contribution of the cells in the different cell cycle phases and counterregulation. However, it could be concluded that already in asynchronously growing MEF cells Eri1 expression seems to decrease Hist2h4 mRNA levels.

To investigate the impact of Eri1 in more detail, the change in histone mRNA levels in response to 45 min of HU-treatment was monitored (Figure 23c,d). The change in mRNA abundance was then expressed as x-fold decrease (Figure 23e,f).



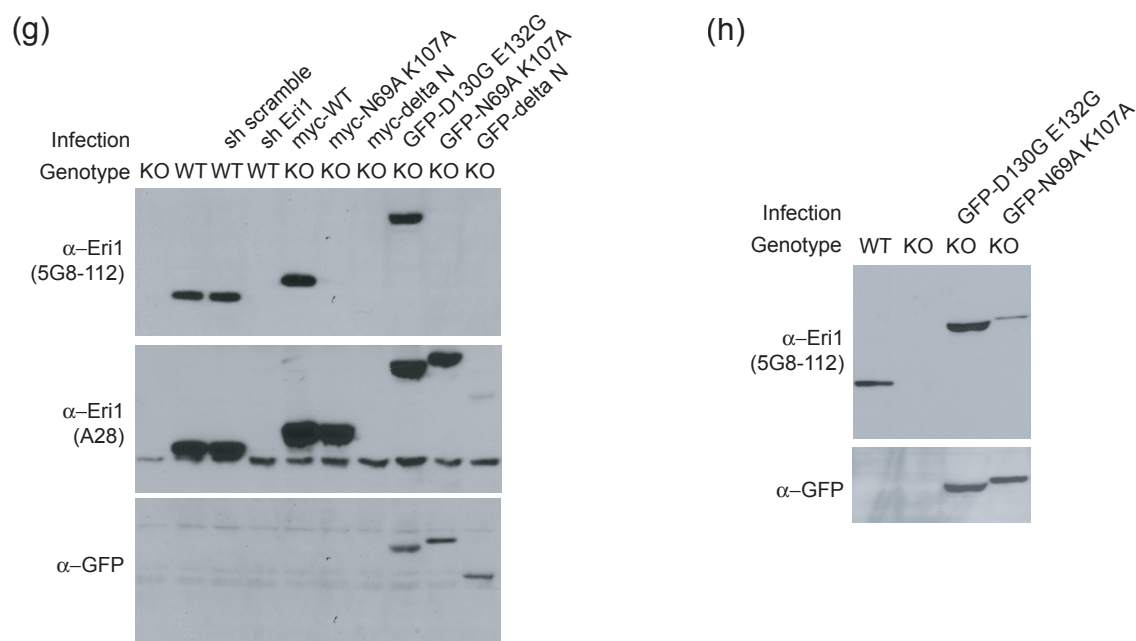


Figure 23: Eri1 initiates Hist2h4 mRNA degradation after HU-treatment, this is supported by sequence-specific binding. (a, b) Two independent experiments measuring Hist2h4 mRNA levels in the indicated MEF cells after retroviral infection using the pSUPER-puro for knockdown of Eri1 and the pMSCV-puro for reconstitution with wildtype-*Eri1* and mutants. Hist2h4 was detected by qRT-PCR and normalized to HPRT as well as a calibrator using the Light cycler 480 software (Roche). Then the Hist2h4 mRNA in wildtype MEF cells was set 100%. The normalized Target/Ref (Hist2h4/HPRT) value for wildtype MEF cells constituted 2.79 in the first experiment (a) and 2.72 in the second experiment (b). Duplicates were measured in the Light cycler to calculate error bars. (c, d) Hist2h4 mRNA levels in the indicated MEF cells after 45 min HU-treatment. Again, values were normalized to HPRT and the calibrator. (e, f) Degradation of Hist2h4 mRNA during incubation with hydroxyurea. For this depiction the Hist2h4 mRNA value measured before HU-treatment was divided by the Hist2h4 mRNA value measured after HU-treatment. The calculated result represents the factor of Hist2h4 mRNA degradation during 45 min HU-treatment. (g, h) Immunoblots using monoclonal anti-Eri1 (5G8-112), polyclonal anti-Eri1 (A28) and polyclonal anti-GFP antibodies to detect Eri1, myc-tagged Eri1 and GFP-tagged Eri1 expression in the MEF cells that were examined in the acrylamide-urea gels and in the HU-experiments. The monoclonal anti-Eri1 antibody recognizes an epitope in the SAP domain, that is why the deletion and point mutants are not or less detected.

Although the basal level of Hist2h4 mRNA was similar in the wildtype MEF cells of both experiments (calibrator-normalized Hist2h4/HPRT value: 2.79 in the first experiment and 2.72 in the second experiment, Figure 23a,b), the reduction upon HU-treatment differed. In the first experiment the Hist2h4 mRNA was reduced by a factor of 16.8 after HU-treatment (Figure 23e), whereas in the second experiment the Hist2h4 mRNA was only reduced by a factor of 9.5 (Figure 23f). Again, this could be due to the variability of the cell culture system. However, only a 2-fold reduction of Hist2h4 was measured in the Eri1-knockout cells in both experiments (Figure 23e,f), confirming that the Eri1 protein is an important factor for the degradation of replication-dependent histone mRNAs. The catalytically inactive (D130G E132G)

mutant as well as the N-terminal deletion mutant, were not able to initiate rapid Hist2h4 mRNA degradation (Figure 23e,f). Thus, catalytic activity as well as stable binding via the SAP domain to the histone mRNA target seemed to be crucial for Eri1 to initiate histone mRNA degradation. Importantly, the new SAP/linker sequence (N69A K107A) mutant could not lead to rapid degradation of Hist2H4 mRNA in the first experiment, represented by a degradation factor of 4.4 for myc-tagged N69A K107A, and by a factor of 1.8 for GFP-tagged N69A K107A (Figure 23e). This experiment suggested that the two amino acids in close proximity to the U13 of stem-loop histone mRNAs are indeed critical for the binding of histone mRNA. Conversely, in the second experiment the SAP/linker sequence (N69A K107A) mutant could decrease the levels of histone Hist2H4 mRNA with a degradation factor of 10.1 (Figure 23f). No significant difference in the Eri1 expression levels could be detected by Western blotting (Figure 23g,h). Hence, the different outcome in the first and second experiment concerning the ability of the SAP/linker sequence (N96A K107A) mutant to initiate degradation of Hist2h4 mRNA may have been caused by altered cell conditions. It can be concluded from these two experiments that although the two amino acids, N69 and K107, support binding to histone mRNA they are not crucial for specific binding of Eri1 to histone mRNA.

Thomas Mullen and William Marzluff have published that upon a 80-90% Eri1 knockdown the degradation rate of cell cycle dependent histones in response to HU-treatment did not change (Mullen and Marzluff, 2008). In contrast, quantitative RT-PCR analysis of Hist2h4 mRNA levels in MEF cells before and after HU-treatment, showed that complete knockdown or knockout of Eri1 did indeed strongly impair the degradation of Hist2H4 mRNA (Figure 23e,g). Additionally, the level of Hist2h4 mRNA in normal growing cell cultures was already increased in Eri1-knockout MEF cells or after Eri1 knockdown. These findings make Eri1 an important factor in the regulation of replication-dependent histone mRNA in growing MEF cells, initiating the degradation of histone mRNAs at the end of S-phase.

3.2 Dymorphology phenotype of *Eri1*-knockout mice

From the list of phenotypes that have been found in the systematic screen of *Eri1*-deficient mice in the German Mouse Clinic (section 3.1.1.3), the skeletal anomalism was chosen for a detailed description (section 3.2.1) and for an investigation of its underlying molecular mechanism (section 3.2.2, 3.2.3, 3.2.4, 3.2.5). This has led to the analysis of the impact of *Eri1* on miR-196a (section 3.2.6) and *Eri1*'s function on miRNA-mediated Hox mRNA silencing (section 3.2.7).

3.2.1 *Eri1*-knockout mice show a homeotic transformation

3.2.1.1 Additional rib pair in *Eri1*-knockout mice

In the primary screen in the German Mouse Clinic 10 NMRI x C57BL/6 *Eri1*-knockout and wildtype control mice, females and males each, were subjected to dual-energy X-ray analysis. The obtained images revealed a dymorphology phenotype: 80% of NMRI x C57BL/6 *Eri1*-knockout mice developed an additional 14th rib pair on vertebra #21 (Table 8). Heterozygous mice, analyzed during secondary screens, were identical to wildtype animals showing a normal number of 13 rib pairs and thoracic vertebrae. Interestingly, all female animals that developed the additional thoracic rib pair, also displayed an additional vertebra. Thus, the number of lumbar vertebrae, defined as those vertebrae without ribs that are posterior to the thorax and anterior to the vertebrae linked to the pelvic bones (sacral vertebrae), remained at the normal number of 6 in female mice. In contrast, male *Eri1*-knockout animals developed the additional 14th rib pair either in the presence or in the absence of an additional vertebra. Hence, in male *Eri1*-knockout mice the number of lumbar vertebrae varied between 6 and 5.

To exclude that the developmental phenotype of *Eri1*-knockout mice depends on the mixed NMRI x C57BL/6 background, one of the rare surviving litters on a pure C57BL/6 background was analyzed. The *Eri1*-knockout phenotype could be confirmed to also occur in mice on inbred C57BL/6 background as shown on the X-ray microtomography (μ CT) pictures (Figure 24). Again, both the female and male *Eri1*-knockout mouse, showed an additional 14th rib pair, but only the female mouse also developed an additional vertebra.

Table 8: Skeletal dysmorphology in *Eri1*-knockout mice. The results from X-ray absorptiometry have been grouped according to the presence of a normal or an aberrant number of ribs, thoracic and lumbar vertebrae. wildtype, *Eri1*-heterozygous, and *Eri1*-knockout mice were analyzed from the F2 generation of a mixed NMRI x C57BL/6 background. (Primary and secondary screen in the German Mouse Clinic.)

Phenotype		Females			Males		
		WT	HET	KO	WT	HET	KO
Number of ribs	normal (26)	10	4	3	10	4	1
	aberrant (28)	-	-	7	-	-	9
Number of thoracic vertebrae*	normal (13)	10	4	3	10	4	1
	aberrant (14)	-	-	7	-	-	9
Number of lumbar vertebrae*	normal (6)	10	4	10	10	4	7
	aberrant (5)	-	-	-	-	-	3
Total number of mice		10	4	10	10	4	10

* In this table, the rib bearing vertebrae were defined as thoracic vertebrae and vertebrae posterior to rib bearing vertebrae and anterior to the first sacral vertebra were defined as lumbar vertebrae.

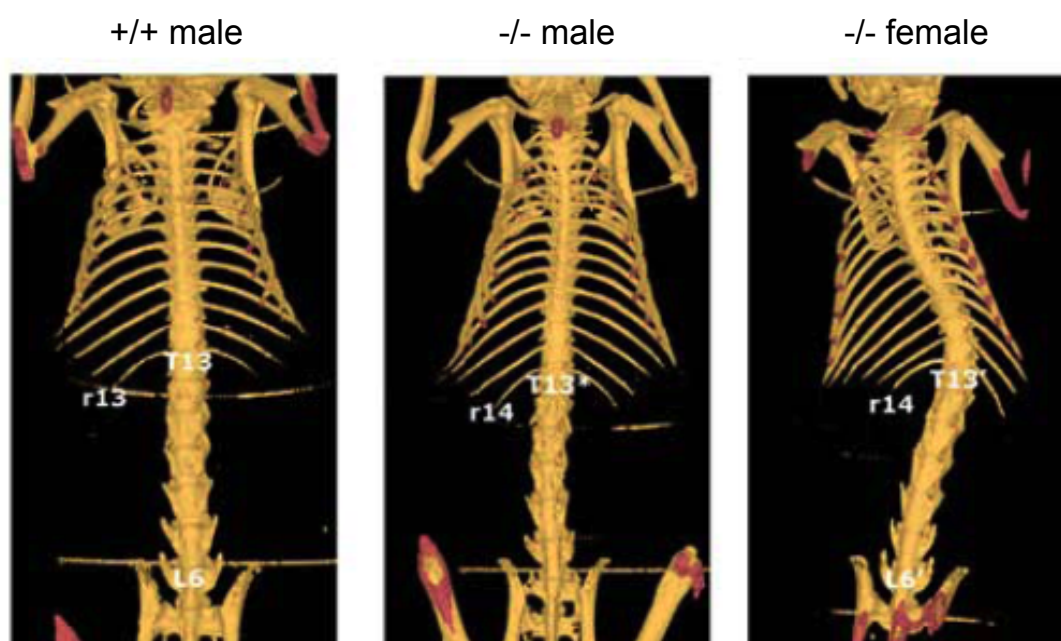


Figure 24: *Eri1*-knockout mice show a skeletal dysmorphology phenotype. μ CT pictures of one female and one male *Eri1*-knockout mouse with an aberrant 14th rib pair, compared to the normal number of 13 pairs of ribs in wildtype mice (C57BL/6). Additionally, the female *Eri1*-knockout mouse revealed an extra vertebra. (In collaboration with Wolfgang Hans.)

3.2.1.2 In *Eri1*-knockout mice 8 pairs of ribs are fused to the sternum

In wildtype mice 7 of the 13 rib pairs are fused to the sternum. La Theta scans of *Eri1*-knockout mice revealed the fusion of an 8th pair of ribs to the sternum (Figure 25a). For a more detailed investigation skeletal stains were performed on adult and newborn *Eri1*-knockout and control mouse skeletons. The method uses alcian blue to stain the cartilage and alizarin red to stain the bones. The skeletons confirmed the additional 14th rib pair in *Eri1*-knockout mice as well as the aberrant fusion of the 8th rib pair adjacent to the 7th rib pair at the sternum. Through this fusion a bony process at the last sternebra developed in several *Eri1*-knockout animals. In contrast, all wildtype animals showed the normal fusion of only the 6th and 7th rib pairs to that sternebra (Figure 25b).

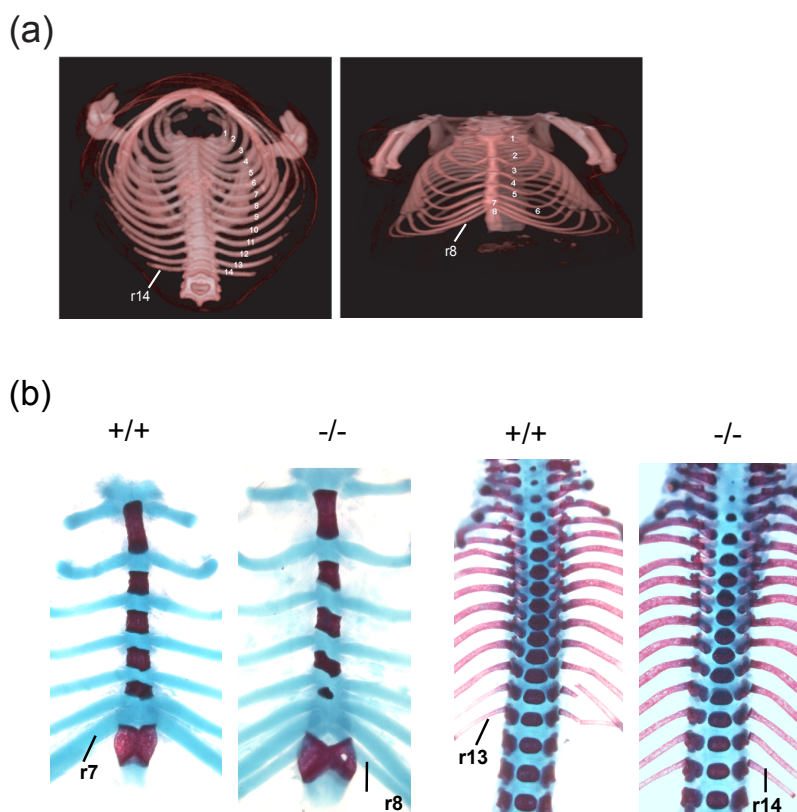


Figure 25: In *Eri1*-knockout mice an 8th rib pair is fused to the sternum. (a) The La Theta scanner was used to take pictures of the ribcage of *Eri1*-knockout mice. Representative picture of an *Eri1*-knockout male (NMRI x C57BL/6) showing an additional 8th pair of ribs attached to the sternum. (b) Skeletons stained with alcian blue (staining the cartilage) and alizarin red (staining the bone). Representative pictures of one wildtype and one *Eri1*-knockout newborn (NMRI x C57BL/6). The wildtype newborn shows the normal number of 13 rib pairs and the fusion of the 6th and 7th pair of ribs to the last sternebra. The *Eri1*-knockout newborn reveals the aberrant number of 14 rib pairs and the fusion of the 6th, 7th and 8th pair of ribs to the same sternebra. (In collaboration with Christian Cohrs.)

3.2.1.3 Anteriorization of vertebrae in *Eri1*-knockout mice

In depth analysis of the thoracic and lumbar vertebrae demonstrated that *Eri1* deficiency led to a full transformation of the 8th thoracic vertebra (T8) to a 7th thoracic vertebra (T7') (Figure 26a). Consequently, the vertebrae T7 and T7' looked identical in *Eri1*-knockout mice. This kind of homeotic transformation is called anteriorization.

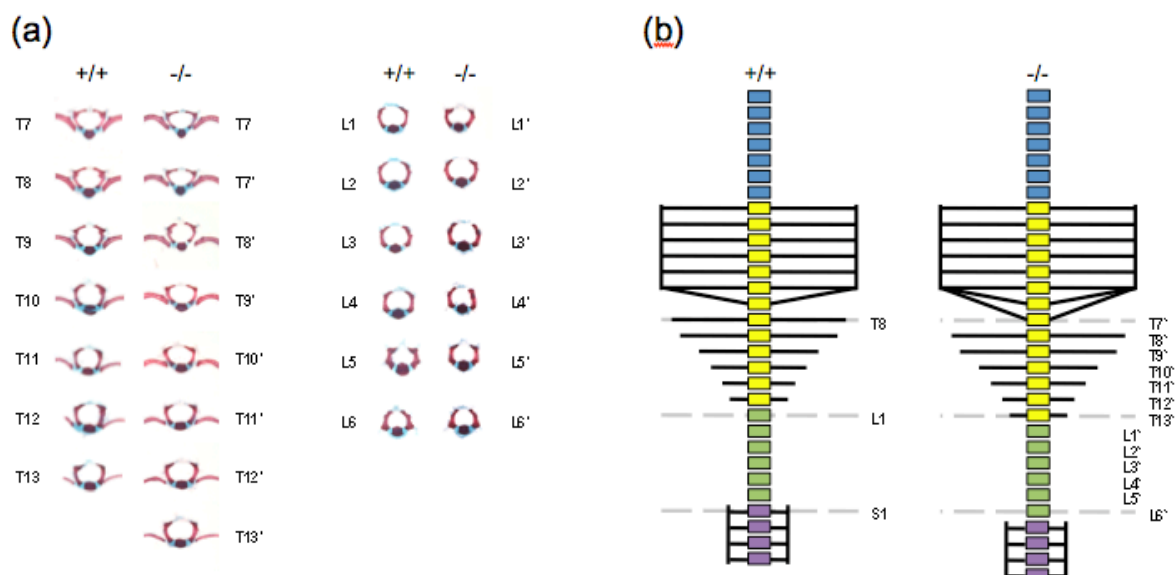


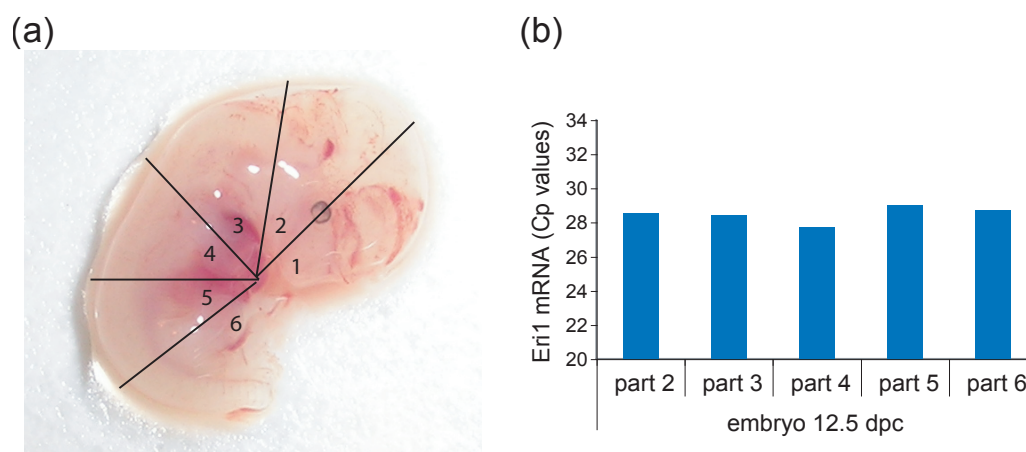
Figure 26: Anteriorization of thoracic, lumbar, and sacral vertebrae in *Eri1*-knockout mice. (a) Individual thoracic vertebrae from skeletal stains of wildtype and *Eri1*-knockout newborns (NMRI x C57BL/6). (In collaboration with Christian Cohrs.) (b) Schematic representation of the skeletal phenotype of *Eri1*-knockout mice compared to wildtype control mice.

Furthermore, the duplication of the 7th vertebra resulted in an extension of the anteriorization towards the sacral vertebrae and included the homeotic transformation of L1 to T13' and S1 to L6' (Figure 26a,b). This phenotype was observed in all female *Eri1*-knockout mice as well as in those male *Eri1*-knockout mice that developed the additional 14th rib pair in presence of an additional vertebra. In contrast, the male *Eri1*-knockout mice with 14 pairs of ribs with no additional vertebra, only showed a partial transformation (T8 to T7'). This partial transformation did only lead to anteriorization of the more posterior located vertebrae up to the 3rd lumbar (L3). Hence the lumbar vertebra L1 still adopted a T13' phenotype, but the sacral vertebra S1 did not transform into L6 identity. Consequently, the number of thoracic vertebrae rose to a total of 14 vertebrae, but the number of lumbar vertebrae dropped to 5 (Table 8). These results argued for the development of an additional

true rib in the *Eri1*-knockout mice caused by a homeotic transformation into the anterior direction of each vertebra starting at the 8th thoracic (T8).

3.2.2 High expression of *Eri1* in the prevertebrae of embryos

To investigate *Eri1* expression in the embryo during development, *Eri1* mRNA and *Eri1* protein levels were measured by qRT-PCR and Western blot methods. Embryos at 12.5 dpc were sliced into 6 parts along their anterior-posterior axis and the abundance of *Eri1* RNA or protein was examined in the individual tissue extracts (Figure 27a). *Eri1* mRNA as well as *Eri1* protein detection revealed that already at early embryonic developmental stages *Eri1* is expressed all over the body (Figure 27b,c). To show the distribution of *Eri1* in the embryo in more detail immunohistochemistry stains using affinity-purified polyclonal anti-*Eri1* antibodies was performed. Despite the fact that *Eri1* was expressed in equal amount in the different sections of the embryo, there was higher *Eri1* expression in the prevertebrae and in the brain, here especially in the cortex and in the plexus choroideus. The intensive stain of the liver might be due to a non-specific peroxidase activity in hepatocytes and abundant *Eri1* protein in proliferating hematopoietic cells (Figure 27d,e,f,g). The predominant expression of *Eri1* protein in the prevertebrae of embryos gave a strong indication of *Eri1* function in the development of vertebrae as well as ribs.



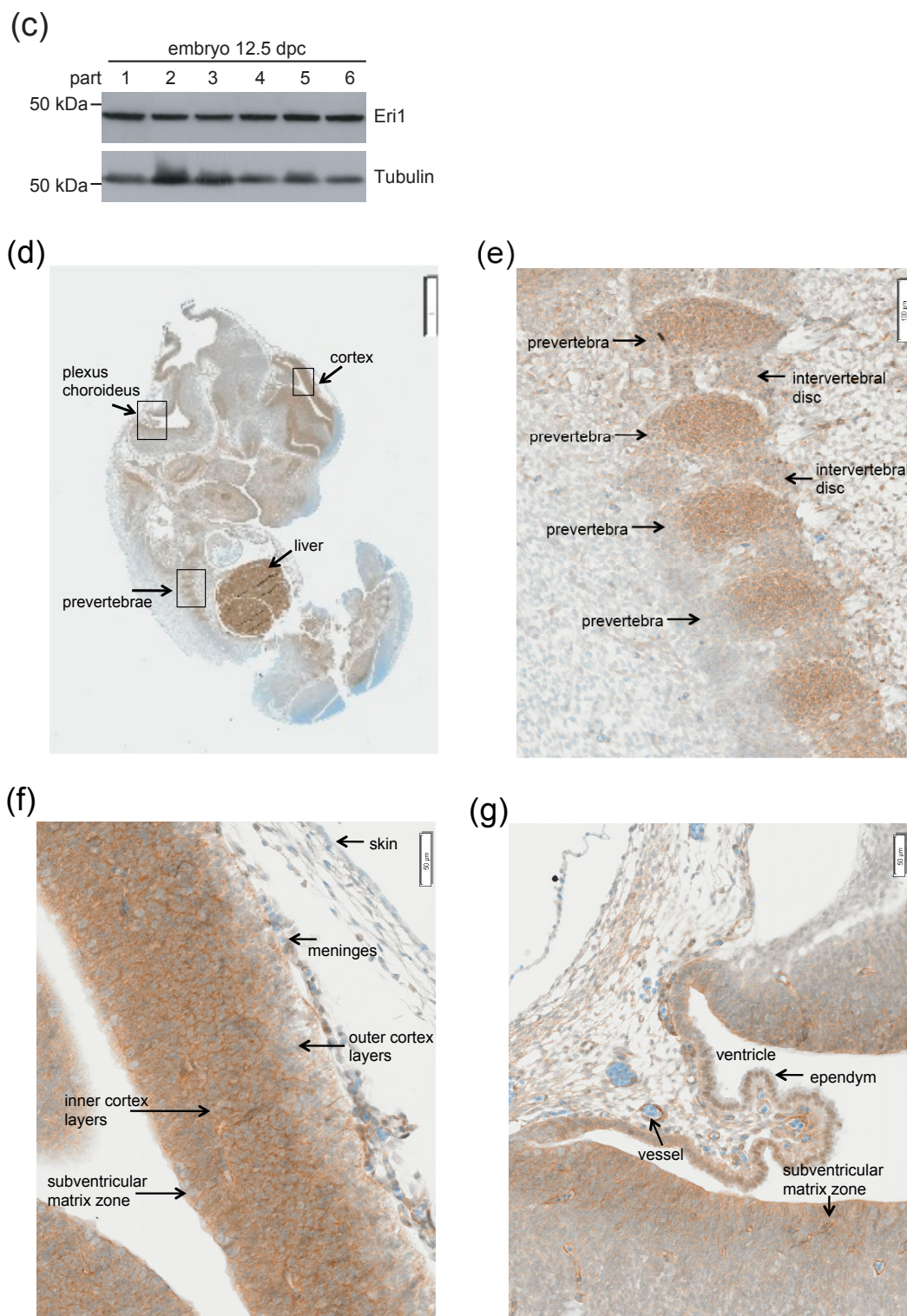


Figure 27: Eri1 expression pattern in the mouse embryo. (a) Mouse embryos (E12.5) were sliced into 6 parts along their anterior-posterior axis. (b) Eri1 mRNA levels in part 2-6 from a wildtype embryo (C57BL/6) was detected by qRT-PCR. Part 1 was not analyzed, but was used for genotyping. (c) The ubiquitous expression of Eri1 protein is shown by immunohistochemistry using a monoclonal anti-Eri1 antibody. Tubulin was included as loading control. The Western blot of the wildtype embryo on BalB/c background is a representative out of eight BALB/c and two C57BL/6 embryos analyzed. (d-g) Immunohistochemistry stains using affinity-purified polyclonal anti-Eri1 antibody on an embryo at E12.5 (BALB/c). (d) Depiction of the whole embryo. (e) Blow-up of the prevertebrae. (f) Blow-up of the plexus choroideus. (g) Blow-up of the cortex. (In collaboration with Frauke Neff.)

3.2.3 Molecular phenotyping of *Eri1*-knockout embryos

To investigate *Eri1*-knockout dysmorphology on the molecular basis, close to genome-wide microarrays were used for mRNA expression profiling of embryos (E12.5). Total RNA was isolated from the trunk, omitting the heads, of four *Eri1*-knockout and four wildtype control animals (C57BL/6) and sent for a secondary screen analysis to the German Mouse Clinic. Table 9 summarizes the results of three chip hybridizations; the statistical analysis identified 34 significantly down-regulated mRNAs in the experiments of three animals (*Eri1*-knockout 2, 3 and 4). Interestingly, no up-regulated mRNAs were found.

The expression pattern of *Eri1*-knockout 1 was different from the other three embryos (Table 10) and was therefore excluded from the statistical analysis. The calculated false discovery rate of 6.3% and the different brightness of the color in the heat plot (Table 10) indicated high biological variability of the expression patterns across the analyzed embryos.

In *Eri1*-knockout 2, 3 and 4 the differential expression of *Hba-a1* and *Hba-a2* was confirmed by four independent probes on the array. These different probes for the identical gene showed similar regulation providing confidence for the expression profiling data. In order to analyze whether specific functional annotations were over-represented among the regulated genes, 12 of the down-regulated genes were classified into two categories of Gene Ontology terms: molecular functions and biological processes (Table 11). Over-representation of four molecular functions was detected: transporter and catalytic activity as well as binding of adenyly nucleotides and metal ions. In the category of biological processes cell growth, metabolism of proteins and nucleotides as well as defense response, signal transduction and homeostasis were over-represented pathways. Only 2 of the 12 genes are associated with developmental processes: *Afp* (alpha feto protein) is a major plasma protein produced by the yolk sac and the liver during fetal life (Jin et al., 2009). *Abr* (active BCR-related gene) plays an important role during vestibular morphogenesis (Kaartinen et al., 2002).

Finally, although smaller differences in the expression of several genes were found in this molecular phenotyping approach, the results did not reveal a candidate gene being a key player in skeletal patterning during embryogenesis.

Table 9: Heat plot of gene expression profiles from six DNA microarray experiments of *Eri1*-mutant versus control embryos. One dye-flip pair represents two experimental replicates of each analyzed animal. One Array TAG ID is the unique probe identifier from the Lion Bioscience clone set. Official gene symbols are given. The scale bar encodes the ratio of the fold induction (red is up-regulation and green down-regulation in mutant mice). (In collaboration with Marion Horsch.)



Mean ratio	K02	K03	K04	Array TAG ID	Gene symbol	Gene name
-2.17				MG-8-71j2	Nup155	nucleoporin 155
-2.59				MG-4-146n10	Hbb-b1	hemoglobin, beta adult major chain
-2.08				MG-8-84a9	Eraf	erythroid associated factor
-2.07				MG-6-69d8	Gripap1	GRIP1 associated protein 1
-1.87				MG-4-2p9	DQ012052	
-1.70				MG-4-2j8	H2-Ab1	histocompatibility 2, class II antigen A, beta 1
-1.81				MG-8-118e21	Alb	albumin
-1.95				MG-8-10b11	Hbb-b2	hemoglobin, beta adult minor chain
-1.58				MG-6-19n14	Abr	active BCR-related gene
-1.66				MG-4-4k23	Uhrf1bp1l	UHRF1 (ICBP90) binding protein 1-like
-1.83				MG-4-145j12	Hba-a1	hemoglobin alpha, adult chain 1
-1.74				MG-4-3k1	Hba-a1	hemoglobin alpha, adult chain 1
-1.84				MG-4-148e12	Hba-a2	hemoglobin alpha, adult chain 2
-1.68				MG-15-165i2	AY438023	
-1.77				MG-6-22j19	CR514268	
-1.94				MG-6-1o11	Rab5b	RAB5B, member RAS oncogene family
-1.77				MG-4-148e3	Hba-a2	hemoglobin alpha, adult chain 2
-1.49				MG-4-146d10	Tysnd1	trypsin domain containing 1
-1.79				MG-4-86f7	Hba-a2	hemoglobin alpha, adult chain 2
-1.76				MG-8-54o6	Rif	rearranged L-myc fusion sequence
-1.81				MG-4-5m17	Hba-a2	hemoglobin alpha, adult chain 2
-1.66				MG-4-5j21	Il6st	interleukin 6 signal transducer
-1.66				MG-4-147o3	Hba-a1	hemoglobin alpha, adult chain 1
-1.75				MG-15-226i17	Uba5	ubiquitin-like modifier activating enzyme 5
-1.69				MG-8-86g2	1110017116Rik	
-1.59				MG-12-199o10	Cpeb4	cytoplasmic polyadenylation protein 4
-1.57				MG-8-35j22	Afp	alpha fetoprotein
-1.55				MG-8-11g1	Slc4a1	solute carrier family 4, member 1
-1.71				MG-4-3b2	Hba-a1	hemoglobin alpha, adult chain 1
-1.69				s1-Fbxo32	Fbxo32	F-box protein 32
-1.46				MG-6-32i2	1190017012Rik	
-1.67				MG-14-64n9	Mark3	MAP/microtubule affinity-regulating kinase 3
-1.50				MG-3-80m18	Txndc3	thioredoxin domain containing 3
-1.80				MG-26-270k2	Rnaseh2b	ribonuclease H2, subunit B

Table 10: Heat plot of gene expression profiles from eight DNA microarray experiments of *Eri1*-mutant versus control embryo. *Eri1*-knockout 1 shows a different expression pattern in the regulated genes. (In collaboration with Marion Horsch.)

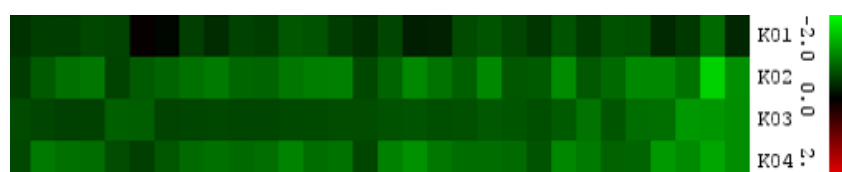


Table 11: Functional classification of the regulated genes in *Eri1*-knockout embryos. In order to analyze whether specific functional annotations were over-represented among the regulated genes EASE (a module of the DAVID database) was used to classify the genes for two categories of Gene Ontology (GO) terms. (In collaboration with Marion Horsch.)

Category	GO term	Gene symbol
Molecular function	transporter activity	AFP ; ALB; NUP155; SLC4A1; TXNDC3
	catalytic activity	GRIPAP1; MARK3; RAB5B; TXNDC3
	adenyl nucleotide binding	MARK3; TXNDC3
	transition metal ion binding	AFP ; RLF
Biological processes	cell growth and/or maintenance	AFP ; ALB; FBXO32; NUP155; SLC4A1
	protein metabolism	ERAF; MARK3
	nucleotide and nucleic acid metabolism	RLF; TXNDC3
	defense response	AFP ; IL6ST
	signal transduction	ABR ; IL6ST
	homeostasis	ALB; SLC4A1

3.2.4 Literature and database research to reveal *Eri1* target candidates

The MGI (Mouse Genome Informatics) database is a resource for information about the laboratory mouse, providing integrated genetic, genomic and biological data (The Jackson Laboratory, <http://www.informatics.jax.org/>).

In order to find other laboratory mice displaying the same or a similar phenotype as the *Eri1*-knockout mice, the search term: *increased rib number* was used to obtain a list of 64 genotypes. Looking closer at these candidates, the development of an additional rib pair at the first lumbar vertebra in wildtype mice, vertebra #21, has been reported for mouse mutants with a single and combined deletion of the *Hoxc8*, *Hoxa9*, *Hoxc9* and *Hoxa10* gene (Chen and Capecchi, 1997; Fromental-Ramain et al., 1996a; Le Mouellic et al., 1992; Rijli et al., 1995; Satokata et al., 1995; Suemori, 1995; van den Akker et al., 2001; Wellik and Capecchi, 2003). All gene deletion mutants showing an additional rib pair on vertebra #21 are summarized in Table 12. However, only *Hoxc8* and *Hoxc9*-deficient animals also share the other prominent skeletal abnormality of the *Eri1*-deficient mice, which is the fusion of the 8th rib pair to the sternum (Le Mouellic et al., 1992; Suemori et al., 1995; van den Akker et al., 2001). In the case of *Hoxc9*-deficient animals the 9th rib was found to partially fuse to

the sternum as well (Suemori, 1995), indicating that Hoxc9 deficiency may result in a slightly different abnormality compared to *Eri1*-deficient mice.

Finally, the perinatal lethality due to an unknown cause is shared between *Eri1*- and *Hoxc8*-deficient mice. Individuals of both genotypes die within a few days after birth, and in both cases mortality of knockout animals was partially rescued if they were generated on an outbred strain background (section 3.1.1.2) (Ansel et al., 2008; Le Mouellic et al., 1992; Tiret et al., 1998; van den Akker et al., 2001)

Table 12: All published Hox gene(s) deletion mutants showing an additional rib pair on vertebra #21.

Type of mutant	Hox gene(s)	Publication(s)
Single deletion mutants	Hoxc8	Le Mouellic et al., 1992; van den Akker et al., 2001
	Hoxa9	Fromental-Ramain et al., 1996(a)
	Hoxc9	Suemori, 1995
	Hoxa10	Rijli et al., 1995; Satokata et al., 1995
Double deletion mutants	Hoxc8/d8	van den Akker et al., 2001
	Hoxa9/d9	Fromental-Ramain et al., 1996(a)
	Hoxa9/b9	Chen and Capecchi, 1997
Deletion of all homologous genes from one cluster	Hoxb8/c8/d8	van den Akker et al., 2001
	Hoxa9/b9/c9/d9 ^{*1}	Chen and Capecchi, 1997
	Hoxa10/c10/d10 ^{*2}	Wellik and Capecchi, 2003

^{*1} Additional rib pair on vertebra #21, #22, #23 and #24.

^{*2} Rib processes on all lumbar and sacral vertebrae.

It seemed unlikely that the Eri1 protein directly upregulates Hoxc8 gene expression, because so far Eri1 has not been described in the context of transcription activation. However, the homologue of Eri1 in *C. elegans* was published to inhibit RNAi in neurons and it was suggested that Eri1 degrades siRNAs (Kennedy et al., 2004). SiRNAs and miRNAs show pronounced similarities in their biogenesis and silencing activity, and it has been shown that some proteins are active in several RNAi pathways (section 1.3.1). This made mouse Eri1 a promising candidate for miRNA regulation.

The Targetscan database (Targetscan 5.1, <http://www.targetscan.org/>), which predicts mRNA targets of mammalian miRNAs and vice versa, was used to find promising miRNAs for Hoxc8 mRNA regulation. The database research revealed, that the Hoxc8 UTR exhibits 4 conserved and 1 non-conserved recognition motifs for miR-196a/b. This makes Hoxc8 the first hit on the list of predicted target proteins for miR-196a/b. The list is ranked due to the calculation of the total context score, which

is based on the type, the number and the context of miRNA-binding sites on the target mRNA (Grimson et al., 2007). Importantly miR-196a and miR-196b are expressed from Hox clusters as well, so that they are regulated by the same epigenetic temporal and spatial control mechanisms (Soshnikova and Duboule, 2009b). The Hoxc9 mRNA is not on the list of predicted targets of miR-196a/b, suggesting that Hoxc9 is less likely to be affected by miRNA overexpression in the *Eri1*-deficient mice. Another published target of miR-196a/b is Hoxb8, which has a nearly perfect complementary sequence for miR-196a/b in its UTR. This makes Hoxb8 a pronounced target because its mRNA was rather degraded than translationally inhibited upon miR-196a expression (Hornstein et al., 2005; Mansfield et al., 2004; Yekta et al., 2004). Very recently, it has also been shown that during chick development knockdown of miR-196 induces expansion of the anterior limit of Hoxb8 and thereby induces a cervical to thoracic homeotic transformation (McGlinn et al., 2009). Together, these findings gave a strong indication to investigate Hoxc8 and also Hoxb8 expression in *Eri1*-deficient embryos.

3.2.5 Shift of Hox gene expression in *Eri1*-knockout embryos

3.2.5.1 Posterior shift of Hoxc8 expression in *Eri1*-knockout embryos

Embryos were analyzed at 12.5 dpc, a time at which the anterior boundary of Hox expression has been established in embryonic development (Wellik, 2007). In section 3.1.2 it was shown that *Eri1* protein expression could be detected in all embryo parts along the anterioposterior axis and the detailed analysis in immunohistochemistry stains supported *Eri1* function in prevertebrae by revealing enhanced *Eri1* expression levels. Analyzing Hoxc8 expression in embryo sections by Western blot, high protein levels were found only in part 4 and 5, whereas a faint band was present in part 3 and 6 and no Hoxc8 protein was determined in the most anterior parts 1 and 2 (Figure 28a).

Similar to the protein levels, Hoxc8 mRNA could not be detected at significant levels by qRT-PCR in the anterior part 2; with a mean Cp-value of 39.2 in wildtype embryos the detection border was reached. But Hoxc8 mRNA was measured at strongly increased levels in the posterior half of the embryo. Different from the protein level, the mRNA showed a steep increase of Hoxc8 expression that was already observed in part 3 of the wildtype embryo. And, in contrast to the rapidly declining Hoxc8

protein levels in the most posterior part 6, its mRNA expression declined much less (Figure 28a,b). A similar expression profile was determined in wildtype embryo parts for Hoxb8 mRNA levels (Figure 28c).

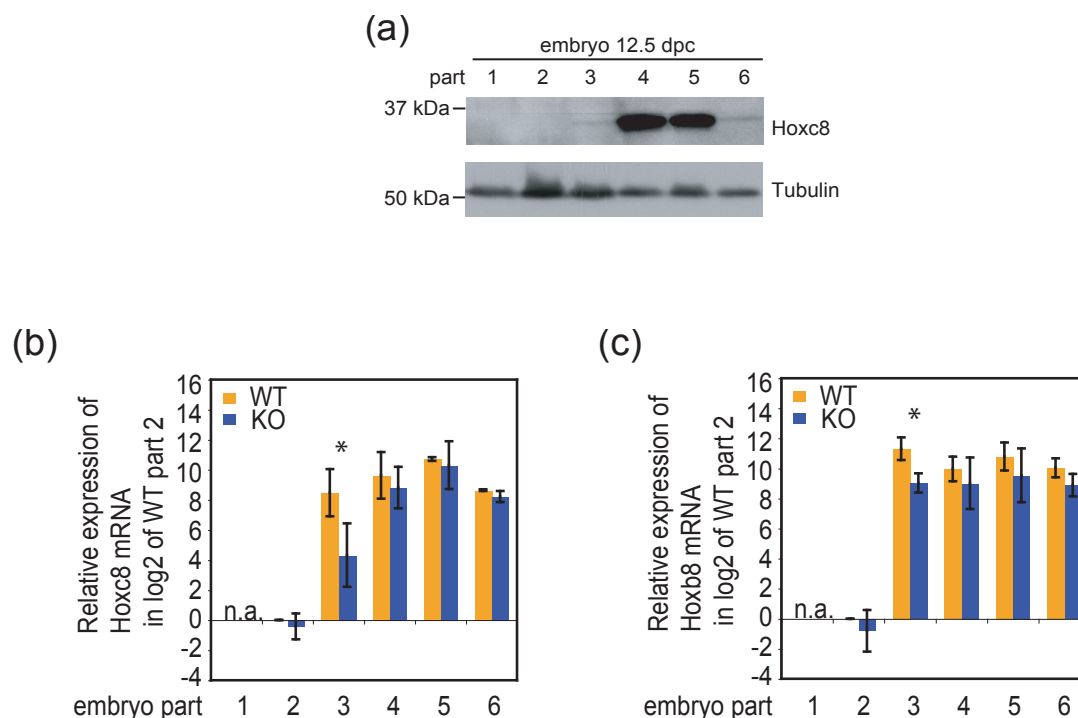


Figure 28: The anterior border of Hoxc8 and Hoxb8 expression is shifted posterior in *Eri1*-knockout mice. (a) Mouse embryos were sliced into 6 parts along their anterior-posterior axis at 12.5 dpc (Figure 3-18a). The position specific expression pattern of Hoxc8 protein is shown by immunohistochemistry using a monoclonal anti-Hoxc8 antibody. Tubulin was included as loading control. The Western blot of the wildtype embryo on BALB/c background is one representative out of eight BALB/c and two C57BL/6 embryos analyzed. (b, c) Hoxc8 and Hoxb8 mRNA levels were detected by qRT-PCR in three *Eri1*-knockout and wildtype embryos (C57BL/6) and normalized to the pbgd housekeeping gene. The mean Cp-value of the three wildtype embryos in part 2 was 39.2 measuring Hoxc8 mRNA and 39.2 measuring Hoxb8 mRNA, compared to 26.4 measuring pbgd mRNA. The Δ Cp Hoxc8/pbgd or Hoxb8/pbgd of wildtype part 2 was set 1 (log₂ of 0). The expression of Hoxc8/Hoxb8 mRNA in the six embryo parts is shown on a logarithmic scale as multiples of the mRNA expression in part 2 of the wildtype embryos. (b) * Significantly less Hoxc8 mRNA in part 3 of *Eri1*-knockout embryos (T test, one-tailed, unpaired, P = 0.026). (c) * Significantly less Hoxb8 mRNA in part 3 of *Eri1*-knockout embryos (T test, unpaired, P = 0.008). (The single embryo measurements are shown in the supplementary.)

Comparing Hoxc8 mRNA expression in *Eri1*-knockout and wildtype embryos, on average a ~16-fold decreased expression of Hoxc8 mRNA in part 3 of *Eri1*-knockout embryos was measured. A statistically significant ~4 fold decrease was also observed for the Hoxb8 mRNA in part 3 of *Eri1*-knockout embryos (Figure 28b,c). Both Hoxc8 and Hoxb8 mRNAs only displayed significant regulation by *Eri1* in the embryo part 3, which, in the wildtype embryo, may include the first anterior segments

with high *Hoxc8* and *Hoxb8* expression. These findings suggest an exclusive regulation at the anterior boundary of *Hoxc8* and *Hoxb8* mRNA expression by *Eri1* and the posterior shifted expression of these mRNAs in the absence of *Eri1*.

3.2.5.2 miR-196a expression pattern in wildtype and *Eri1*-knockout embryos

The miRNAs miR-10 and miR-196 have been proposed to restrict expression of Hox target genes at their anterior boundaries (Mansfield et al., 2004; McGlenn et al., 2009; Yekta et al., 2004; Yekta et al., 2008). Importantly, the 3' UTR of the *Hoxc8* mRNA has 4 highly conserved and one non-conserved binding site for miR-196a/b (section 3.2.4). Analyzing the mature miR-196a expression in embryo parts 1-6 using qRT-PCR miR-196a can already be detected in anterior regions (Figure 28a), but the steep increase to high expression of mature miR-196a was shifted into the posterior direction compared to *Hoxc8* mRNA expression in the wildtype situation (Figure 28a, Figure 29a). This is consistent with the spatial and temporal colinearity of Hox cluster gene expression, because the loci encoding miRNAs of the miR-196 family are positioned 5' to group 8 Hox cluster genes, so that they are predicted to be highly expressed more posterior and later during development (Figure 6).

Although increased expression of miRNA-196a in part 3 was observed in two *Eri1*-knockout embryos compared to their wildtype littermates, in the unmatched *Eri1*-knockout and wildtype pair there was slightly more miR-169a in part 3 of the wildtype embryo (Supplementary Figure S-36). Hence, the difference was not statistically significant when comparing 3 wildtype and knockout counterparts (Figure 29a). Other predicted regulatory miRNAs for *Hoxc8* are miR-181a/b/c/d with 2 conserved binding sites on the UTR. The qRT-PCR results for miR-181a showed neither an anterior-posterior expression gradient nor a difference between *Eri1* wildtype and knockout embryos (Figure 29b).

Whole mount *in situ* hybridization for miR-196a revealed that in wildtype embryos at 12.5 dpc miR-196a can be detected from vertebra #23 up to the tip of the tail (Figure 29c). The *in situ* hybridization technique is probably less sensitive than qRT-PCR analysis. This would explain restricted detection of miR-196a in the posterior part of the embryos using a probe for *in situ* hybridization, while qRT-PCR amplified also low levels of miR-196a in more anterior regions (Figure 29a,c). In the discussion further experiments will be proposed how to analyze miR-196a levels in *Eri1*-knockout and wildtype embryos more precisely.

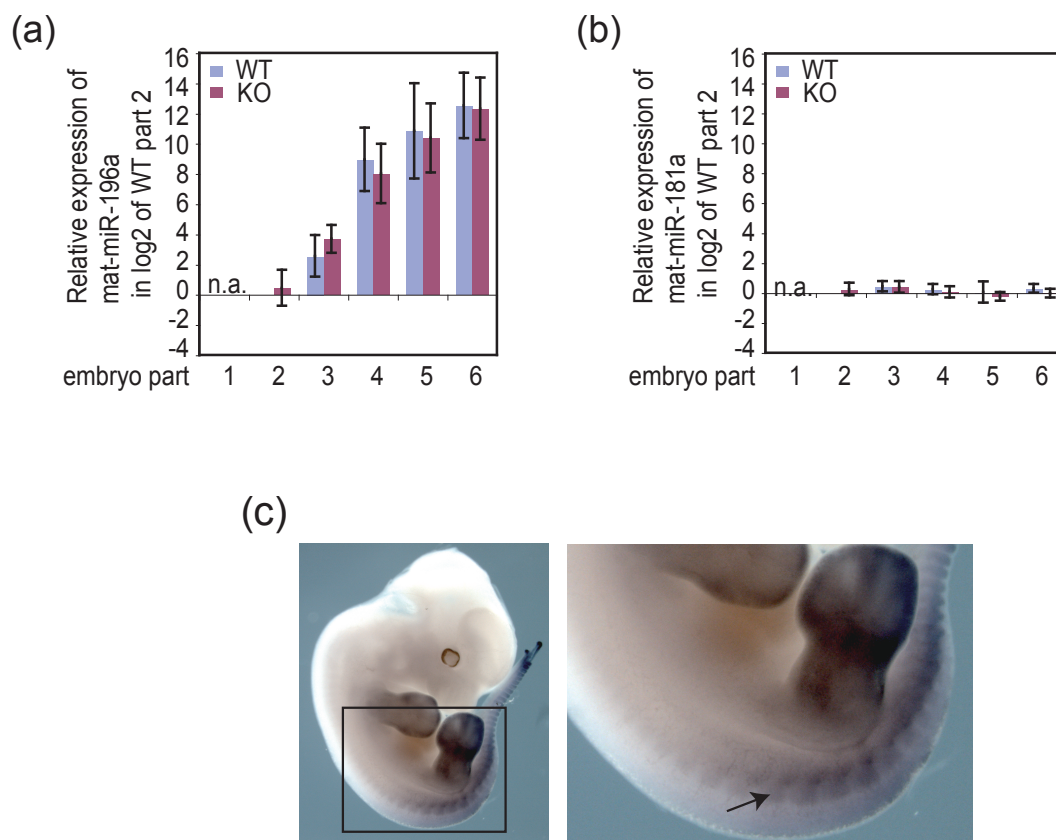


Figure 29: Expression of mature miR-196a in mouse embryos. (a, b) Mature miRNA levels for miR-196a, and miR-181a were detected by qRT-PCR in three *Eri1*-knockout and wildtype embryos (C57BL/6) and normalized to the U6 snRNA housekeeping gene. The mean Cp-value of the three wildtype embryos in part 2 was 37.1 measuring miR-196a and 25.8 measuring miR-181a, compared to 29.1 or 29.8 measuring U6 snRNA. The ΔC_p , mature miRNA/U6 mRNA, in wildtype part 2 was set 1 (log₂ of 0). The expression of mat-miR-196a and miR-181a in the six embryo parts is shown on a logarithmic scale as multiples of the miRNA expression in part 2 of the wildtype embryos. (The single embryo measurements are shown in the supplementary.) (c) In situ hybridization for miR-196a on an embryo at 12.5 dpc. (In collaboration with Bastian Hösel.)

3.2.6 *Eri1* reduces mature miR-196a levels in MEF cells

To test the effect of *Eri1* on miR-196a in fibroblasts, *Eri1*-knockout MEF cells were infected with adenoviruses coding for pri-miR-196a and *Eri1* or pri-miR-196a and GFP control, respectively. For pri-miRNA infection a titration series was performed. The depicted MOI values of 250 and 10 represent overexpression and approximately endogenous miRNA expression levels. The pri-miR-196a and mat-miR-196a levels were analyzed by quantitative RT-PCR and normalized to pbgd or U6 snRNA, respectively (Figure 30). Slightly more pri-miR-196a was obtained in the *Eri1* reconstituted MEF cells. In contrast, decreased levels of mature miR-196a were detected in the very same cells. In *Eri1*-deficient cells the mature miR-196a level was

1.34-fold increased in the case of higher miR-196a expression (MOI 250) and even 1.68-fold increased in the case of lower miR-196a expression (MOI 10).

This result supported the notion that Eri1 has an impact of on the miRNA-mediated RNAi pathway in mammalian cells, either by negatively influencing the processing of precursor miRNAs to their mature form or by reducing the half-life of mature miRNAs.

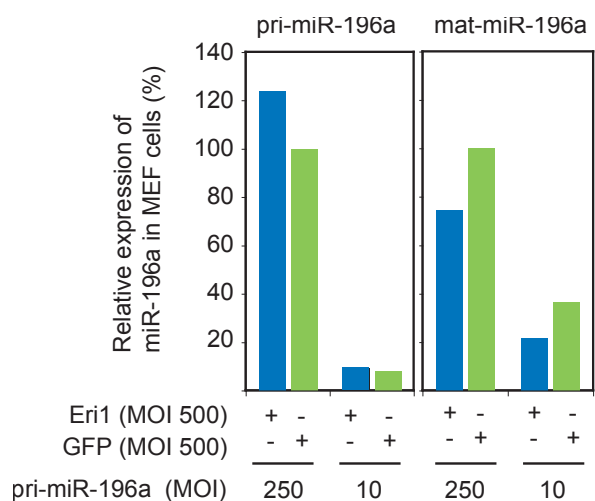


Figure 30: Eri1 reduces mature miR-196a levels in MEF cells. To analyse the impact of Eri1 on miRNAs, Eri1-knockout MEF cells were transduced with both an Eri1 or GFP expression plasmid (MOI 500), and a pri-miR-196a expression plasmid (MOI 250 or 10). The levels of pri-miR-196a and mat-miR-196a were measured by qRT-PCR in a Light cycler 480 and normalized to pbgd or U6 snRNA, respectively.

3.2.7 The exonuclease activity of Eri1 inhibits miR-196-mediated silencing of Hoxc8 through its 3' UTR

3.2.7.1 Generation of a dual-luciferase reporter system for MEF cells

A dual-luciferase reporter system was set up as a functional assay for testing the impact of Eri1 on miR-196a-dependent Hoxc8 mRNA regulation. The term 'dual' refers to the simultaneous expression and measurement of two individual reporter enzyme activities in the system. The experimental reporter (Renilla luciferase, Rluc) is linked to the specific conditions, while the activity of the second 'control' reporter (Firefly luciferase, Luc) provides an internal control that serves as a baseline for infection efficiency. The psiCHECK2 vector from Promega encodes for both reporter genes on the same plasmid. For the application of this project, psiCHECK2 was cloned into the context of an adenoviral backbone (pAd-PI, Invitrogen) to produce reporter constructs suitable for the infection of MEF cells.

In the following assays, a reporter construct was co-transduced with adenoviruses encoding pri-miR-196a and *Eri1*, or appropriate GFP controls. The infection was performed at constant multiplicities of infection (MOI). Importantly, the MOI values of the adenoviruses were determined according to their efficiency to infect A549 cells.

These cells are highly infectable with adenoviruses compared to the much lower infection efficiency of MEF cells. For example, *Eri1*-knockout MEF cell infections with pCAGAdDU + myc-tagged *Eri1* adenoviruses at an MOI of 50 was barely reconstituting the cells with levels that matched endogenous *Eri1* expression (Figure 33).

In a first experiment the repression of the *Hoxc8* 3' UTR by miR-196a in MEF cells was tested. The activity of RLuc that was linked to the *Hoxc8*-3'UTR was strongly repressed upon co-expression of pri-miR-196a in wildtype MEF cells, whereas a control reporter was unaffected by miR-196a expression. The repression of the *Hoxc8* 3' UTR was only observed in wildtype but not in a Dicer-deficient MEF cell clone (Figure 32a). These findings show that miR-196a-dependent repression of the *Hoxc8* 3' UTR only occurred in cells with intact miRNA-biogenesis. Furthermore, the comparable activity of the *Hoxc8* 3' UTR reporter in the absence of ectopic miR-196a expression in wildtype and Dicer knockout cells indicated that this 3'UTR is not repressed substantially through endogenous miRNAs in MEF cells (Figure 31).

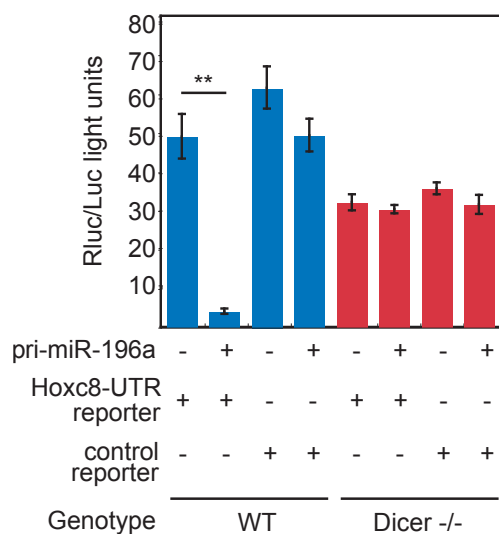


Figure 31: Repression of the *Hoxc8* 3' UTR by miR-196a in MEF cells. The 3' UTR of *Hoxc8* was linked to RLuc and tested for repression by a pri-miR-196a expression plasmid. *Dicer*-knockout and wildtype MEF cells were co-transduced with pri-miR-196a expression plasmid or GFP (MOI 500) and with either the *Hoxc8* 3' UTR reporter or a control reporter plasmid, without a 3' UTR linked to RLuc. Luc is co-expressed from the luciferase reporter plasmid and used to normalize for the transduction efficiency. * Very significantly less RLuc light units after pri-miR-196a co-transduction (T test, one-tailed, paired, $P = 0.002$).

3.2.7.2 *Eri1* inhibits miR-196a-mediated silencing of the *Hoxc8* 3' UTR and interferes with the miRNA-mediated RNAi pathway

In the following experiments *Eri1* was titrated into *Eri1*-knockout MEF cells on a GFP background. The cells were co-transduced to express constant amounts of a reporter (the *Hoxc8* 3' UTR reporter or the control reporter) and a miRNA (the pri-miR-196a or the pri-miR-150).

Increasing levels of Eri1 were indeed able to attenuate miR-196a-dependent Hoxc8 3' UTR repression, represented by the increase of Rluc light units. But Eri1 did not derepress the control reporter, which misses the 3' UTR (Figure 32a). Consequently, adding Eri1 to a system in which miR-196a silences the Hoxc8 3' UTR, Eri1 had a positive effect on Hoxc8 expression.

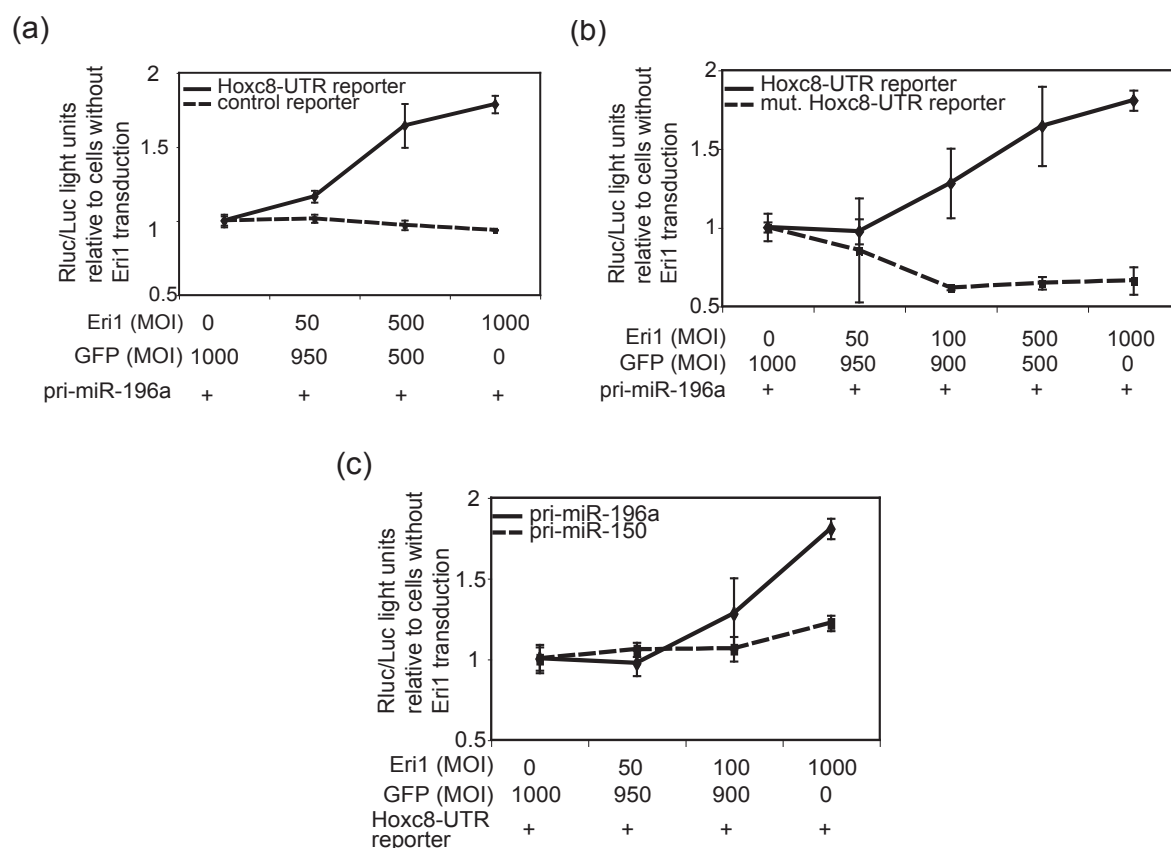


Figure 32: Eri1 inhibits miR-196a-mediated Hoxc8 3' UTR silencing and Eri1 interferes with the RNAi pathway. (a) *Eri1*-knockout MEF cells were co-transduced with either of the luciferase reporter plasmids and the pri-miR-196a expression plasmid (MOI 500), while an expression plasmid for Eri1 was titrated in on GFP background. For the diagram the expression of the Rluc reporter activity without Eri1 co-transduction was set 1. (b) *Eri1*-knockout MEF cells were transduced with a luciferase reporter plasmid, encoding either the intact Hoxc8 3' UTR or a mutated Hoxc8 3' UTR, in which all four conserved miR-196a binding sites have been disrupted. The pri-miR-196a expression plasmid (MOI 500) and a titration series of the Eri1 expression plasmid on a GFP background were co-transduced. (c) *Eri1*-knockout MEF cells were co-transduced with the Hoxc8 3' UTR reporter and the pri-miR-196a or pri-miR-150 expression plasmid (MOI 500), while an expression plasmid for Eri1 was titrated in on GFP background.

It should further be investigated, if Eri1 inhibits the miR-196a-mediated Hoxc8 3' UTR silencing using the RNAi pathway. Therefore all four conserved miR-196a binding site sequences were mutated (actaCCt>actaAAt) within the seed sequence to create a 'mutated Hoxc8-UTR reporter construct'. The mutations of the miRNA-binding sites

for miR-196a abolished derepression of the Rluc-reporter by Eri1 (Figure 32b). Eri1-dependent derepression of the Hoxc8 3' UTR was also not observed when the Hoxc8 3' UTR reporter was co-expressed with pri-miR-150 (Figure 32c). MiR-150 has no predicted binding site in the Hoxc8 3' UTR and could therefore serve as a negative control. Hence, these experiments provided proof that Eri1 affects the RNAi pathway and that Eri1 needs mat-miR-196a binding to the conserved binding sites on the Hoxc8-UTR sequence to show an effect.

3.2.7.3 The exonuclease activity of Eri1 is required for its impact on miR-196a mediated silencing of the Hoxc8 3' UTR

An interesting question was whether the derepression of Hoxc8 3' UTR requires the exonuclease activity of Eri1. Indeed, the catalytically inactive (D130G E132G) Eri1 mutant was not effective compared to its wildtype form to increase the expression level of the Hoxc8 3' UTR reporter (Figure 33a). Equal protein expression of the wildtype Eri1 protein and the catalytic inactive Eri1 protein was confirmed by immunoblotting (Figure 33b). This result supported the idea of Eri1 being a negative regulator of miRNAs using its exonuclease activity to reduce miRNA levels.

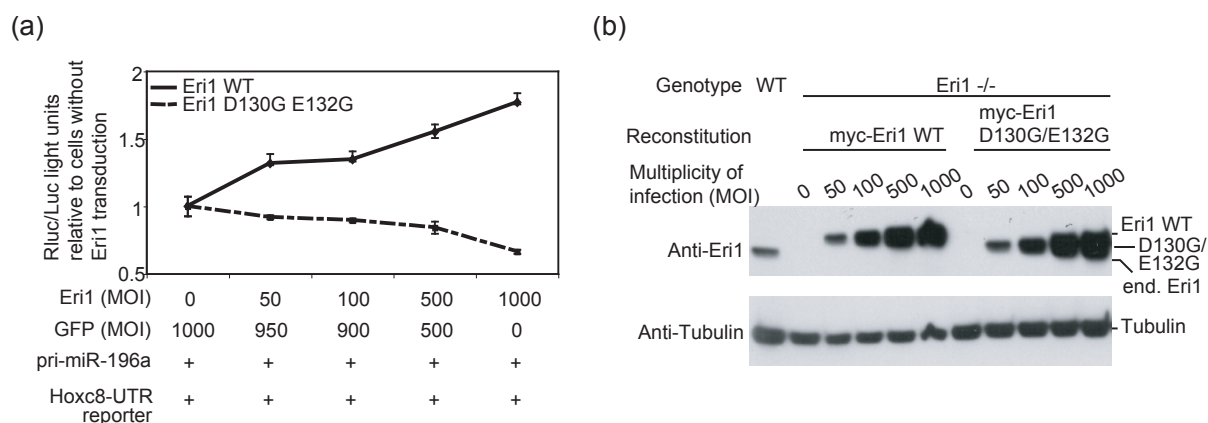


Figure 33: The exonuclease activity of Eri1 is required for its impact on miR-196a mediated Hoxc8 3' UTR silencing. (a) *Eri1*-knockout MEF cells were co-transduced with the luciferase reporter plasmid and the pri-miR-196a expression plasmid (MOI 500), while an expression plasmid for Eri1 wildtype or the catalytically inactive Eri1 D130G E132G mutant was titrated in on a GFP background. (b) The comparable titration series of Eri1 wildtype and Eri1 (D130G E132G) mutant are shown by immunoblotting using monoclonal anti-Eri1 antibody. For comparison to endogenous Eri1 expression levels wildtype MEF cell extract was loaded in the first lane. Tubulin was included as loading control.

4 Discussion

In this work, the impact of Eri1 in mice has been investigated using an *Eri1*-knockout mouse model. Critical findings from the different areas of this investigation have contributed to the demonstration of several distinct molecular roles of Eri1. For example, it has been shown that the catalytic activity of Eri1 is essential for 5.8S rRNA 3' end formation during ribosome biogenesis (Ansel et al., 2008) and for histone mRNA degradation at the end of S-phase (Höfig et al., in preparation). Further, it has been found that Eri1 limits cellular miR196a-abundance and it counter-regulates miR-196a-dependent Hoxc8 3' UTR silencing in MEF cells. Eri1 affects Hox gene expression in embryos and thereby controls skeletal patterning in mouse development (Rath et al., in preparation).

4.1 Severe phenotypes in *Eri1*-knockout mice

4.1.1 Growth defects, postnatal death and male sterility

The *Eri1*-knockout mice were systematically analyzed for their phenotypes to get an impression of the function of murine Eri1. It was observed that *Eri1*-knockout mice show a reduced body size and weight throughout development and till adulthood (Figure 10). Consistent with this finding, it could be shown that primary MEF cell cultures from *Eri1*-knockout embryos have a prolonged doubling time (Figure 19). The cell screen analysis cannot distinguish between (1) prolonged duration between cell divisions of all cells in the culture or (2) some of the cells in the culture dividing normally while others become impaired to divide. Experiments to test cell apoptosis were not performed in the frame of this thesis, so this cannot be excluded.

The growth defects resemble those associated with Minute *Drosophila* mutants, Belly spot and tail (Bst) mouse mutants and Diamond-Blackfan anemia patients. All three of them have been linked to mutations in ribosomal genes (Draptchinskaia et al., 1999; Lambertsson, 1998; Oliver et al., 2004). In this work it could be shown, that Eri1 binds to and processes 5.8S ribosomal RNA (section 3.1.4). Therefore a connection might be suggested between impaired ribosome biogenesis, a prolonged doubling time of primary *Eri1*-deficient MEF cells and decreased growth of *Eri1*-knockout mice.

Mice of an inbred strain are genetically as alike as possible by being homozygous for virtually all alleles. This makes them favorable for knockout studies, because the phenotypic variability between individual animals is very small. On the other hand, inbred strain animals are more vulnerable to mutations, because they are less able to compensate for experimentally generated loss of function of specific gene products. In the case of *Eri1* deletion, deficient mice on an inbred C57BL/6 strain background died soon after birth (Figure 11, Table 6). A strategy to combat this neonatal mortality was found by crossing in an outbred strain that had strongly increased allelic variability. Generating *Eri1*-knockout mice on an NMRI x C57BL/6 background could indeed largely rescue the phenotype (Table 6). These data suggest that *Eri1* deficiency in combination with one or many specific other alleles decreases survival, which can be overcome by compensatory mechanisms present in mixed strains.

Tissue Western blotting revealed relatively high levels of Eri1 in the testes of mice (Figure 13). The deficiency of Eri1 led to the phenotype of male sterility, which was also reflected by an underdevelopment of the testes (Figure 12). It may be speculated that this phenotype is a consequence of Eri1's impact on cell cycle-dependent histone mRNAs (Figure 23). A unique regulation of histones occurs in mammalian spermatogenesis. During meiosis, the replication-dependent histones are replaced with testis-specific variants and these themselves are then substituted by protamines in the mature sperm (Kimmins and Sassone-Corsi, 2005). Potentially, Eri1 could be involved in the exchange of replication-dependent histones to testis-specific histones. If in the *Eri1*-deficient testis this crucial step is impaired one could imagine that spermatogenesis is arrested.

4.1.2 Results from the screen in the German Mouse Clinic

For a more detailed analysis of phenotypes in *Eri1*-deficient mice, *Eri1*-knockout, *Eri1*-heterozygous and wildtype littermates were sent to the German Mouse Clinic to test them in a number of standardized screens. Tests were performed in 14 different categories. In five categories no abnormalities were found: allergy, cardiovascular function, eye, lung function and nociception, but in nine categories *Eri1*-dependent phenotypes were discovered: behavior, clinical chemistry and hematology, dysmorphology, energy metabolism, immunology, molecular phenotyping, neurology, pathology, and steroid metabolism (Table 7). The diversity of categories exhibiting a

phenotype already suggests that Eri1 is a regulator in many different cell types either of the same cellular pathway or even of several different pathways. This work has provided support for the latter by showing that Eri1 is involved in such crucial processes as ribosome biogenesis, canonical histone mRNA regulation and RNAi.

For example, in the clinical chemistry and hematology screen *Eri1*-deficient mice showed a macrocytic anemia phenotype. The cause of Diamond-Blackfan anemia has been described to be abnormal processing of ribosomal RNA due to mutations in the ribosomal protein S19, which leads to abnormalities in ribosomal function (Draptchinskaia et al., 1999). Consistent with this finding, the macrocytic anemia in *Eri1*-deficient mice might be connected to impaired ribosomal RNA processing as well (Figure 18). The behavior phenotype of increased anxiety in the *Eri1*-knockout mice could be due to loss of Eri1 function in neurons. Eri1 has been shown to be highly expressed in a subset of neurons in *C. elegans* (Kennedy et al., 2004). Further, in *Eri1*-deficient worms an increased RNAi sensitivity was reported. Testing the worms for siRNA-mediated silencing of a neuron-specific reporter gene, the *Eri1*-knockout worms showed a 70% decrease in reporter gene expression upon feeding with dsRNA, while the dsRNA had no effect in wildtype animals (Kennedy et al., 2004). These findings suggest that Eri1 might have an important function on miRNAs in the neurons of mice, but this has not been demonstrated yet.

4.2 Limitations of molecular phenotyping of embryos

Comparative genome-wide expression profiling is a powerful tool in the effort to annotate the mouse genome with biological function. The analysis of mRNA expression data of knockout mice may support the understanding of the molecular biology in the mutants. Within the German Mouse Clinic the efficiency of systematic genome-wide expression profiling for the detection of molecular phenotypes in organs of a mammalian model organism has been demonstrated (Horsch et al., 2008).

To address the question, which genes cause the phenotype of dysmorphology in the development of *Eri1*-deficient mice, the mRNA expression of whole embryos, excluding the head, was analyzed instead of singular organs. A number of mRNAs coding for hemoglobin have been found to be down-regulated in *Eri1*-knockout embryos (Table 9). This might be linked to the macrocytic anemia phenotype of adult

mice, which is often associated with an insufficient concentration of hemoglobin in the cells. However, only two developmentally regulated genes, *Abr* (active BCR-related gene) and *Afp* (alpha feto protein), could be found in the pool of 13 diverse regulated genes (Table 11). *Abr* is important during the vestibular morphogenesis of the inner ear in mice. The vestibular system has important sensory functions and contributes to spatial orientation. Probably, the increased expression of *Abr* in *Eri1*-knockout mice does not induce a noticeable phenotype, because in the screen of the German Mouse Clinic only small problems were noticed in behavior tests (Table 7). AFP is the main fetus serum glycoprotein, which is produced by the fetal yolk sac and the fetal liver. In pregnant women increased levels are indicative of open neural tube defects in the fetus (Leighton et al., 1975) and decreased levels are indicative of the Down syndrome (Cuckle et al., 1984). Contrary, it has been proposed that AFP is not required during mouse embryonic development. Furthermore, it has been shown that AFP null females are infertile whereas males are fertile (Gabant et al., 2002). However, it has not been solved in the framework of this thesis whether the increased level of *Afp* expression in *Eri1*-knockout embryos has an influence on any of the observed phenotypes.

All down-regulated mRNAs show only about a 2-fold regulation (Table 9). Probably, the analyses of whole embryos were not precise enough to reveal greater differences between *Eri1*-knockout and wildtype embryos. Additionally, a high variability among the four *Eri1*-knockout embryos was discovered (Table 10). Biological variability in gene expression, oscillation of stress responsive genes and technical variability of the dissection or the blood content of the embryos might bear potential for anti-correlation in the gene expression patterns between individuals of one genotype. In addition, several recent publications have provided evidence for biological variability of expression levels for particular genes (Churchill, 2002; Drobyshev et al., 2003; Oishi et al., 2003; Pritchard et al., 2001; Selmann et al., 2005).

Altogether, the molecular phenotyping approach did not reveal potential genes that are involved in the prominent *Eri1*-knockout phenotype of skeletal dysmorphology.

4.3 Expression and intracellular localization of *Eri1*

The EST (expressed sequence tags) profile of *Eri1* in *M. musculus* is shown on the NCBI-Unigene webpage (<http://www.ncbi.nlm.nih.gov/UniGene/ESTProfileViewer.cgi>)

uglist=Mm.207534). The profile gives numbers for the Eri1 specific EST versus all EST in the pool of each organ analyzed. Relative high mRNA levels were found in the bladder, bone, dorsal root ganglion, spleen and thymus. The EST profile further shows Eri1 expression in various developmental stages. Eri1 mRNA is expressed as early as cleavage to the morula stage occurs. High mRNA expression was found in the developmental stages of gastrula, organogenesis, fetus neonate and juvenile.

These data on Eri1 mRNA expression are largely consistent with the protein expression described in this thesis work. Analyzing Eri1 protein expression in adult mice, it was found to be expressed ubiquitously with especially high levels in tissue protein extracts from spleen, thymus and testis (Figure 13). High mRNA and protein levels in spleen and thymus indicate a possible, increased impact of Eri1 on blood cell maturation. Initial experiments have been performed to analyze the differentiation of bone marrow cells *in vitro*. Although changes in differentiation between the hematopoietic cells from *Eri1*-knockout and wildtype mice were observed, a high variability in both groups was determined and excluded to describe statistically significant changes (data not shown). However, the macrocytic anemia phenotype of *Eri1*-knockout mice indicates a function of Eri1 at least in the erythroid lineage (Table 7). Immunohistochemistry stains of embryos at 12.5 dpc revealed Eri1 protein expression all over the embryo with higher Eri1 protein levels in the prevertebrae and in the brain (Figure 27). The elevated Eri1 protein abundance in prevertebrae and the higher mRNA levels in the bones of adult mice (NCBI-Unigene) are in line with the skeletal anomalism of *Eri1*-knockout mice.

In previous studies intracellular localization of the human homolog of mouse Eri1, 3'hExo, was investigated in HeLa cells. Human Eri1 linked to a C-terminal GFP tag accumulated in the cytoplasm and the nucleoli (Yang et al., 2006). In *C. elegans*, functional Eri1-GFP fusion proteins seemed to be strictly cytoplasmic, and Flag-tagged Eri1 localized only to the cytoplasm in *S. pombe* (Bühler et al., 2006; Gabel and Ruvkun, 2008; Kennedy et al., 2004).

Consistent with the observations for human Eri1 and in contrast to worm and fission yeast, analysis of the intracellular localization of GFP-tagged mouse Eri1 revealed localization to the cytoplasm and the nucleus (Figure 14). Inside the nucleus Eri1 was especially enriched in the nucleoli, the site of ribosomal RNA biogenesis. An extended analysis employing point mutants of Eri1 showed that this localization

depends on an intact SAP domain and linker sequence. Although the exchange of single amino acids did not impair the entry into the nucleus, no enrichment was seen in the nucleoli any more. Probably, the adherence of the Eri1 mutants to attach to the RNA or DNA in the nucleolar structures was reduced. This is supported by analysis of the mutants in RNA immunoprecipitation assays, which revealed that the very same amino acids support binding to 5.8S rRNA (Figure 17).

4.4 The RNA target molecules of Eri1

The Eri1 protein contains an amino-terminal SAP domain, a linker sequence and a carboxy-terminal exonuclease domain. A structure-based comparison with other known 3' exonucleases of the DEDD family revealed that the human homolog of Eri1 is more similar to DNA-specific exonucleases than to RNases (Cheng and Patel, 2004). Nevertheless, in this work it could be shown that the exonuclease domain of mouse Eri1 is crucial for the regulation of at least three RNA target molecules: ribosomal RNA, canonical histone mRNA and miRNA.

4.4.1 Ribosomal RNA processing

The synthesis of ribosomes is among the most fundamental of biological processes in each cell. Yet our understanding of ribosome biogenesis remains incomplete. Gabel and Ruvkun have demonstrated that Eri1 is essential for the maturation of the 3' end of 5.8S rRNA in *C. elegans* and *S. pombe* (Gabel and Ruvkun, 2008). Together with the finding of mouse Eri1 being involved in 5.8S rRNA processing (Ansel et al., 2008), this leads to the conclusion that Eri1 has a conserved function in rRNA processing.

In this work it was shown that Eri1 is directly associated with 5.8S rRNA in living cells and that the 5.8S rRNA 3' end is extended in *Eri1*-deficient MEF cells (Figure 15, Figure 18). In an *in vitro* assay of 5.8S rRNA maturation, recombinant Eri1 was able to access and convert the 3' end of the 5.8S rRNA of intact ribosomes from *Eri1*-deficient liver extract to exactly the same size as mature wildtype 5.8S rRNA (Ansel et al., 2008). Taken together, these findings strongly support the conclusion that Eri1 binds to and removes the unpaired nucleotides from the 3' end of 5.8S rRNA *in vitro* and *in vivo*.

In the mature ribosome structure, the 3' end of 5.8S rRNA forms a duplex with the 5' end of 28S rRNA, leaving a 3' overhang in *Eri1*-deficient cells (Ansel et al., 2008). This 5.8S-28S rRNA duplex resembles the structure of siRNA duplexes. Previous work on homologs of Eri1 have shown that a characteristic of Eri1 activity is its enhanced exonucleolytic function on free 3' overhangs compared to single-stranded RNA or duplexes (Iida et al., 2006; Kennedy et al., 2004; Yang et al., 2006). Hence, it could be reasoned that the Eri1 protein recognizes duplex RNA structures. These duplex structures are also present in hairpins for which Eri1 would then be able to process the 3' unpaired end. This feature is shared with the canonical histone mRNAs for which our group has demonstrated that Eri1 processes the 3' end (Höfig et al., in preparation).

RIP assays proved that Eri1 already interacts with the longer 45S rRNA precursor (Figure 16). No significant association could be detected with the 3' ETS, which is the sequence that is transcribed last in the generation of the 47S rRNA precursor. One possible explanation would be, that Eri1 binds to the precursor at its 5' part before the 47S rRNA has been fully transcribed. It has been shown for *S. cerevisiae*, that co-transcriptional cleavage takes place within the 3' ETS (Henras et al., 2004). If this was true for mammalian cells as well, the 45S precursor, lacking the 3' ETS sequence, would be the earliest detectable species that can be visualized by the applied method. Consequently, it cannot be excluded that Eri1 binds to the entire 47S rRNA precursor as well. Interestingly, an impact of Eri1 on earlier processing steps could not be detected, because (1) *Eri1*-deficient and wildtype cells showed equal levels of 5.8S rRNA (Figure 15) and (2) pulse chase experiments in these cells to analyze rRNA precursor processing did not reveal a difference (Ansel et al., 2008). Hence the importance of the binding of Eri1 to the ribosomal RNA during early processing steps remains unclear.

4.4.2 Histone mRNA degradation

As cells approach the end of S-phase, the need for new canonical histone proteins vanishes and the levels of replication-dependent histone mRNAs decrease. Recently, it has been demonstrated in human cells that degradation of histone mRNAs requires SLBP, which is involved in recruiting the proteins necessary to add a short oligo(U) tail to the histone mRNA that is being translated (Mullen and Marzluff, 2008) (Figure 2). The oligo(U) tail is an optimal binding site for the LSM1-7 complex, which binds to

oligo(U) tails as well as poly(A) tails. The binding leads to the degradation of the histone mRNA by pathways that are similar to those involved in the degradation of poly(A) mRNA after deadenylation induced shortening of the poly (A) tail towards an oligo(A) tail (Parker and Song, 2004; Tharun et al., 2000). SLBP itself is cell cycle-regulated; but although the levels of SLBP and canonical histone mRNA parallel each other during cell cycle, the molecular signals that regulate these two factors are distinct (Marzluff et al., 2008). Hydroxyurea-induced inhibition of DNA replication in the middle of S-phase resulted in rapid degradation of replication-dependent histone mRNA, but there was no effect on SLBP levels (Whitfield et al., 2004). In addition, stabilizing SLBP did not prevent replication-dependent histone mRNA degradation at the end of S-phase (Zheng et al., 2003). Consequently, an additional protein has to trigger histone mRNA degradation.

In this work mouse Eri1 has been shown to directly interact with the replication-dependent Hist2h4 mRNA (Figure 20). Furthermore, it could be demonstrated that Eri1 initiates Hist2h4 mRNA degradation upon hydroxyurea-treatment simulating the end of S-phase (Figure 23). This finding disproved the current results from Mullen and Marzluff. In HeLa cells, they could not detect a contribution of Eri1 to the degradation of canonical histone mRNAs after hydroxyurea treatment (Mullen and Marzluff, 2008). One possible explanation for these contrary results could be that Mullen and Marzluff did only achieve an 80-90% knockdown in HeLa cells. In the experiment presented in this work, a knockdown with undetectable Eri1 levels on a Western blot was attained in MEF cells (Figure 23g). Furthermore, Mullen and Marzluff did only induce a short-term knockdown by the transfection of siRNAs, whereas retroviral infection of shRNAs, as performed in this thesis work, induces a longterm knockdown. These differences did probably lead to diverse starting conditions for the hydroxyurea experiments, which would explain the different outcome.

Further, it could be demonstrated in this study that the exonuclease activity of Eri1 is crucial for the initiation of histone mRNA degradation (Figure 23). Consequently, not only the binding of Eri1 to canonical histone mRNA, probably in cooperation with a larger protein complex, but also the enzymatic activity of Eri1 is needed for histone mRNA degradation. Further experiments have been performed that reveal the effect of Eri1 on canonical histone mRNAs in T cells and that provide a detailed insight into

the mechanism how Eri1 cooperates in the canonical histone mRNA degradation pathway (Hoefig et al., in preparation).

4.4.3 How does Eri1 recognize its target RNAs?

The SAP (SAF-A/B, Acinus and PIAS) domain of Eri1 has been found to facilitate binding of proteins to double stranded DNA and RNA. The domain codes for a scaffold attachment factor (SAF)-box, which was shown to recognize AT-rich regions in the chromosomal DNA known as scaffold-attachment regions (Aravind and Koonin, 2000; Kipp et al., 2000). Furthermore, it had been claimed that the SAP domain and linker sequence of human Eri1 are essential for sequence-specific binding to the histone mRNA stem loop and its conserved 3' terminal ACCCA sequence (Yang et al., 2006).

In this work, binding of Eri1 to the histone mRNA could be confirmed in the mouse cell system *in vivo* (Figure 20). Furthermore, it was shown that Eri1 associates with the 5.8S rRNA and its precursor (Figure 15, Figure 16). The RNA immunoprecipitation assays did not reveal a direct contact to the 5S rRNA, which is also present in the 60S large ribosomal subunit. These findings supported the hypothesis that Eri1 selects its RNA substrates. Further evidence was given in experiments testing point mutations in the RNA-binding linker sequence of Eri1. These impaired direct binding to 5.8S rRNA and histone mRNA at low, endogenous expression levels (Figure 17a, Figure 20). Unfortunately, the function of the SAP domain could not be tested, because the monoclonal anti-Eri1 antibody recognizes an epitope in this domain. Generating monoclonal antibodies against the exonuclease domain, these were not specific enough for the use in RIP assays (data not shown). Therefore, GFP-tagged Eri1 wildtype and mutants were immunoprecipitated by a polyclonal anti-GFP antibody. Contrary to the earlier experiments, the SAP domain and the linker sequence were now functionally dispensable (Figure 17c). GFP-tagged proteins are often several fold higher expressed than the endogenous protein. Consequently, it has to be concluded that the here investigated residues in the SAP domain and the linker domain as well as the SAP domain itself are not required for 5.8S rRNA processing in cells under conditions at which a mutant of Eri1 is expressed at a significantly higher level than endogenous expression.

The analysis of an additional Eri1 SAP/linker sequence (N69A K107A) mutant was based on the crystal structure of human Eri1 bound to histone mRNA (Y. Cheng and D. Patel, submitted to the Protein Data Bank). The open question was, whether these two amino acids in the SAP domain and linker sequence are crucial for binding to the histone mRNA, but not to the 5.8S rRNA. In this thesis work, it could indeed be shown that the two amino acids, N69 and K107, are supportive for histone mRNA binding. While the mutant could reconstitute processing of the 3' end of 5.8S rRNA in *Eri1*-knockout cells (Figure 22), the same cells were impaired to initiate degradation of Hist2h4 mRNA upon hydroxyurea-treatment (Figure 23e). Consequently, it can be proposed that different amino acids in the SAP domain or linker sequence support the binding of Eri1 to each of the RNA substrates. Nevertheless, in a second experiment the very same mutant could initiate histone mRNA degradation, probably because of slightly higher expression levels or varying cellular conditions or more efficient introduction of the mutant protein into endogenous complexes. This result is partly consistent with the findings on human Eri1 binding to histone mRNA *in vitro*. Inherent substrate specificity of Eri1 protein towards the histone loop was lost at high Eri1 concentrations, testing binding to histone mRNA loops comprising nucleotide replacements or truncations (Dominski et al., 2003; Yang et al., 2006).

Together, the data suggest that single amino acids in the Eri1 protein support binding to specific RNA target molecules, but at higher expression levels they are dispensable. Hence, additional protein-protein contacts between Eri1 and ribosomal proteins or factors associated with histone mRNA degradation have to participate in the substrate selection of Eri1 RNA targets.

4.5 Eri1 regulates skeletal patterning

This work contributes new data concerning the genetic basis of skeletal patterning in mice. It is shown that (1) a homeotic transformation is present in *Eri1*-deficient mice, (2) the *Hoxc8* expression border is shifted in *Eri1*-knockout embryos relative to wildtype and (3) Eri1 has an impact on miR-196a-mediated silencing of the *Hoxc8* 3' UTR.

4.5.1 Shared phenotypes of *Eri1*- and *Hoxc8*-knockout mice

Homeotic transformations are characterized by the change of segment identity during development. This is induced by a mutation or misexpression of developmentally critical genes, for example the Hox genes in animals. Several Hox gene knockout mice show the phenotype of an additional rib pair at vertebrae #21. This has been reported for mouse mutants with a single or combined deletion of *Hoxc8*, *Hoxa9*, *Hoxc9* and *Hoxa10* (Chen and Capecchi, 1997; Fromental-Ramain et al., 1996a; Le Mouellic et al., 1992; Rijli et al., 1995; Satokata et al., 1995; Suemori, 1995; van den Akker et al., 2001; Wellik and Capecchi, 2003) (Table 12). Accordingly, an overlap of function between the gene products of these paralogues as well as non-paralogues Hox genes may be suggested.

In *Eri1*-knockout mice a skeletal anomalism was detected with a high penetrance of 80% (Table 8). A duplication of the 7th thoracic vertebra was observed resulting in a total number of 14 rib bearing vertebrae (Figure 24, Figure 26). Furthermore, *Eri1*-deficient mice showed the fusion of an 8th rib pair to the sternum (Figure 25). This is a logic consequence of a duplication of exactly the 7th rib, which is the last rib attached to the sternum. This *Eri1*-knockout mouse phenotype is only shared with the *Hoxc8*- and *Hoxc9*-deficient mice (Le Mouellic et al., 1992; Suemori, 1995; van den Akker et al., 2001). Although, the phenotype of *Hoxc9*-deficient mice resembled closely that of *Eri1*- and *Hoxc8*-deficient mice, in some of the *Hoxc9*-knockout animals the anteriorization effect seemed to be even more prominent. The 9th rib was partially found to fuse to the sternum as well. The *Hoxc9*-knockout mouse phenotype might also develop due to an altered expression of *Hoxc8* which was suggested to be regulated by *Hoxc9* (Suemori, 1995).

Hoxc8 expression is particularly high in the lower thoracic prevertebrae compared to levels of *Hoxb8* and *Hoxd8*. Hence, it was this domain, in which the most penetrant phenotypes were found in *Hoxc8*-knockout mutants. *Hoxb8*-knockout mutants showed predominantly abnormalities in the upper rib cage. *Hoxd8* was found to be expressed in the region of sacral vertebrae but only with low levels of gene expression. *Hoxd8* deficiency rather increased the phenotype in double or triple mutants, than developing abnormalities as a single knockout (van den Akker et al., 2001).

Interestingly, different from *Hox*-knockout mice in *Eri1*-knockout animals there was never a rudimentary rib or a one-sided additional rib observed on vertebra #21. The additional rib pair was always fully developed. It may be speculated that the *Eri1* deletion leads to a different outcome than *Hox* gene deletion, because *Eri1* works on the secondary, post-transcriptional level.

A detailed analysis of the vertebrae in *Eri1* mutants revealed that the duplication of the 7th thoracic vertebra leads to an anteriorization of all following vertebrae down to the lumbar or sacral region (Figure 26). This anteriorization stopped in the lumbar domain in some of the male mice, while in the other male mice as well as in all female animals the anteriorization was extended to the sacral domain. Both cases have been seen occasionally in *Hoxc8*-, *Hoxc8/d8*- or *Hoxb8/c8/d8*-deficient mice as well (van den Akker et al., 2001). The diversity of the phenotypes probably results from partially incomplete homeotic transformation of thoracic, lumbar and sacral vertebrae.

Altogether, it may be concluded that the *Eri1*-knockout dysmorphology phenotype resembles closely the *Hoxc8* single and combined deletion mutants. Apart from the shared skeletal anomalies the *Hoxc8* mutant mouse line did show the phenotype of postnatal death as well. Most *Hoxc8*-deficient mice die shortly after birth from a still unknown cause (van den Akker et al., 2001). Another shared phenotype is the reduced fore-limb grip strength that was also observed in *Hoxc8*- knockout animals (Tiret et al., 1998).

4.5.2 Hox expression pattern in embryos

Hox genes have been shown to play important roles in the establishment of the body axis during development (Krumlauf, 1994). *Hox* genes are a particular subgroup of homeobox genes, which code for a group of transcription factors. Special of *Hox* genes is not only their organization in chromosomal clusters, but the striking phenomenon of spatial colinearity (McGinnis and Krumlauf, 1992). In vertebrates, also a temporal colinearity has been detected (Duboule, 1994; Kmita and Duboule, 2003).

Hox proteins have been proved to be difficult to stain in whole mount immunohistochemistry approaches. Reviewing the current literature, the sensitivity of the different methodical approaches resulted in diverse *Hoxc8* gene expression borders (Juan et al., 2006; Kwon et al., 2005b; Le Mouellic et al., 1992; van den

Akker et al., 2001). Recently, researchers replaced the *Hoxc8* allele with either a GFP or a LacZ reporter. It could be shown that already the introduction of a reporter may lead to differences in endogenous Hox gene expression (Blackburn et al., 2009). The embryonic stage also seems to play an important role because the expression domains are labile within larger domains till embryonic day 12.5 dpc (McIntyre et al., 2007). In this study *Hoxc8* expression in mouse embryos was analyzed using the Western blot method. The analysis of embryo parts revealed a specific protein expression in the posterior half of the embryo (Figure 28a).

Comparing mRNA and protein levels of *Hoxc8* in wildtype embryos at 12.5 dpc, *Hoxc8* mRNA could be detected in a broader area, while high expression of protein was restricted to a smaller region in the center of the mRNA expression area (Figure 28a,b). This difference in the mRNA and protein expression pattern do not exclude a regulation on the protein level, but strongly suggest a regulation on the post-transcriptional level causing an absence of *Hoxc8* protein at the anterior and posterior expression borders. MiRNAs have been shown to repress the translation of target genes as well as to reduce the target mRNA expression levels and they have been proposed to act as fine-tuners of developmental gene expression programs (Stark et al., 2005). Consequently, it may be assumed that miRNAs inhibit *Hoxc8* mRNA translation at sites of low expression.

Hoxc8 and *Hoxb8* mRNAs could be identified to be targets of *Eri1* during embryonic development. The *Hoxc8* and *Hoxb8* mRNA expression levels showed distinct phenotypes in *Eri1*-knockout and wildtype littermates (Figure 28b,c, Figure S-35). In the mutants the anterior expression border of *Hoxc8* as well as *Hoxb8* was shifted into posterior direction on the A-P axis of the embryo. In the critical expression area (embryo part 3) a 16-fold change for *Hoxc8* and a 4-fold change for *Hoxb8* was measured. However, no significant impact of *Eri1* was seen in the posterior region of high *Hoxc8* and *Hoxb8* expression. The shift of Hox gene expression into the posterior direction in *Eri1*-knockout mice may account for both *Eri1*-knockout mouse phenotypes, the attachment of an 8th rib pair to the sternum as well as the development of an additional rib pair at the first lumbar vertebra. The posterior dominance model predicts that the more posterior expressed Hox genes have a greater effect on the patterning information than the more anterior expressed genes (Duboule, 1994). It can therefore be proposed that the *Hoxc8* and *Hoxb8* prevalence

starts only in the more posterior situated lower thoracic region in the *Eri1*-knockout situation.

Although the presented data cannot rule out a possible positive effect of Eri1 on the transcription rate of Hoxc8 and Hoxb8 mRNAs, there is compelling evidence for Eri1-mediated derepression of posttranscriptional silencing of Hoxc8. In support of this proposed mechanism, a very recently published paper showed an anterior expansion of Hoxb8 gene expression as the consequence of antagomir-mediated neutralization of the Hox miR-196 in chicken embryos (McGlenn et al., 2009).

The levels of mature miR-196a were measured in *Eri1*-knockout and wildtype animals. Although a tendency for a shift into the anterior direction was observed in *Eri1*-knockout mice, no significant difference could be detected comparing three *Eri1*-knockout and wildtype pairs by quantitative reverse transcription PCRs (Figure 29a, Figure S-36). This might be due to various reasons: First, the analyses were performed at 12.5 dpc, a time point when the identity of the segments has already been established. And second, the analysis is imprecise by measuring whole slices including the limbs, which express miR-196 as well. Therefore follow-up experiments using microdissection are planned in which exclusively the somites will be examined for their mature miR-196a expression. Further, whole mount *in situ* hybridizations on embryos at 11.5 and 12.5 dpc have been performed (Figure 29c), but the protocol still has to be established for earlier developmental stages closer to the time period of vertebrae anlage. A problem for the *Eri1*-knockout and wildtype comparison by *in situ*-hybridization is that the locked nucleic acids probe recognizes mature miR-196a as well as its precursor molecules, pre-miR-196a and pri-miR-196a. Regulation of precursor miRNAs by Eri1 has not been demonstrated yet.

4.5.3 Eri1 regulates mature miR-196a levels

Although much is known about the synthesis of miRNAs, up to now, very little is known about the regulatory mechanisms controlling the spatiotemporal expression pattern of miRNAs and nothing is known about their downregulation. Eri1 has been suggested to regulate exogenous as well as endogenous siRNA pathways in *C. elegans* (Duchaine et al., 2006; Kennedy et al., 2004). Kennedy and colleagues proposed a direct impact of Eri1 on exogenous siRNAs by degrading the 3' overhangs of siRNAs, whereas Duchaine and colleagues suggested that Eri1 affects

the exogenous RNAi pathway only indirectly through its role in endo-siRNA production. In this model, Eri1-dependent endo-siRNA pathways inhibit RNAi by competing for cellular factors involved in the production or activity of both endo- and exo-siRNAs.

Data from *Eri1*-deficient mice have shown that in T cells all analyzed miRNAs were enriched with a factor of 1.25, while other noncoding RNAs, such as U6 snRNA were unaffected (Rath et al. in preparation, data from KM. Ansel). Mature miR-196a levels have been analyzed in MEF cells in this work. The data revealed that in *Eri1*-deficient cells a 1.34-fold to 1.68-fold increase of mature miR-196a levels could be measured comparing to *Eri1*-reconstituted cells (Figure 30). These results uncovered a consistent increase in mature miRNA abundance in *Eri1*-deficient cells. Further investigations have to reveal, if the biogenesis of mature miRNAs is impaired through *Eri1*-deficiency, or rather if the half-life of mature miRNAs is reduced.

4.5.4 The impact of Eri1 on miR-196-mediated Hoxc8 silencing

Reporter assays in HeLa cells have indicated that miR-196 limits or dampens Hoxc8, Hoxd8 and Hoxa7 expression using Hox 3' UTR fragments. In the case of Hoxb8 even degradation of the reporter RNA was initiated (Yekta et al., 2004).

Luciferase assays on MEF cells using the complete 3' UTR of Hoxc8 have confirmed negative regulation of Hoxc8 by miR-196a through its 3' UTR (Figure 31). Importantly, it was shown that Eri1 could attenuate this suppression. Increasing the amount of Eri1 did lead to higher expression levels of the Hoxc8 3' UTR reporter (Figure 32a). Further experiments, in which all four conserved miR-196 binding sites in the Hoxc8 3' UTR had been mutated revealed that Eri1 affects indeed the RNAi pathway and it could be shown that the exonucleolytic activity of Eri1 is crucial for its impact on miR-196a-mediated Hoxc8 silencing (Figure 32b, Figure 33). Together with the finding that Eri1 reduces mature miR-196a levels in MEF cells (Figure 30), it may be proposed that Eri1 has a negative influence on the accumulation of mature miRNAs in the cell through its exonuclease domain. Thus, through the reduction of miR-196a levels, silencing of Hoxc8 mRNA will be released and more Hoxc8 protein is expressed in the wildtype situation.

4.5.5 Model depicting the role of Eri1 in skeletal patterning

Analyzing the skeletal phenotype in *Eri1*-knockout mice, the data suggest the following model (Figure 34). In wildtype mice, *Eri1* expression leads to a decreased level of mature miR-196a, especially at sites of low expression of miR-196a. This is the case at the anterior expression border in the embryo. Consequently, *Eri1* counteracts the silencing of *Hoxc8* mRNA by miR-196a and *Hoxc8* protein will be expressed. In *Eri1*-knockout mice higher levels of functionally active miR-196a are expressed in more anterior segments of the embryo. Accordingly, the RNAi pathway inhibits *Hoxc8* mRNA and thus the *Hoxc8* protein expression will be shifted into the posterior direction in the embryo. According to the posterior prevalence model this may lead to the anteriorization phenotype observed in *Eri1*-deficient mice due to a lack of *Hoxc8* prevalence over the more anterior Hox genes in prevertebrae of the lower thoracic region of the embryo.

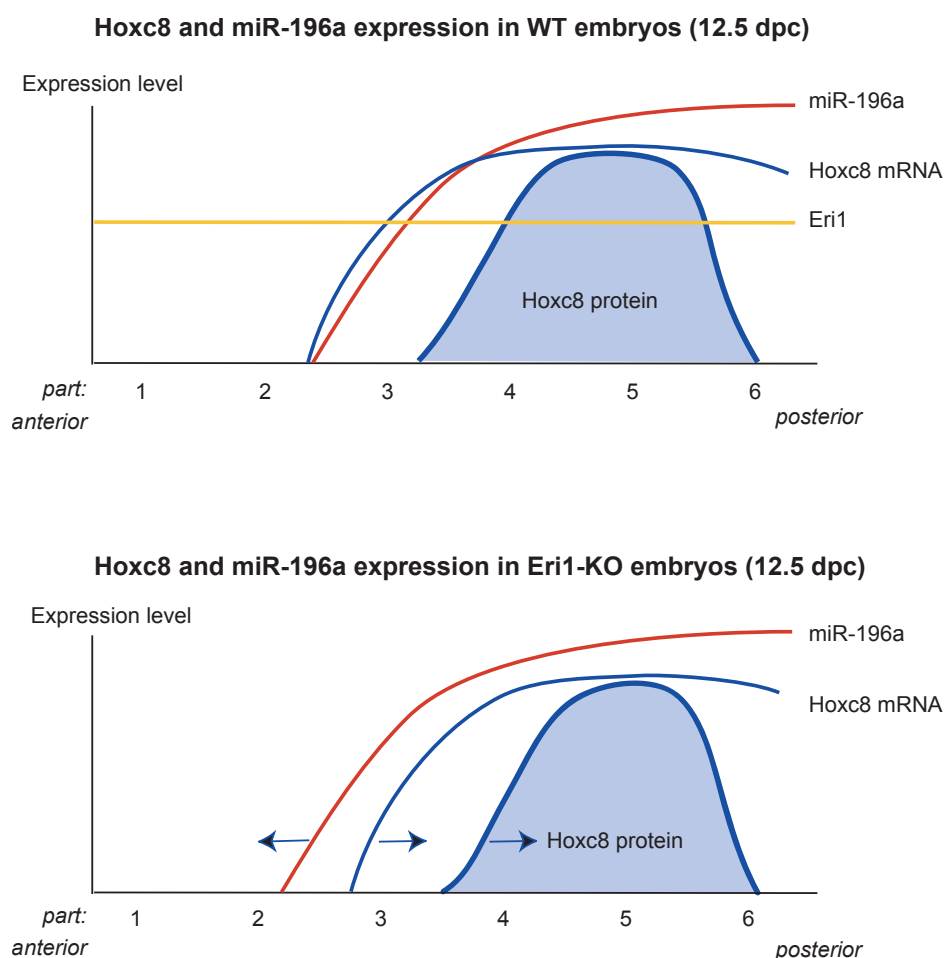


Figure 34: Model depicting the role of *Eri1* in skeletal patterning.

4.6 Conclusion

In this study the conserved exonuclease Eri1 could be shown to be involved in at least three RNA pathways: ribosomal RNA processing, histone mRNA degradation and miRNA-mediated RNAi.

Eri1 was found to be enriched in nucleoli and to directly bind to and process 5.8S rRNA. Contrary to the proposed model of Mullen and Marzluff that excludes a contribution of Eri1 in histone mRNA degradation (Mullen and Marzluff, 2008), it could be demonstrated that the exonuclease activity of Eri1 initiates cell cycle-dependent histone mRNA degradation. Furthermore, the findings on Eri1 binding to 5.8S rRNA and Hist2h4 mRNA support the view that specific residues in the Eri1 SAP domain and linker sequence facilitate binding to RNA duplex structures, as they are inherent in the ribosomal RNA or the histone mRNA stem loop. However, this binding acts in concert with one or more so far unknown cellular binding partners to determine substrate specificity.

Eri1-knockout mice revealed a number of phenotypes, most prominently growth defects, postnatal death, male sterility and skeletal dysmorphology. Detailed analyses of the skeleton discovered high similarity to *Hoxc8*-knockout mice (van den Akker et al., 2001). Consistently, molecular analyses detected a shift of the anterior expression boundary of *Hoxc8* in embryos. A negative regulatory function of Eri1 on mature miR-196a levels could be shown and Eri1 was demonstrated to inhibit miR-196-mediated *Hoxc8* 3' UTR silencing. These findings suggested a model, in which Eri1 defines the *Hoxc8* expression pattern in the embryo and is consequently required for the correct patterning of the skeleton.

References

- Ambros, V. 2004. The functions of animal microRNAs. *Nature*. 431:350-5.
- Andersen, J.S., Y.W. Lam, A.K. Leung, S.E. Ong, C.E. Lyon, A.I. Lamond, and M. Mann. 2005. Nucleolar proteome dynamics. *Nature*. 433:77-83.
- Andersen, J.S., C.E. Lyon, A.H. Fox, A.K. Leung, Y.W. Lam, H. Steen, M. Mann, and A.I. Lamond. 2002. Directed proteomic analysis of the human nucleolus. *Curr Biol*. 12:1-11.
- Ansel, K.M., W.A. Pastor, N. Rath, A.D. Lapan, E. Glasmacher, C. Wolf, L.C. Smith, N. Papadopoulou, E.D. Lamperti, M. Tahiliani, J.W. Ellwart, Y. Shi, E. Kremmer, A. Rao, and V. Heissmeyer. 2008. Mouse Eri1 interacts with the ribosome and catalyzes 5.8S rRNA processing. *Nat Struct Mol Biol*. 15:523-30.
- Aravin, A., D. Gaidatzis, S. Pfeffer, M. Lagos-Quintana, P. Landgraf, N. Iovino, P. Morris, M.J. Brownstein, S. Kuramochi-Miyagawa, T. Nakano, M. Chien, J.J. Russo, J. Ju, R. Sheridan, C. Sander, M. Zavolan, and T. Tuschl. 2006. A novel class of small RNAs bind to MILI protein in mouse testes. *Nature*. 442:203-7.
- Aravin, A.A., M. Lagos-Quintana, A. Yalcin, M. Zavolan, D. Marks, B. Snyder, T. Gaasterland, J. Meyer, and T. Tuschl. 2003. The small RNA profile during *Drosophila melanogaster* development. *Dev Cell*. 5:337-50.
- Aravind, L., and E.V. Koonin. 2000. SAP - a putative DNA-binding motif involved in chromosomal organization. *Trends Biochem Sci*. 25:112-4.
- Battle, D.J., and J.A. Doudna. 2001. The stem-loop binding protein forms a highly stable and specific complex with the 3' stem-loop of histone mRNAs. *RNA*. 7:123-32.
- Blackburn, J., M. Rich, N. Ghitani, and J.P. Liu. 2009. Generation of conditional *Hoxc8* loss-of-function and *Hoxc8*-->*Hoxc9* replacement alleles in mice. *Genesis*. 47:680-7.
- Boisvert, F.M., S. van Koningsbruggen, J. Navascues, and A.I. Lamond. 2007. The multifunctional nucleolus. *Nat Rev Mol Cell Biol*. 8:574-85.
- Brennecke, J., D.R. Hipfner, A. Stark, R.B. Russell, and S.M. Cohen. 2003. bantam encodes a developmentally regulated microRNA that controls cell proliferation and regulates the proapoptotic gene *hid* in *Drosophila*. *Cell*. 113:25-36.
- Brummelkamp, T.R., R. Bernards, and R. Agami. 2002. Stable suppression of tumorigenicity by virus-mediated RNA interference. *Cancer Cell*. 2:243-7.
- Bühler, M., A. Verdel, and D. Moazed. 2006. Tethering RITS to a nascent transcript initiates RNAi- and heterochromatin-dependent gene silencing. *Cell*. 125:873-86.
- Cam, H., and S.I. Grewal. 2004. RNA interference and epigenetic control of heterochromatin assembly in fission yeast. *Cold Spring Harb Symp Quant Biol*. 69:419-27.
- Cam, H.P., T. Sugiyama, E.S. Chen, X. Chen, P.C. Fitzgerald, and S.I. Grewal. 2005. Comprehensive analysis of heterochromatin- and RNAi-mediated epigenetic control of the fission yeast genome. *Nat Genet*. 37:809-19.
- Castelli-Gair, J., and M. Akam. 1995. How the Hox gene *Ultrabithorax* specifies two different segments: the significance of spatial and temporal regulation within metameres. *Development*. 121:2973-82.
- Chen, C.Z., L. Li, H.F. Lodish, and D.P. Bartel. 2004. MicroRNAs modulate hematopoietic lineage differentiation. *Science*. 303:83-6.
- Chen, F., and M.R. Capecchi. 1997. Targeted mutations in *hoxa-9* and *hoxb-9* reveal synergistic interactions. *Dev Biol*. 181:186-96.

- Cheng, Y., and D.J. Patel. 2004. Crystallographic structure of the nuclease domain of 3'hExo, a DEDDh family member, bound to rAMP. *J Mol Biol.* 343:305-12.
- Churchill, G.A. 2002. Fundamentals of experimental design for cDNA microarrays. *Nat Genet.* 32 Suppl:490-5.
- Condie, B.G., and M.R. Capecchi. 1994. Mice with targeted disruptions in the paralogous genes *hoxa-3* and *hoxd-3* reveal synergistic interactions. *Nature.* 370:304-7.
- Cuckle, H.S., N.J. Wald, and R.H. Lindenbaum. 1984. Maternal serum alpha-fetoprotein measurement: a screening test for Down syndrome. *Lancet.* 1:926-9.
- Davis, A.P., D.P. Witte, H.M. Hsieh-Li, S.S. Potter, and M.R. Capecchi. 1995. Absence of radius and ulna in mice lacking *hoxa-11* and *hoxd-11*. *Nature.* 375:791-5.
- de Fougères, A., H.P. Vornlocher, J. Maraganore, and J. Lieberman. 2007. Interfering with disease: a progress report on siRNA-based therapeutics. *Nat Rev Drug Discov.* 6:443-53.
- DeLisle, A.J., R.A. Graves, W.F. Marzluff, and L.F. Johnson. 1983. Regulation of histone mRNA production and stability in serum-stimulated mouse 3T6 fibroblasts. *Mol Cell Biol.* 3:1920-9.
- Deschamps, J. 2007. Ancestral and recently recruited global control of the Hox genes in development. *Curr Opin Genet Dev.* 17:422-7.
- Dominski, Z., and W.F. Marzluff. 1999. Formation of the 3' end of histone mRNA. *Gene.* 239:1-14.
- Dominski, Z., X.C. Yang, H. Kaygun, M. Dadlez, and W.F. Marzluff. 2003. A 3' exonuclease that specifically interacts with the 3' end of histone mRNA. *Mol Cell.* 12:295-305.
- Draptchinskaja, N., P. Gustavsson, B. Andersson, M. Pettersson, T.N. Willig, I. Dianzani, S. Ball, G. Tchernia, J. Klar, H. Matsson, D. Tentler, N. Mohandas, B. Carlsson, and N. Dahl. 1999. The gene encoding ribosomal protein S19 is mutated in Diamond-Blackfan anaemia. *Nat Genet.* 21:169-75.
- Drobyshev, A.L., C. Machka, M. Horsch, M. Selmann, V. Liebscher, M. Hrabe de Angelis, and J. Beckers. 2003. Specificity assessment from fractionation experiments (SAFE): a novel method to evaluate microarray probe specificity based on hybridisation stringencies. *Nucleic Acids Res.* 31:E1-1.
- Duboule, D. 1994. Temporal colinearity and the phylotypic progression: a basis for the stability of a vertebrate Bauplan and the evolution of morphologies through heterochrony. *Dev Suppl.* 135-42.
- Duboule, D., and P. Dolle. 1989. The structural and functional organization of the murine HOX gene family resembles that of Drosophila homeotic genes. *EMBO J.* 8:1497-505.
- Duboule, D., and G. Morata. 1994. Colinearity and functional hierarchy among genes of the homeotic complexes. *Trends Genet.* 10:358-64.
- Duchaine, T.F., J.A. Wohlschlegel, S. Kennedy, Y. Bei, D. Conte, Jr., K. Pang, D.R. Brownell, S. Harding, S. Mitani, G. Ruvkun, J.R. Yates, 3rd, and C.C. Mello. 2006. Functional proteomics reveals the biochemical niche of *C. elegans* DCR-1 in multiple small-RNA-mediated pathways. *Cell.* 124:343-54.
- Eichler, D.C., and N. Craig. 1994. Processing of eukaryotic ribosomal RNA. *Prog Nucleic Acid Res Mol Biol.* 49:197-239.
- Elbashir, S.M., J. Harborth, W. Lendeckel, A. Yalcin, K. Weber, and T. Tuschl. 2001. Duplexes of 21-nucleotide RNAs mediate RNA interference in cultured mammalian cells. *Nature.* 411:494-8.
- Fire, A., S. Xu, M.K. Montgomery, S.A. Kostas, S.E. Driver, and C.C. Mello. 1998. Potent and specific genetic interference by double-stranded RNA in *Caenorhabditis elegans*. *Nature.* 391:806-11.

- Fromental-Ramain, C., X. Warot, S. Lakkaraju, B. Favier, H. Haack, C. Birling, A. Dierich, P. Dollé, and P. Chambon. 1996a. Specific and redundant functions of the paralogous Hoxa-9 and Hoxd-9 genes in forelimb and axial skeleton patterning. *Development*. 122:461-72.
- Fromental-Ramain, C., X. Warot, N. Messadecq, M. LeMeur, P. Dolle, and P. Chambon. 1996b. Hoxa-13 and Hoxd-13 play a crucial role in the patterning of the limb autopod. *Development*. 122:2997-3011.
- Gabant, P., L. Forrester, J. Nichols, T. Van Reeth, C. De Mees, B. Pajack, A. Watt, J. Smits, H. Alexandre, C. Szpirer, and J. Szpirer. 2002. Alpha-fetoprotein, the major fetal serum protein, is not essential for embryonic development but is required for female fertility. *Proc Natl Acad Sci U S A*. 99:12865-70.
- Gabel, H.W., and G. Ruvkun. 2008. The exonuclease ERI-1 has a conserved dual role in 5.8S rRNA processing and RNAi. *Nat Struct Mol Biol*. 15:531-3.
- Gilbert, C., A. Kristjuhan, G.S. Winkler, and J.Q. Svejstrup. 2004. Elongator interactions with nascent mRNA revealed by RNA immunoprecipitation. *Mol Cell*. 14:457-64.
- Graham, A., N. Papalopulu, and R. Krumlauf. 1989. The murine and Drosophila homeobox gene complexes have common features of organization and expression. *Cell*. 57:367-78.
- Grimson, A., K.K. Farh, W.K. Johnston, P. Garrett-Engele, L.P. Lim, and D.P. Bartel. 2007. MicroRNA targeting specificity in mammals: determinants beyond seed pairing. *Mol Cell*. 27:91-105.
- Gruss, P., and M. Kessel. 1991. Axial specification in higher vertebrates. *Curr Opin Genet Dev*. 1:204-10.
- Harris, M.E., R. Bohni, M.H. Schneiderman, L. Ramamurthy, D. Schumperli, and W.F. Marzluff. 1991. Regulation of histone mRNA in the unperturbed cell cycle: evidence suggesting control at two posttranscriptional steps. *Mol Cell Biol*. 11:2416-24.
- Heard, E., and W. Bickmore. 2007. The ins and outs of gene regulation and chromosome territory organisation. *Curr Opin Cell Biol*. 19:311-6.
- Hegde, P., R. Qi, K. Abernathy, C. Gay, S. Dharap, R. Gaspard, J.E. Hughes, E. Snesrud, N. Lee, and J. Quackenbush. 2000. A concise guide to cDNA microarray analysis. *Biotechniques*. 29:548-50, 552-4, 556
- Henras, A.K., E. Bertrand, and G. Chanfreau. 2004. A cotranscriptional model for 3'-end processing of the *Saccharomyces cerevisiae* pre-ribosomal RNA precursor. *RNA*. 10:1572-85.
- Henras, A.K., J. Soudet, M. Gerus, S. Lebaron, M. Caizergues-Ferrer, A. Mougin, and Y. Henry. 2008. The post-transcriptional steps of eukaryotic ribosome biogenesis. *Cell Mol Life Sci*. 65:2334-59.
- Horan, G.S., E.N. Kovacs, R.R. Behringer, and M.S. Featherstone. 1995. Mutations in paralogous Hox genes result in overlapping homeotic transformations of the axial skeleton: evidence for unique and redundant function. *Dev Biol*. 169:359-72.
- Hornstein, E., J.H. Mansfield, S. Yekta, J.K. Hu, B.D. Harfe, M.T. McManus, S. Baskerville, D.P. Bartel, and C.J. Tabin. 2005. The microRNA miR-196 acts upstream of Hoxb8 and Shh in limb development. *Nature*. 438:671-4.
- Horsch, M., S. Schadler, V. Gailus-Durner, H. Fuchs, H. Meyer, M.H. de Angelis, and J. Beckers. 2008. Systematic gene expression profiling of mouse model series reveals coexpressed genes. *Proteomics*. 8:1248-56.
- Houseley, J., J. LaCava, and D. Tollervey. 2006. RNA-quality control by the exosome. *Nat Rev Mol Cell Biol*. 7:529-39.
- Iida, T., R. Kawaguchi, and J. Nakayama. 2006. Conserved ribonuclease, Eri1, negatively regulates heterochromatin assembly in fission yeast. *Curr Biol*. 16:1459-64.

- Jacquier, A. 2009. The complex eukaryotic transcriptome: unexpected pervasive transcription and novel small RNAs. *Nat Rev Genet.* 10:833-44.
- Jin, L., L. Long, M.A. Green, and B.T. Spear. 2009. The alpha-fetoprotein enhancer region activates the albumin and alpha-fetoprotein promoters during liver development. *Dev Biol.* 336:294-300.
- Johnston, R.J., and O. Hobert. 2003. A microRNA controlling left/right neuronal asymmetry in *Caenorhabditis elegans*. *Nature.* 426:845-9.
- Juan, A.H., H. Lei, P. Bhargava, M. Lebrun, and F.H. Ruddle. 2006. Multiple roles of *hoxc8* in skeletal development. *Ann NY Acad Sci.* 1068:87-94.
- Kaartinen, V., A. Nagy, I. Gonzalez-Gomez, J. Groffen, and N. Heisterkamp. 2002. Vestibular dysgenesis in mice lacking *Abr* and *Bcr Cdc42/RacGAPs*. *Dev Dyn.* 223:517-25.
- Kennedy, S., D. Wang, and G. Ruvkun. 2004. A conserved siRNA-degrading RNase negatively regulates RNA interference in *C. elegans*. *Nature.* 427:645-9.
- Kessel, M., and P. Gruss. 1991. Homeotic transformations of murine vertebrae and concomitant alteration of Hox codes induced by retinoic acid. *Cell.* 67:89-104.
- Kim, V.N. 2005. MicroRNA biogenesis: coordinated cropping and dicing. *Nat Rev Mol Cell Biol.* 6:376-85.
- Kimmins, S., and P. Sassone-Corsi. 2005. Chromatin remodelling and epigenetic features of germ cells. *Nature.* 434:583-9.
- Kipp, M., F. Gohring, T. Ostendorp, C.M. van Drunen, R. van Driel, M. Przybylski, and F.O. Fackelmayer. 2000. SAF-Box, a conserved protein domain that specifically recognizes scaffold attachment region DNA. *Mol Cell Biol.* 20:7480-9.
- Kiss, T. 2002. Small nucleolar RNAs: an abundant group of noncoding RNAs with diverse cellular functions. *Cell.* 109:145-8.
- Kloosterman, W.P., E. Wienholds, E. de Bruijn, S. Kauppinen, and R.H. Plasterk. 2006. In situ detection of miRNAs in animal embryos using LNA-modified oligonucleotide probes. *Nat Methods.* 3:27-9.
- Kmita, M., and D. Duboule. 2003. Organizing axes in time and space; 25 years of colinear tinkering. *Science.* 301:331-3.
- Kornberg, R.D. 1974. Chromatin structure: a repeating unit of histones and DNA. *Science.* 184:868-71.
- Kornberg, R.D., and J.O. Thomas. 1974. Chromatin structure; oligomers of the histones. *Science.* 184:865-8.
- Krumlauf, R. 1994. Hox genes in vertebrate development. *Cell.* 78:191-201.
- Kupsco, J.M., M.J. Wu, W.F. Marzluff, R. Thapar, and R.J. Duronio. 2006. Genetic and biochemical characterization of *Drosophila* Snipper: A promiscuous member of the metazoan 3'hExo/ERI-1 family of 3' to 5' exonucleases. *RNA.* 12:2103-17.
- Kwon, C., Z. Han, E.N. Olson, and D. Srivastava. 2005a. MicroRNA1 influences cardiac differentiation in *Drosophila* and regulates Notch signaling. *Proc Natl Acad Sci U S A.* 102:18986-91.
- Kwon, Y., J. Shin, H.W. Park, and M.H. Kim. 2005b. Dynamic expression pattern of *Hoxc8* during mouse early embryogenesis. *Anat Rec A Discov Mol Cell Evol Biol.* 283:187-92.
- Lagos-Quintana, M., R. Rauhut, A. Yalcin, J. Meyer, W. Lendeckel, and T. Tuschl. 2002. Identification of tissue-specific microRNAs from mouse. *Curr Biol.* 12:735-9.
- Lambertsson, A. 1998. The minute genes in *Drosophila* and their molecular functions. *Adv Genet.* 38:69-134.
- Landgraf, P., M. Rusu, R. Sheridan, A. Sewer, N. Iovino, A. Aravin, S. Pfeffer, A. Rice, A.O. Kamphorst, M. Landthaler, C. Lin, N.D. Socci, L. Hermida, V. Fulci, S. Chiaretti, R.

- Foa, J. Schliwka, U. Fuchs, A. Novosel, R.U. Muller, B. Schermer, U. Bissels, J. Inman, Q. Phan, M. Chien, D.B. Weir, R. Choksi, G. De Vita, D. Frezzetti, H.I. Trompeter, V. Hornung, G. Teng, G. Hartmann, M. Palkovits, R. Di Lauro, P. Wernet, G. Macino, C.E. Rogler, J.W. Nagle, J. Ju, F.N. Papavasiliou, T. Benzing, P. Lichter, W. Tam, M.J. Brownstein, A. Bosio, A. Borkhardt, J.J. Russo, C. Sander, M. Zavolan, and T. Tuschl. 2007. A mammalian microRNA expression atlas based on small RNA library sequencing. *Cell*. 129:1401-14.
- Lau, N.C., L.P. Lim, E.G. Weinstein, and D.P. Bartel. 2001. An abundant class of tiny RNAs with probable regulatory roles in *Caenorhabditis elegans*. *Science*. 294:858-62.
- Le Mouellic, H., Y. Lallemand, and P. Brulet. 1992. Homeosis in the mouse induced by a null mutation in the Hox-3.1 gene. *Cell*. 69:251-64.
- Lee, R.C., and V. Ambros. 2001. An extensive class of small RNAs in *Caenorhabditis elegans*. *Science*. 294:862-4.
- Lee, R.C., R.L. Feinbaum, and V. Ambros. 1993. The *C. elegans* heterochronic gene *lin-4* encodes small RNAs with antisense complementarity to *lin-14*. *Cell*. 75:843-54.
- Lee, R.C., C.M. Hammell, and V. Ambros. 2006. Interacting endogenous and exogenous RNAi pathways in *Caenorhabditis elegans*. *RNA*. 12:589-97.
- Leighton, P.C., M.J. Kitau, T. Chard, Y.B. Gordon, and A.E. Leek. 1975. Levels of alpha-fetoprotein in maternal blood as a screening test for fetal neural-tube defect. *Lancet*. 2:1012-5.
- Lewis, E.B. 1978. A gene complex controlling segmentation in *Drosophila*. *Nature*. 276:565-70.
- Licatalosi, D.D., and R.B. Darnell. 2010. RNA processing and its regulation: global insights into biological networks. *Nat Rev Genet*. 11:75-87.
- Lippman, Z., and R. Martienssen. 2004. The role of RNA interference in heterochromatic silencing. *Nature*. 431:364-70.
- Liu, C.G., G.A. Calin, B. Meloon, N. Gamliel, C. Sevignani, M. Ferracin, C.D. Dumitru, M. Shimizu, S. Zupo, M. Dono, H. Alder, F. Bullrich, M. Negrini, and C.M. Croce. 2004. An oligonucleotide microchip for genome-wide microRNA profiling in human and mouse tissues. *Proc Natl Acad Sci U S A*. 101:9740-4.
- Manley, N.R., and M.R. Capecchi. 1997. Hox group 3 paralogous genes act synergistically in the formation of somitic and neural crest-derived structures. *Dev Biol*. 192:274-88.
- Manley, N.R., and M.R. Capecchi. 1998. Hox group 3 paralogs regulate the development and migration of the thymus, thyroid, and parathyroid glands. *Dev Biol*. 195:1-15.
- Mansfield, J.H., B.D. Harfe, R. Nissen, J. Obenauer, J. Srineel, A. Chaudhuri, R. Farzan-Kashani, M. Zuker, A.E. Pasquinelli, G. Ruvkun, P.A. Sharp, C.J. Tabin, and M.T. McManus. 2004. MicroRNA-responsive 'sensor' transgenes uncover Hox-like and other developmentally regulated patterns of vertebrate microRNA expression. *Nat Genet*. 36:1079-83.
- Martin, F., F. Michel, D. Zenklusen, B. Muller, and D. Schumperli. 2000. Positive and negative mutant selection in the human histone hairpin-binding protein using the yeast three-hybrid system. *Nucleic Acids Res*. 28:1594-603.
- Marzluff, W.F., E.J. Wagner, and R.J. Duronio. 2008. Metabolism and regulation of canonical histone mRNAs: life without a poly(A) tail. *Nat Rev Genet*. 9:843-54.
- McGinnis, W., and R. Krumlauf. 1992. Homeobox genes and axial patterning. *Cell*. 68:283-302.
- McGlenn, E., S. Yekta, J.H. Mansfield, J. Soutschek, D.P. Bartel, and C.J. Tabin. 2009. In ovo application of antagomiRs indicates a role for miR-196 in patterning the chick axial skeleton through Hox gene regulation. *Proc Natl Acad Sci U S A*. 106:18610-5.

- McIntyre, D.C., S. Rakshit, A.R. Yallowitz, L. Loken, L. Jeannotte, M.R. Capecchi, and D.M. Wellik. 2007. Hox patterning of the vertebrate rib cage. *Development*. 134:2981-9.
- Mello, C.C., and D. Conte, Jr. 2004. Revealing the world of RNA interference. *Nature*. 431:338-42.
- Mendes Soares, L.M., and J. Valcarcel. 2006. The expanding transcriptome: the genome as the 'Book of Sand'. *EMBO J*. 25:923-31.
- Mitchell, P., E. Petfalski, A. Shevchenko, M. Mann, and D. Tollervy. 1997. The exosome: a conserved eukaryotic RNA processing complex containing multiple 3'→5' exoribonucleases. *Cell*. 91:457-66.
- Mowry, K.L., and J.A. Steitz. 1987. Identification of the human U7 snRNP as one of several factors involved in the 3' end maturation of histone premessenger RNA's. *Science*. 238:1682-7.
- Mullen, T.E., and W.F. Marzluff. 2008. Degradation of histone mRNA requires oligouridylation followed by decapping and simultaneous degradation of the mRNA both 5' to 3' and 3' to 5'. *Genes Dev*. 22:50-65.
- Niranjanakumari, S., E. Lasda, R. Brazas, and M.A. Garcia-Blanco. 2002. Reversible cross-linking combined with immunoprecipitation to study RNA-protein interactions in vivo. *Methods*. 26:182-90.
- Oishi, K., K. Miyazaki, K. Kadota, R. Kikuno, T. Nagase, G. Atsumi, N. Ohkura, T. Azama, M. Mesaki, S. Yukimasa, H. Kobayashi, C. Iitaka, T. Umehara, M. Horikoshi, T. Kudo, Y. Shimizu, M. Yano, M. Monden, K. Machida, J. Matsuda, S. Horie, T. Todo, and N. Ishida. 2003. Genome-wide expression analysis of mouse liver reveals CLOCK-regulated circadian output genes. *J Biol Chem*. 278:41519-27.
- Olins, A.L., and D.E. Olins. 1974. Spheroid chromatin units (v bodies). *Science*. 183:330-2.
- Oliver, E.R., T.L. Saunders, S.A. Tarle, and T. Glaser. 2004. Ribosomal protein L24 defect in belly spot and tail (Bst), a mouse Minute. *Development*. 131:3907-20.
- Parker, R., and H. Song. 2004. The enzymes and control of eukaryotic mRNA turnover. *Nat Struct Mol Biol*. 11:121-7.
- Pasquinelli, A.E., B.J. Reinhart, F. Slack, M.Q. Martindale, M.I. Kuroda, B. Maller, D.C. Hayward, E.E. Ball, B. Degnan, P. Muller, J. Spring, A. Srinivasan, M. Fishman, J. Finnerty, J. Corbo, M. Levine, P. Leahy, E. Davidson, and G. Ruvkun. 2000. Conservation of the sequence and temporal expression of let-7 heterochronic regulatory RNA. *Nature*. 408:86-9.
- Pearson, J.C., D. Lemons, and W. McGinnis. 2005. Modulating Hox gene functions during animal body patterning. *Nat Rev Genet*. 6:893-904.
- Pritchard, C.C., L. Hsu, J. Delrow, and P.S. Nelson. 2001. Project normal: defining normal variance in mouse gene expression. *Proc Natl Acad Sci U S A*. 98:13266-71.
- Raijmakers, R., G. Schilders, and G.J. Pruijn. 2004. The exosome, a molecular machine for controlled RNA degradation in both nucleus and cytoplasm. *Eur J Cell Biol*. 83:175-83.
- Reinhart, B.J., F.J. Slack, M. Basson, A.E. Pasquinelli, J.C. Bettinger, A.E. Rougvie, H.R. Horvitz, and G. Ruvkun. 2000. The 21-nucleotide let-7 RNA regulates developmental timing in *Caenorhabditis elegans*. *Nature*. 403:901-6.
- Rijli, F.M., R. Matyas, M. Pellegrini, A. Dierich, P. Gruss, P. Dolle, and P. Chambon. 1995. Cryptorchidism and homeotic transformations of spinal nerves and vertebrae in Hoxa-10 mutant mice. *Proc Natl Acad Sci U S A*. 92:8185-9.
- Saiki, R.K., D.H. Gelfand, S. Stoffel, S.J. Scharf, R. Higuchi, G.T. Horn, K.B. Mullis, and H.A. Erlich. 1988. Primer-directed enzymatic amplification of DNA with a thermostable DNA polymerase. *Science*. 239:487-91.

- Salser, S.J., and C. Kenyon. 1996. A *C. elegans* Hox gene switches on, off, on and off again to regulate proliferation, differentiation and morphogenesis. *Development*. 122:1651-61.
- Satokata, I., G. Benson, and R. Maas. 1995. Sexually dimorphic sterility phenotypes in Hoxa10-deficient mice. *Nature*. 374:460-3.
- Scherl, A., Y. Coute, C. Deon, A. Calle, K. Kindbeiter, J.C. Sanchez, A. Greco, D. Hochstrasser, and J.J. Diaz. 2002. Functional proteomic analysis of human nucleolus. *Mol Biol Cell*. 13:4100-9.
- Schneider, D.A., A. Michel, M.L. Sikes, L. Vu, J.A. Dodd, S. Salgia, Y.N. Osheim, A.L. Beyer, and M. Nomura. 2007. Transcription elongation by RNA polymerase I is linked to efficient rRNA processing and ribosome assembly. *Mol Cell*. 26:217-29.
- Schwartz, Y.B., and V. Pirrotta. 2007. Polycomb silencing mechanisms and the management of genomic programmes. *Nat Rev Genet*. 8:9-22.
- Seltmann, M., M. Horsch, A. Drobyshev, Y. Chen, M.H. de Angelis, and J. Beckers. 2005. Assessment of a systematic expression profiling approach in ENU-induced mouse mutant lines. *Mamm Genome*. 16:1-10.
- Shuman, S. 1997. Origins of mRNA identity: capping enzymes bind to the phosphorylated C-terminal domain of RNA polymerase II. *Proc Natl Acad Sci U S A*. 94:12758-60.
- Siomi, H., and M.C. Siomi. 2009. On the road to reading the RNA-interference code. *Nature*. 457:396-404.
- Soshnikova, N., and D. Duboule. 2009a. Epigenetic regulation of vertebrate Hox genes: a dynamic equilibrium. *Epigenetics*. 4:537-40.
- Soshnikova, N., and D. Duboule. 2009b. Epigenetic temporal control of mouse Hox genes in vivo. *Science*. 324:1320-3.
- Stark, A., J. Brennecke, N. Bushati, R.B. Russell, and S.M. Cohen. 2005. Animal MicroRNAs confer robustness to gene expression and have a significant impact on 3'UTR evolution. *Cell*. 123:1133-46.
- Suemori, H., N. Takahashi, and S. Noguchi. 1995. Hoxc-9 mutant mice show anterior transformation of the vertebrae and malformation of the sternum and ribs. *Mech Dev*. 51:265-73.
- Sweetman, D., K. Goljanek, T. Rathjen, S. Oustanina, T. Braun, T. Dalmay, and A. Munsterberg. 2008. Specific requirements of MRFs for the expression of muscle specific microRNAs, miR-1, miR-206 and miR-133. *Dev Biol*. 321:491-9.
- Tharun, S., W. He, A.E. Mayes, P. Lennertz, J.D. Beggs, and R. Parker. 2000. Yeast Sm-like proteins function in mRNA decapping and decay. *Nature*. 404:515-8.
- Tiret, L., H. Le Mouellic, M. Maury, and P. Brulet. 1998. Increased apoptosis of motoneurons and altered somatotopic maps in the brachial spinal cord of Hoxc-8-deficient mice. *Development*. 125:279-91.
- Tschochner, H., and E. Hurt. 2003. Pre-ribosomes on the road from the nucleolus to the cytoplasm. *Trends Cell Biol*. 13:255-63.
- van den Akker, E., C. Fromental-Ramain, W. de Graaff, H. Le Mouellic, P. Brulet, P. Chambon, and J. Deschamps. 2001. Axial skeletal patterning in mice lacking all paralogous group 8 Hox genes. *Development*. 128:1911-21.
- Verdel, A., S. Jia, S. Gerber, T. Sugiyama, S. Gygi, S.I. Grewal, and D. Moazed. 2004. RNAi-mediated targeting of heterochromatin by the RITS complex. *Science*. 303:672-6.
- Volpe, T.A., C. Kidner, I.M. Hall, G. Teng, S.I. Grewal, and R.A. Martienssen. 2002. Regulation of heterochromatic silencing and histone H3 lysine-9 methylation by RNAi. *Science*. 297:1833-7.
- Wellik, D.M. 2007. Hox patterning of the vertebrate axial skeleton. *Dev Dyn*. 236:2454-63.

- Wellik, D.M., and M.R. Capecchi. 2003. Hox10 and Hox11 genes are required to globally pattern the mammalian skeleton. *Science*. 301:363-7.
- Wetterberg, I., G. Bauren, and L. Wieslander. 1996. The intranuclear site of excision of each intron in Balbiani ring 3 pre-mRNA is influenced by the time remaining to transcription termination and different excision efficiencies for the various introns. *RNA*. 2:641-51.
- Whitfield, M.L., H. Kaygun, J.A. Erkmann, W.H. Townley-Tilson, Z. Dominski, and W.F. Marzluff. 2004. SLBP is associated with histone mRNA on polyribosomes as a component of the histone mRNP. *Nucleic Acids Res.* 32:4833-42.
- Wightman, B., I. Ha, and G. Ruvkun. 1993. Posttranscriptional regulation of the heterochronic gene *lin-14* by *lin-4* mediates temporal pattern formation in *C. elegans*. *Cell*. 75:855-62.
- Williams, A.S., and W.F. Marzluff. 1995. The sequence of the stem and flanking sequences at the 3' end of histone mRNA are critical determinants for the binding of the stem-loop binding protein. *Nucleic Acids Res.* 23:654-62.
- Xu, P., S.Y. Vernooy, M. Guo, and B.A. Hay. 2003. The Drosophila microRNA Mir-14 suppresses cell death and is required for normal fat metabolism. *Curr Biol*. 13:790-5.
- Yang, X.C., M. Purdy, W.F. Marzluff, and Z. Dominski. 2006. Characterization of 3'hExo, a 3' exonuclease specifically interacting with the 3' end of histone mRNA. *J Biol Chem*. 281:30447-54.
- Yekta, S., I.H. Shih, and D.P. Bartel. 2004. MicroRNA-directed cleavage of HOXB8 mRNA. *Science*. 304:594-6.
- Yekta, S., C.J. Tabin, and D.P. Bartel. 2008. MicroRNAs in the Hox network: an apparent link to posterior prevalence. *Nat Rev Genet*. 9:789-96.
- Zheng, L., Z. Dominski, X.C. Yang, P. Elms, C.S. Raska, C.H. Borchers, and W.F. Marzluff. 2003. Phosphorylation of stem-loop binding protein (SLBP) on two threonines triggers degradation of SLBP, the sole cell cycle-regulated factor required for regulation of histone mRNA processing, at the end of S phase. *Mol Cell Biol*. 23:1590-601.
- Zuo, Y., and M.P. Deutscher. 2001. Exoribonuclease superfamilies: structural analysis and phylogenetic distribution. *Nucleic Acids Res.* 29:1017-26.

Supplementary

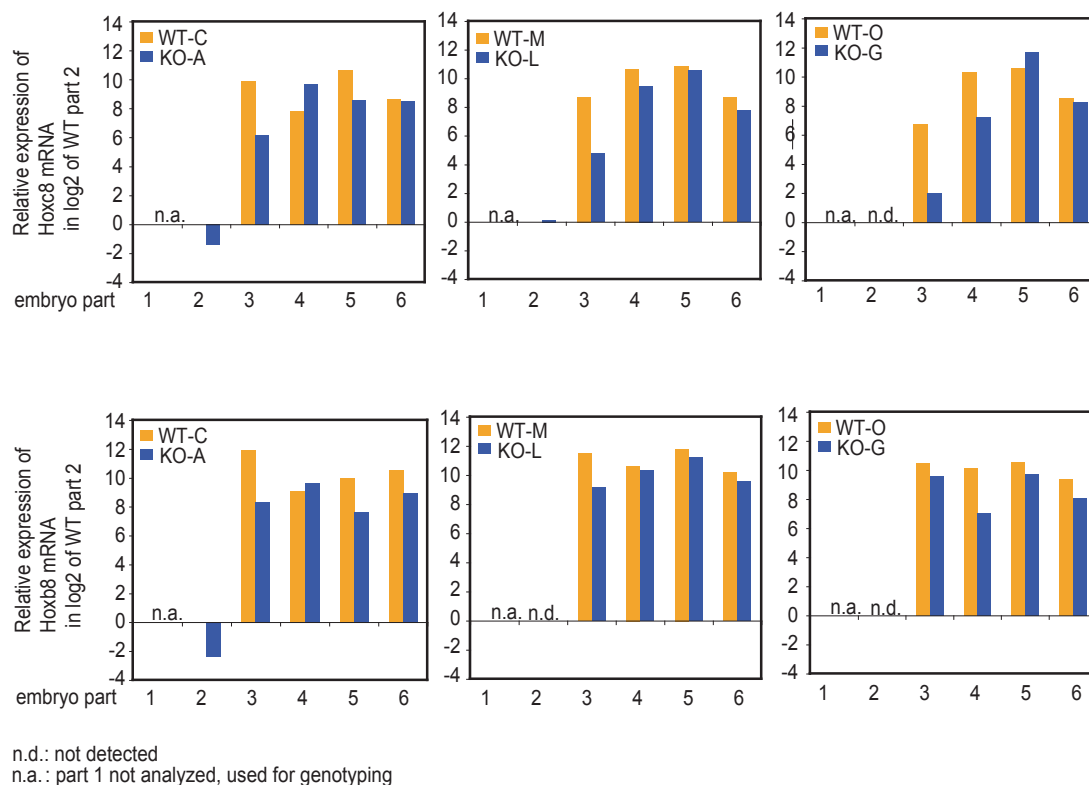


Figure S-35: Hoxc8 and Hoxb8 expression in three *Eri1*-knockout and wildtype embryos. Hoxc8 and Hoxb8 mRNA levels were detected by qRT-PCR in three *Eri1*-knockout and wildtype embryos from two litters (litter one: knockout-A, wildtype-C, knockout-G and litter two: knockout-L, wildtype-M, wildtype-O; C57BL/6). The values were normalized to the pbgd housekeeping gene. The ΔCp Hoxc8/pbgd or Hoxb8/pbgd in wildtype part 2 was set 1 (\log_2 of 0). The expression of Hoxc8/Hoxb8 mRNA in the six embryo parts is shown on a logarithmic scale as multiples of the mRNA expression in part 2 of the wildtype embryos.

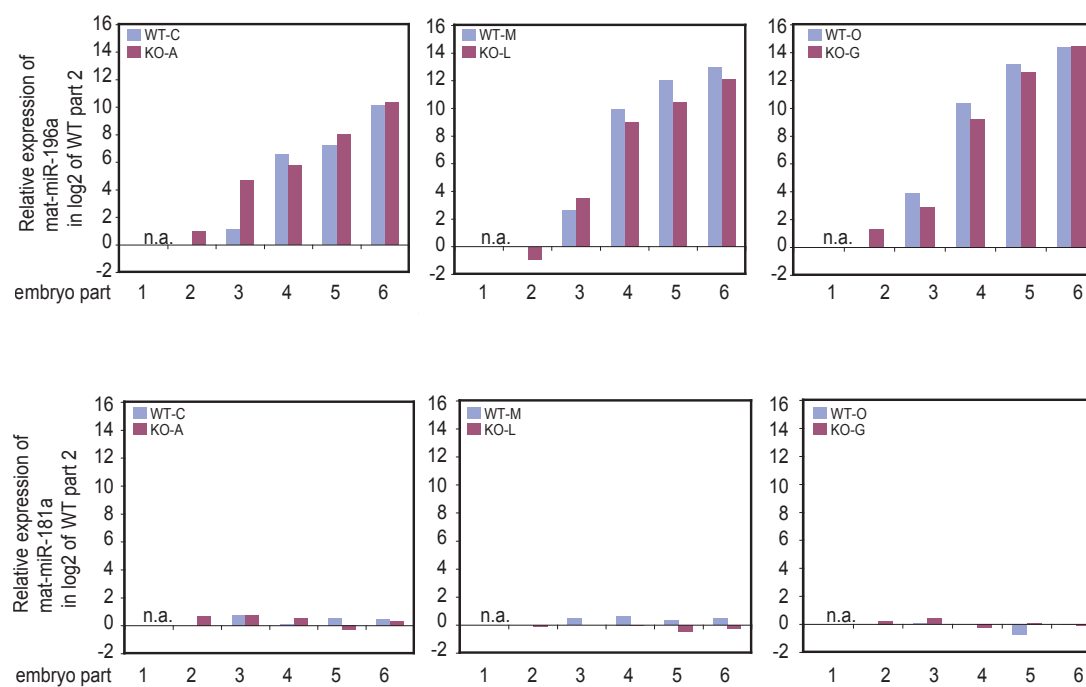


Figure S-36: mat-miR-196a and miR-181a expression in three *Eri1*-knockout and wildtype embryos. Mature miRNA levels for miR-196a and miR-181a were detected by qRT-PCR in three *Eri1*-knockout and wildtype embryos from two litters (litter one: knockout-A, wildtype-C, knockout-G and litter two: knockout-L, wildtype-M, wildtype-O; C57BL/6). The values were normalized to the U6 snRNA housekeeping gene. The ΔC_p , mature miRNA/U6 snRNA, in wildtype part 2 was set 1 (log₂ of 0). The expression of mat-miR-196a and miR-181a in the six embryo parts is shown on a logarithmic scale as multiples of the miRNA expression in part 2 of the wildtype embryos.

Publications

Articles based on this thesis

Ansel KM., Pastor WA.*, **Rath N.***, Lapan AD.*, Glasmacher E., Wolf C., Smith LC., Papadopoulou N., Lamperti ED., Tahiliani M., Ellwart JW., Shi Y., Kremmer E., Rao A., Heissmeyer V. * equal contribution.

‘Mouse Eri1 interacts with the ribosome and catalyzes 5.8S rRNA processing.’

2008. Nat Struct Mol Biol. 15, 523-30.

Rath N. * Abdul-Wajid S. *, Thomas M., Cohrs C., Neff F., Hoesel B., Yanni E., Hattori K., Chen Z., Gajus-Durner V., Beckers J., Esposito I., Hans W., Fuchs H., Hrabe de Angelis M., Heissmeyer V., Ansel KM. * equal contribution.

‘Eri1 inhibits RNAi and the miRNA pathway in T cell differentiation and skeletal patterning.’

Manuscript in preparation.

Hoefig KP., **Rath N.**, Glasmacher E., Schepers A., Heissmeyer V.

‘Eri1 degrades histone mRNA stem-loops’

Manuscript in preparation.

Posters and abstracts based on this thesis

Rath N., Ansel KM., Pastor WA., Rao A., Heissmeyer V.

‘Mouse Eri1 is involved in ribosomal RNA processing.’

Keystone Symposia (2008) on RNAi, microRNA and non-coding RNA, Whistler, British Columbia, Canada

Rath N., Ansel KM., Rao A., Heissmeyer V.

‘Characterization of mouse ERI-1 in the binding and processing of RNA target molecules.’

Interact symposium 2007, MPI research campus, Martinsried, Germany

Curriculum vitae

PERSONAL DATA

Name	Nicola Maria Rath
Date of Birth	02.01.1981
Place of Birth	Belo Horizonte, Brazil
Nationality	German
Contact	nicola.rath@helmholtz-muenchen.de

EDUCATION

10/2003 – 02/2006	Undergraduate Studies in Molecular Biology, Cell Biology and Zoology at the Ruprecht-Karls-University of Heidelberg, Germany (Final Grade: 1.3)
09/2002 – 06/2003	Undergraduate Studies in Genetics, Microbiology and Biochemistry at the Trinity College Dublin, Ireland
10/2000 – 08/2002	Undergraduate Studies in General Biology at the Rheinische Friedrich-Wilhelms-University of Bonn, Germany

PRACTICAL EXPERIENCE

Since 10/2006	PhD thesis at the Institute of Molecular Immunology, Helmholtz Center Munich, Supervisors: Dr. Vigo Heissmeyer and Prof. Dr. Dirk Eick
04/2006 – 09/2006	Research assistant at the Dr. von Hauner Children`s Hospital, Ludwig-Maximilians-University of Munich, Germany, Group: Molecular Pneumology and Experimental Therapy Research, PD Dr. Joseph Rosenecker
05/2005 – 02/2006	Diploma thesis in the Division of Molecular Genetics, German Cancer Research Center (DKFZ), Heidelberg, Germany, Topic: “Stable complementation of the deregulated microRNAs miR-15a and miR-16 -1 in mantle cell lymphoma”, Supervisors: Dr. Armin Pscherer and Prof. Dr. Peter Lichter
06/2003 – 09/2003	Research internship in the Division of Functional Genome Analysis, German Cancer Research Center (DKFZ), Heidelberg, Germany, Supervisors: Dr. Marcus Frohme and Dr. Jörg Hoheisel

Acknowledgements

I would especially like to express my thanks to Dr. Vigo Heissmeyer for the kind opportunity to perform my PhD in his laboratory. Thanks for the continuous and outstanding support, our scientific discussions, the excellent ideas and endless input, this work achieved success.

I would like to thank Prof. Dr. Dirk Eick and Prof. Dr. Michael Schleicher for the evaluation of this thesis work.

Special thanks applies to Dr. K. Mark Ansel from the University of California, San Francisco for the fruitful collaboration in the ribosomal RNA as well as the miRNA project.

I would like to thank Dr. Kai Höfig for the weekly discussions about the course and progress of this work and for his excellent support in the histone mRNA project.

Moreover, I appreciate the valuable cooperation with the German Mouse Clinic. A special thanks goes to Dr. Wolfgang Hans and Christian Cohrs for their contributions to the description of the skeletal phenotype. Thanks goes also to Dr. Marion Horsch for the molecular phenotyping analysis.

Further, I would like to thank Dr. Frauke Neff from the HMGU Institute of Pathology who contributed the Eri1 embryo stains and Bastian Hösel from the HMGU Institute of Experimental Genetics for his highly qualified help to establish an *in situ* hybridization assay for miR-196 in embryos.

Furthermore, I want to thank Elke Glasmacher for her expertise and great help with the confocal microscopy pictures and Lirui Du for the generation of the adenoviral vector pCAGAdDu that is an excellent tool for the infection of cells.